NTNU – Trondheim
Norwegian University of
Science and Technology

Sintering of lead-free piezoelectric materials

Kristine Bakken

Materials Science and Engineering
Submission date: July 2015
Supervisor: Mari-Ann Einarsrud, IMTE
Co-supervisor: Tor Grande, IMTE
Guttorm Syvertsen-Wiig, CerPoTech AS

Norwegian University of Science and Technology
Department of Materials Science and Engineering

Thesis description

CerPoTech AS in Trondheim is a spin-off company from NTNU producing advanced ceramic powders for applications like electroceramics, fuel cells, membranes, batteries and sensors. The powder is produced by spray pyrolysis where aqueous solutions are atomized and sprayed through a furnace. Spray pyrolysis is a flexible and scalable method giving high-quality powders.

The development of new piezo/ferroelectric materials and technology has led to a significant number of industrial and commercial applications. Among these applications are high-dielectric-constant capacitors, piezoelectric sonar and ultrasonic transducers, gas ignitors, sensors and switches as well as ferroelectric thin-film memories. Lead zirconate titanate (PZT) based ceramic materials have been the most common material for these applications for decades, however there is a huge interest in lead-free piezoelectric/ferroelectric materials since PZT will be phased out because of the lead content (toxic in electronic waste). The most attractive materials to replace PZT are $K_{0.5}Na_{0.5}NbO_3$ (KNN)-based materials. The main challenge with these materials is to obtain fine-grained and dense ceramics, preferentially with high degree of preferential orientation in order to obtain improved physical properties. Sub-micron powders as produced by spray pyrolysis are therefore very attractive for the development of these lead-free piezoelectric and ferroelectric materials. Poor sinterability also starting from the sub-micron powders has been the main obstacle for the development of these materials however recently we have set up a hypothesis explaining the low densification rate.

The objective of this project is to explore the sintering of KNN-based materials starting from the sub-micron powders to obtain an understanding of the densification and coarsening mechanisms. The sintering will be performed in different atmospheres and conditions and the effect on the microstructure will be followed. The prepared dense materials will be characterized with respect to the following properties: Microstructure (grain size and porosity) will be characterized by scanning electron microscopy. Crystal structure and phase composition will be determined by X-ray diffraction. Dielectric, piezo- and ferroelectric parameters will be characterized of the dense materials.

Preface

This work is a Master Thesis at NTNU. It is part of the study program Materials Science and Engineering, carried out from February to July 2015. It was done in cooperation with CerPoTech AS, who supplied the powder investigated in this thesis. Professor Mari-Ann Einarsrud has supervised the work, Professor Tor Grande and Guttorm Syvertsen-Wiig from CerPoTech AS served as co-supervisors.

This master thesis is the direct continuation of the specialization project titled "Sintering of lead-free piezoelectric materials"[1], which is a mandatory part of the study program. The aim is to complete the work started in the specialization project, and together give a better understanding of the sintering process in KNN based materials.

The materials used in this master thesis were prepared and characterized as part of the specialization project. Some results from the specialization project will be presented as they complement the results obtained in this master thesis. The dilatometry curves in air and nitrogen were recorded as part of the specialization project, as were some of the infrared spectra and X-ray diffractograms. In addition, some of the samples studied in this master thesis were made during the specialization project.

Trondheim, 7 July 2015

Kristine Bakken

Acknowledgements

First, I would like to thank my supervisor Mari-Ann Einarsrud for all her help, advice, and continuous feedback throughout the semester. Her guidance has truly been invaluable. I would also like to thank all my supervisors, including co-superiors Tor Grande and Guttorm Syvertsen-Wiig for the opportunity to work with this interesting topic.

Espen Tjønneland Wefring has been a great help regarding the many challenges of the electrical measurement, going out of his way to help me solve all my problems and giving excellent advice. I would also like to thank Sandra Helen Skjærvø and Gerhard Henning Olsen for taking the time to read my thesis and for providing constructive comments and suggesting possible improvements.

Another thanks goes out to all of the technical staff at the KII-building, for all the help, training and assistance in the laboratories. Pei Na Kui and Malin Sletnes deserve special credit for their contributions during my project work. I would also like to thank the people associated with the "Ferro"-group for our weekly meetings. They were always ready to give constructive feedback, especially on figures, and for forcing me to reflect on my results.

The work of Astri Bjørnetun Haugen in connection with her PhD Thesis[2] has been invaluable for my understanding of the sintering process in KNN materials and for interpreting my results.

I would also like to thank my family for their support. Finally, special thanks also goes to Jarand Nærland for his extraordinary engineering abilities and Berit Johansen Vinje for proof-reading my thesis.

Abstract

Piezoelectric ceramics are used in many types of devices, and today, lead zirconate titanate (PZT) dominates the market due to its superior properties. Environmental and health concerns have made the search for lead-free piezoelectric ceramics an important issue. Potassium sodium niobate (KNN) is a lead-free ceramic material, where good piezoelectric properties are possible through compositional engineering or texturing, but sintering is challenging due to coarsening and alkali evaporation.

The formation of a liquid phase consisting of alkali hydroxides and carbonates at low temperatures is proposed to be the cause of the abnormal grain growth observed in KNN materials. A reducing atmosphere should destabilize these alkali hydroxides and carbonates, which will limit the coarsening and therefore improve the densification and enhance the piezoelectric performance.

The effect of the sintering atmosphere in nominally stoichiometric KNN and KNN with 3 mol% nominal alkali excess was investigated. Conventional sintering and dilatometry was conducted in synthetic air, nitrogen and a reducing atmosphere. Characterization of the sintered pellets was done by XRD, SEM, infrared spectroscopy and piezoelectric measurements.

This work confirms that the liquid phase forming in KNN materials at low temperatures during sintering (or calcination) consists of alkali carbonates and hydroxides. The reducing atmosphere limits the degree of coarsening and gives higher densities. In stoichiometric KNN the coarsening was especially limited, resulting in a microstructure consisting of small cubic grains.

For piezoelectric applications, the samples had to be reoxidized, but this did not deteriorate the microstructure significantly. The piezoelectric measurements show that high density and proper sample preparation is important. The obtained values of the normalized strain and piezoelectric coefficient were generally low compared to the reported values in the literature. The polarization loops were round and had large leakage currents. However, the results suggest that a reducing atmosphere during sintering might be beneficial for enhanced piezoelectric performance.

Sammendrag

Piezoelektriske keramer brukes i mange typer innretninger, og i dag, dominerer blyzirkoniumtitanat (PZT) markedet, på grunn av PZTs overlegne egenskaper. Miljø og helsemessige hensyn gjør det derimot viktig å finne en erstatning for PZT. Kaliumnatriumniobat (KNN) er et bly-fritt piezoelektriske keram, hvor gode piezoelektriske egenskaper er mulig å oppnå ved doping eller teksturering. Dessvere har sintring av KNN har vist seg å være vanskelig, på grunn av forgroving og alkaliefordampning.

Dannelsen av en væskefase bestående av alkaliehydroksider og -karbonater ved lav temperaturer er foreslått å forårsake den anormal kornveksten som er observert i KNN-baserte keramer. En reduserende atmosfære bør virke destabiliserende på disse alkaliehydroksidene og -karbonatene. Dette vil begrense forgrovingen, forbedre fortettingsprosessen og dermed bedre den piezoelektriske ytelsen.

Effekten av sintringsatmosfæren for nominelt støkiometrisk KNN og KNN med 3 mol% nominelt alkalieoverskudd ble undersøkt. Konvensjonell sintring og dilatometri ble gjort i syntetisk luft, nitrogen og en reduserende atmosfære. Karakterisering av de sintrede pelletene ble gjort ved XRD, SEM, infrarødt spektroskopi og piezoelektriske målinger.

Dette arbeidet bekrefter at væskefasen som dannes i KNN keramer, ved lave temperaturer under sintring (eller kalsinering), består av alkaliehydroksider og -karbonater. Den reduserende atmosfæren begrenser graden av forgrovning og fører til høyere tetthet. I støkiometrisk KNN er forgrovningen spesielt begrenset, noe som resulterer i en mikrostruktur bestående av små kubiske kor.

For piezoelektriske målinger måtte prøvene reoksideres, men dette førte ikke til noe betydelig forverring av mikrostrukturen. De piezoelektriske målingene viser at høy tettet og nøyaktig prøvepreparering er viktig. De oppnådde verdiene for normalisert tøyning og piezoelektrisk koeffisient var generelt lave sammenlignet med de verdiene som er rapportert i litteraturen. Polarisasjonskurvene var runde og hadde store lekkasjestrømmer. Disse resultatene indikerer likevel at en reduserende atmosfære under sintring kan være fordelaktig for å bedrede den piezoelektrisk ytelsen.

Contents

Chapter 1

Background

Pierre and Jacques Curie discovered piezoelectricity in 1880, but a real application for this property was only developed a century later. The Curie brothers identified the piezoelectric effect in several crystals, including quartz, topaz and sugar. The piezoelectric behaviour is characterized by a crystal's ability to generate an electrical voltage when subjected to a mechanical stress (Figure 1.1(b)), or by introducing a mechanical strain in the crystal structure when the crystal is subjected to an electrical field (Figure 1.1(c)).[3]

Many devices rely on the piezoelectric effect, such as lighters, medical ultrasound imaging, transformers, accelerometers, sensors, actuators, microphones, phonograph pick-ups, strain gauges, sonar devices and printers, to name a few.[3]

Present piezoelectric devices are dominated by lead zirconate titanate, (PZT or $PbZr_xTi_{x-1}O_3$), due to PZT's superior piezoelectric properties. However, there is a large interest in developing lead free piezoelectric ceramics with comparable properties to PZT. Health and environmental concerns are the main force behind

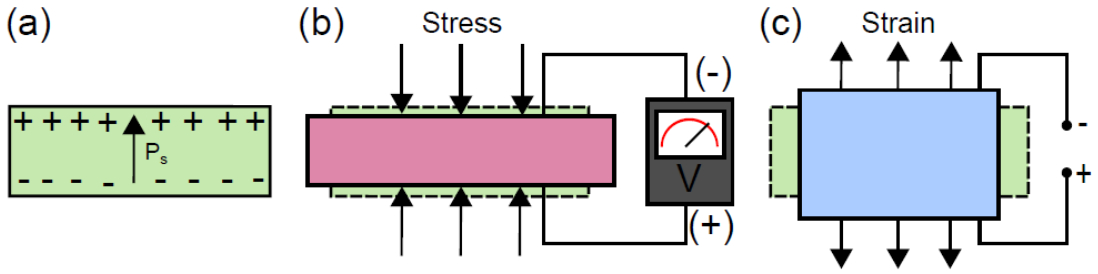

Figure 1.1: *The piezoelectric effect. (a) A crystal with an intrinsic polarization. (b) An applied mechanical stress generates an electrical voltage (direct effect). (c) An applied electric field generates an internal mechanical strain (converse effect). Figure form Haugen[2].*

developing alternatives to lead based piezoelectric ceramics.[4]

In 2003 the European Union issued a directive restricting the use of certain hazardous substances in electrical and electronic equipment, including lead.[5] However, an exception was made for PZT, until a suitable replacement can be found. Other countries, outside the European Union, also have similar regulations in place.[6].

One of the most promising lead free piezoelectric ceramics to replace PZT is potassium sodium niobate ($K_{0.5}Na_{0.5}NbO_3$ or KNN). Excellent piezoelectric properties have been demonstrated for KNN, like high piezoelectric coefficient, or high Curie temperature, which is compatible with the properties of PZT.[7] Still, KNN is challenging to produce, due to high alkali volatility and severe coarsening during conventional sintering and calcination. Therefore have KNNs excellent properties only been achieved using processing techniques not suitable for industrial scale production, like spark plasma sintering[8], hot pressing[9] or two-step sintering[10].

1.1 Aim of Work

The aim of this master thesis is to investigate the sintering process of KNN-based materials. Starting from a sub-micron powder produced by spray pyrolysis, a better understanding of the densification and coarsening mechanisms in KNN is sought.

Several reports of a liquid phase forming during sintering of KNN exist[2, 11, 12, 13, 14], and it is believed that this is the cause of the many challenges when sintering KNN materials for good piezoelectric properties, but especially in relation to the severe coarsening observed.[11, 13] The work of Haugen suggests that this liquid forming at low temperatures (650-700 °C) consists of alkali hydroxides and carbonates, which form by reactions with the humidity and CO_2 in the air.[2] A reducing atmosphere during sintering should destabilize the alkali hydroxides and carbonates, such that the severe coarsening is avoided and a higher density is achieved.

The problem at hand is therefore to see how different sintering atmospheres (air, nitrogen and a reducing atmosphere) affects the properties of nominally stoichiometric KNN and KNN with nominal alkali excess. Special attention will be given to see if sintering in a reducing atmosphere improves the piezoelectric properties compared to a sintering in an oxygen rich atmosphere like air.

To investigate the sintering process of KNN-based material, nominally stoichiometric KNN and KNN with 3 mol% nominal potassium excess and 3 mol% nominal sodium excess was studied. Dilatometry curves were made for all the powders in synthetic air, nitrogen and a reducing atmosphere (2 % H_2 in argon). The powders were conventionally sintered at different temperatures, (700 °C, 1100

°C and 1140 °C) and in different atmospheres (synthetic air, nitrogen and 5 % H_2 in nitrogen). Density measurements were done using Archimedes' method. The sintered pellets were characterized using Scanning electron microscopy (SEM) and X-ray diffraction (XRD). Infrared spectroscopy was used to look for alkali rich secondary phases. The piezoelectric properties of the dense samples were also investigated.

Chapter 2

Introduction

2.1 Sintering

For simple green body geometries, sintering is the most common densifying heat treatment. During the sintering process porosity is removed and particles grow together and bind strongly to the adjacent particles. A mechanism for material transport and an activation energy for the material transport is necessary for sintering to occur. Heat is usually the energy source, and material transport usually occurs through diffusion or viscous flow.[3]

During sintering, initially the particles rearrange themselves by rotation or small movements, Figure 2.1(b). Contact points between particles are established, and bonding occurs in these contact points because material transport is made possible. Secondly the contact between particles grows, particles grow closer together and porosity decreases, Figure 2.1(c). This causes shrinkage of the component, and some grains begin to grow at the expense of others. Finally when the pores are no longer connected, the remaining porosity is removed by vacancy diffusion along the grain boundaries, aided by the movement of grain boundaries and grain growth, Figure 2.1(d).[3]

2.1.1 Mechanisms of Sintering

There are several types of mechanisms to drive sintering, either working alone or together to achieve densification.

In solid-state sintering the driving force is the difference in free energy between the free surface of particles and the points of contact between adjacent particles. The material transport occurs by volume diffusion, i.e. the atoms move by vacancy diffusion through the volume of the material, along a surface or a grain boundary. Volume diffusion results in shrinkage.[3]

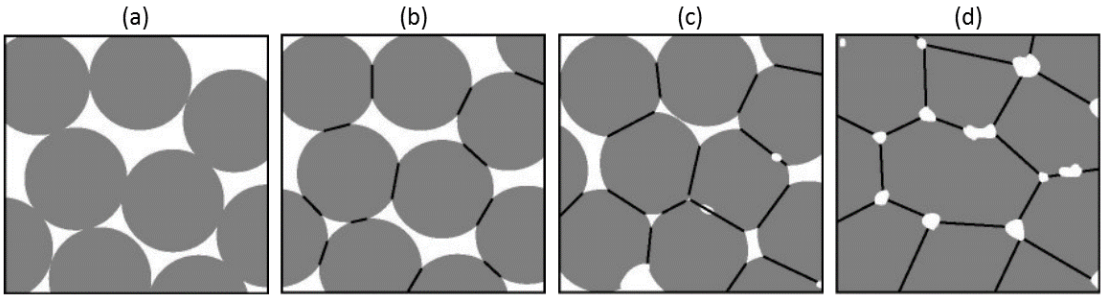

Figure 2.1: *The various stages of sintering. (a) Loose powder with some contact points between particles. (b) Initial stage, some rearrangement of particles occurs and there is bonding between particles at the contact points. (c) Intermediate stage, the contact points starts to grow and the porosity is reduced. (d) Final stage, there are no more open and interconnected pores so the remaining porosity is removed by vacancy diffusion. In the ideal case a density of 100 % will be achieved, but usually some porosity will remain. Figure from Fang[15].*

In liquid-phase sintering a liquid is present at the sintering temperature, and occurs most readily when the liquid completely wets the solid particles. A substantial capillary pressure occurs because of liquid in the narrow channels between the particles. This causes the particles to rearrange in a better packing, and increases the contact pressure between particles and the rate of material transfer.[3] The presence of a liquid phase will in most cases induce faceted grain growth.[15]

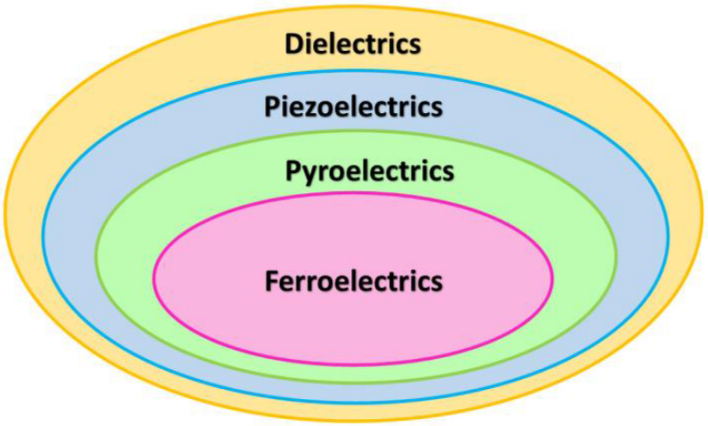

Figure 2.2: *Schematics over the relationship between dielectricity, piezoelectricity, pyroelectricity and ferroelectricity.*

2.2 Piezoelectricity

A dielectric material is an electrical insulator, but can be polarized by an applied electric field. Some dielectric materials respond to an applied electric field by creating a mechanical strain in the material, or a dielectric material can generate an electric polarization in response to an external mechanical stress. The dielectric materials with this kind of properties are termed piezoelectric.[16]

A subgroup of piezoelectric materials also have a spontaneous electrical polarization caused by intrinsic internal strain, resulting in a change in crystal structure to one of lower symmetry. These materials are termed pyroelectric. Among the pyroelectric materials, some are able to reverse the electrical polarization if an external field is applied, these are termed ferroelectric.[16] Figure 2.2 illustrates the relationship between the dielectric subgroups.

The crystals that exhibit piezoelectricity are in general non-centrosymmetric. Of the 32 crystallographic point groups[1], 21 do not possess an inversion symmetry element. One of these 21 point groups has symmetry elements that also exclude piezoelectricity. Therefore only 20 of the point groups can accommodate piezoelectricity.[16] The induced polarization $\boldsymbol{P}$, caused by an external field, is related to the applied stress $\boldsymbol{\sigma}$ by the piezoelectric constant $\boldsymbol{d}$, which is a third-rank tensor.

$$P_i = d_{ijk}\sigma_{jk} \tag{2.1}$$

This relationship is for the direct piezoelectric effect, where an electric polarization

[1] A point group is a group of symmetry elements that leaves one point invariant under these symmetry operations

is created by an applied mechanical stress.[16] For the converse piezoelectric effect, the material responds to an applied electric field by creating internal mechanical strain. The relationship is

$$E_i = d_{ijk}\varepsilon_{jk} \tag{2.2}$$

Where $\boldsymbol{d}$ is the piezoelectric coefficient, $\boldsymbol{\varepsilon}$ is the induced strain and $\boldsymbol{E}$ is the applied electrical field.[16]

Since $\boldsymbol{d}$ is a third-rank tensor, it has 27 components. Intrinsic symmetry *($d_{ijk} = d_{ikj}$)*, reduces these 27 to 18 components. Depending on the Bravais lattice of the crystal, a further reduction based on symmetry is possible.[16]

Discovering the piezoelectric effect has led to a widespread use of piezoelectric ceramics. Today these are used in everything from ultrasonic devices, microphones, phonograph pick-ups, accelerometers, strain gauges and sonar devices.[3]

2.2.1 Ferroelectricity

Pyroelectric crystals have a net electric dipole in each primitive unit cell. In ferroelectric crystals, the spontaneous polarization can be reversed by an applied external electric field, making it possible to align neighbouring domains. The transition from the randomly oriented domains in a paraelectric phase, to an ordered ferroelectric structure occurs at a temperature termed the Curie temperature (T_C) of the material.[16]

The polarization-electric field characteristics of ferroelectrics differ from the linear relationship found in dielectrics. In ferroelectrics, hysteresis occurs due to energy required for domain wall motion. To change the net polarization of a sample, the relative sizes of the various domains need to be altered. This requires domain wall motion between domains having different orientations, which costs energy.[16]

In Figure 2.3 the polarization - electric field hysteresis loop of an ideal ferroelectric is shown. Starting out in the origin, the electric field and the polarization of the material are zero (point O). As the electric field increases the polarization of the material also increases (point O-A). The polarization continues to increase with the applied electrical field until the domain alignment is complete (point B), and the polarization is saturated. P_s refers to the saturation polarization. Further increase of the electric field will not lead to an increase in polarization (point C). If now the external electric field is removed (point D), the material will have some remaining polarization (P_r) termed the remnant polarization. To fully remove the polarization of the material an electric field corresponding to the negative cohesive field (-E_c) must be applied to the material (point F). A further decrease in the electric field will lead to a decrease in polarization, until the negative saturation polarization (-P_s) is reached (point G). Point H indicates the negative

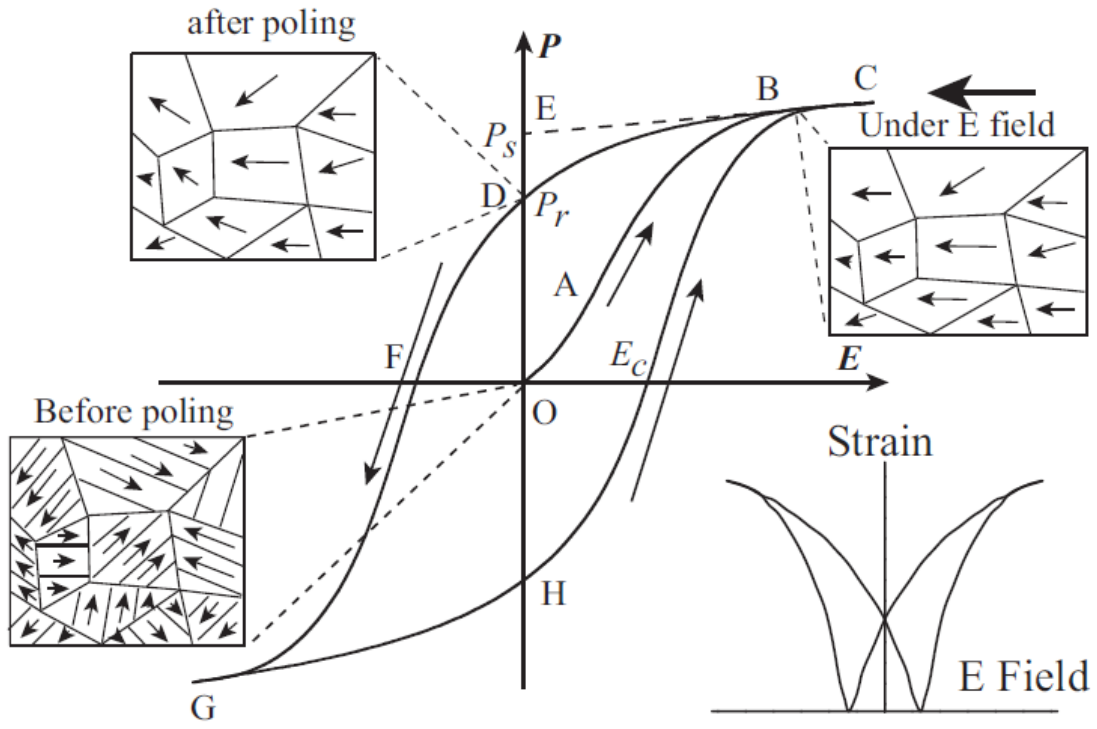

Figure 2.3: *The polarization vs. electric field characteristics of ferroelectrics. The domain structure of the material for some points on the hysteresis loop is indicated. Also included are the strain vs. electric field behaviour of ferroelectrics. Figure from Jin[17].*

remnant polarization of the material, and to again fully remove the polarization of the material, an electric field equal to the coesive field (E_c) of the material must be applied. The hysteresis behaviour can only be removed by heat treating the material.[16]

The strain - electric field hysteresis loop for an ideal ferroelectric is also shown in Figure 2.3. Most ferroelectric materials have ferroelectric domains[2], so when an external electric field is applied, strain is also induced spontaneously in the material. The strain occurs because the electric field lead to switching and movement of domain walls, but also the converse piezoelectric effect contribute to the induced strain.[17]

[2]Ferroelectric domains are areas in a grain which have the polarization of the unit cell ordered in particular direction.[16]

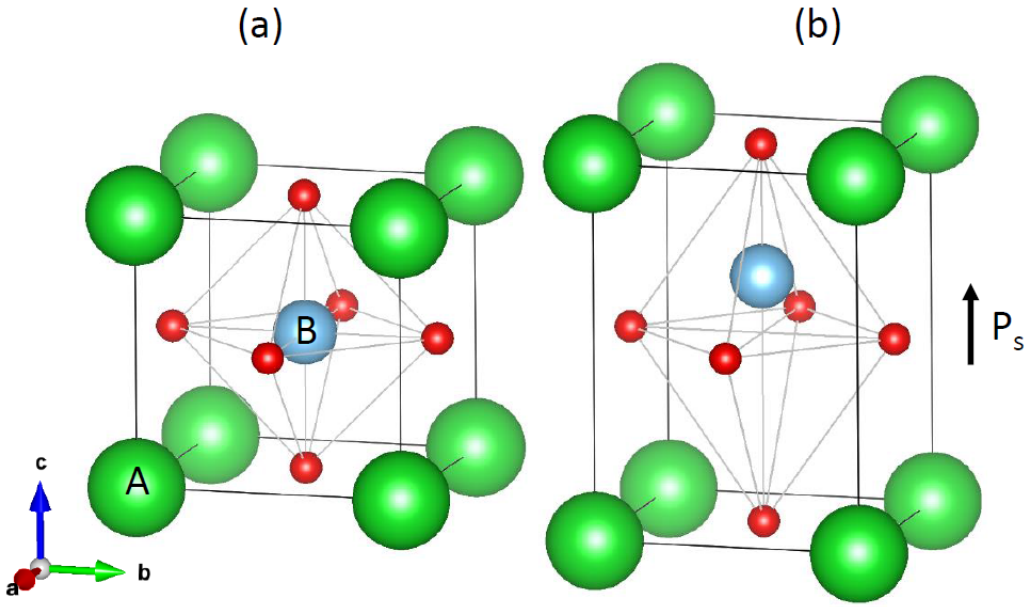

Figure 2.4: *The perovskite structure ABO_3 in (a) paraelectric simple cubic unit cell and (b) ferroelectric tetragonal unit cell where the B-atom is displaced along the [001]-direction. The distortion of the B-atom created a net polarization in the unit cell. The tetragonality and distortion have been exaggerated. Figure made with the software VESTA[18].*

2.3 Piezoelectric materials

The piezoelectric materials used for technical applications are generally polycrystalline ceramics. Single crystals are usually harder to fabricate, and not as suitable for mass production.[6] The crystallites in ceramics are of arbitrary orientation, and the net piezoelectric response from the ceramics cancels. For a net piezoelectric response the symmetry-breaking element, required for overall non-centrosymmetry, has to be externally induced. Ferroelectric materials can be poled which gives the desired symmetry breakage. Therefore only ferroelectric materials can be used as piezoelectric ceramics.[6]

Perovskites

Perovskites are the most common piezoelectric structure, with chemical composition ABO_3. This structure can accommodate all of the 10 polar point groups. The simplest picture of perovskites are a simple cubic unit cell, with the large cations on the corners (A-site), the smaller cations in the body centre (B-site) and oxygen in the face centres (Figure 2.4(a)). The structure can be viewed as a network of

Table 2.1: The properties of lead zirconate titanates

Piezoelectric property	*pure PZT*	*doped PZT*
Curie Temperature, T_c [°C]	400 [7]	250 [7]
Piezoel. coefficient, d_{33} [pC/N]	200 [7]	410 [7]
Dielectric constant, $\varepsilon_{33}^T/\varepsilon_0$	1300 [19]	2300[7]
Piezoel. coupling constant, k_p	0.58 [19]	0.60[7]
Normalized strain, S_{max}/E_{max} [%]		700 [7]

corner-linked oxygen octahedra, where the small cations are filling the octahedral holes and the larger cations are occupying the twelve-coordinated sites.[6]

The perovskite simple cubic unit cell can be distorted in many different ways, often accompanied by tilting of the oxygen octahedra. Distortion of the cubic unit cell into tetragonal, orthorhombic, rhombohedral, monoclinic and triclinic cells are possible.[6] In Figure 2.4(b) a possible distortion of the B-atom along the *c*-axis is shown resulting in a tetragonal unit cell. Most perovskites structures have several phases and change from one crystal system to another with changing temperature. [6]

2.3.1 Lead zirconate titanate - The leading material

Lead zirconate titanates, (PZT or $PbZr_xTi_{x\text{-}1}O_3$), are the most commonly used piezoelectric ceramics today. The extensive use of these materials is due to their excellent piezoelectric properties (see Table 2.1). No other piezoelectric material is a viable alternative for the present technological applications.[7] One of the features of the PZT material systems is the morphotropic phase boundary (MPB)[3].[7] The compositions close to the MPB show the best piezoelectric properties.[4] The piezoelectric properties of the PZT materials can further be enhanced through doping or texturing[4].[4]

However, the high lead-content, more than 60 wt%, in PZT is an increasing concern, in both environmental and health perspectives. PZT is widely used in consumer products such as cars, sound generators and various kinds of smart systems.[4] Although it is believed that PZT itself is not toxic during use, the recycling and disposal of devices containing PZT remains a problem.[4] Fabrication of devices containing lead also poses a health risk. PbO evaporates to the atmosphere during calcination and sintering, and lead also escapes under machining of PZT-components.[6]

[3]Morphotropic phase boundary refers to the phase transition between a tetragonal and rhombohedral phase in ferroelectrics, caused by a variation in chemical composition or an applied mechanical pressure[4]

[4]Texturing refers to a non-random spatial distribution of grains[20]

Table 2.2: The properties of potassium sodium niobates

Piezoelectric property	*KNN*	*Hot pressed*	*textured*	*doped* (Li,Ta)
Curie Temperature, T_c [°C]	413 [7]		253 [7]	
Piezo.coefficient, d_{33} [pC/N]	80-120[22]	160 [9]	416 [7]	206 [14]
Dielectric constant, $\varepsilon_{33}^T/\varepsilon_0$	407 [23]	400 [9]	1570 [7]	690 [24]
Piezo. coupling, k_p	0.305 [23]	0.45 [9]	0.61 [7]	0.38 [14]
S_{max}/E_{max} [%]			700 [7]	400 [7]
Conductivity, σ [pS/cm]	18.2 [25]	1 [9]		

There is no safe exposure dosage of lead, since lead has no natural function in the human body.[21] Lead poisoning will effect almost all of the major organ systems in the body, for instance the central nerve system or the reproduction system, and may cause irreversible damage.[21]

The present state of the art PZT materials suggest that the development of new lead-free piezoelectric materials should be done for each specific application. Currently, there are no lead-free material systems capable to cover all of the present applications.[6] In the search for new materials systems with good electromechanical properties, the presence of a morphotropic phase boundary is sought, since the unit cell of these compositions have more possibilities for distortions.[4] The search is also driven by the desire to find piezoelectric ceramics for high temperature applications, where the current lead-based materials are unsuitable.[4] The low density of some lead-free piezoelectrics is believed to have an advantage in underwater transducers and medical imaging, due to lower acoustical impedance.[4] The prospect of possibly being able to implant sensors and actuators directly into the human body makes the search for biocompatible piezoelectrics even more attractive.[4]

2.3.2 Potassium sodium niobate - A new candidate?

Potassium sodium niobate (KNN or $K_xNa_{1-x}NbO_3$) is one of the most researched and promising replacements for lead-based piezoelectrics. Excellent piezoelectric properties near the morphotropic phase boundary (around x=0.5), but also the biocompatibility of KNN make it a promising material system.[4] KNN is a solid solution between the two perovskites potassium niobate and sodium niobate, both are orthorhombic at room temperature.[6] $KNbO_3$ is ferroelectric and single crystals are used in technological applications, exploiting the non-linear optical properties of potassium niobate.[6] On the other hand, $NaNbO_3$ is antiferroelectric.[6] The KNN material system has many morphotropic phase boundaries, one of which is between two orthorhombic phases near the 50/50-composition.[4] KNN gener-

ally refers to the $K_xNa_{1-x}NbO_3$-material system, but the composition with x=0.5 will be referred to as stoichiometric KNN, unless otherwise specified. Even though KNN materials show good piezoelectric properties compatible with PZT (Table 2.2), there are still some challenges to overcome before KNN can replace PZT.

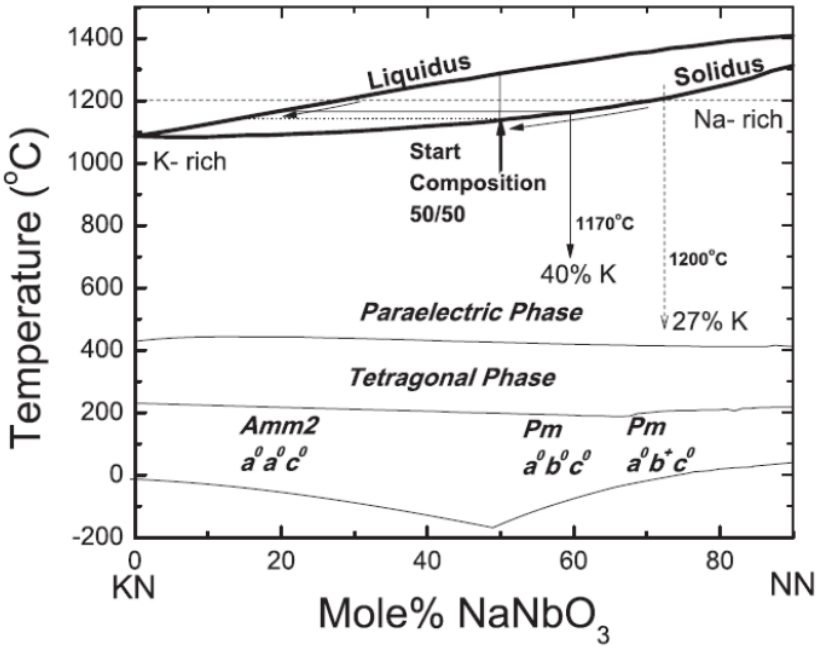

Figure 2.5: *The phase diagram of the $KNbO_3$-$NaNbO_3$ solid solution. Figure from Zang[31].*

2.4 Sintering of potassium sodium niobate

The excellent piezoelectric properties of KNN has only been demonstrated by spark plasma sintering[8], hot pressing[9] or two step sintering[10]. However, none of these techniques are commercially suitable for industrial scale production. Doping or texturing has also been demonstrated to improve the piezoelectric properties although sintering is still challenging.[7, 14, 26] Therefore, great efforts have been done to gain an understanding of the mechanisms at work during the sintering process of KNN.

2.4.1 Densification of stoichiometric KNN

Conventional sintering of KNN based materials has proven to be challenging, through extensive research regarding the densification process of KNN. Several works report a narrow temperature window where sintering occurs[10, 6, 27] and a deviation from these temperatures leads to deteriorated piezoelectric performance.[28, 29, 30]

Sintering normally occurs close to the solid-liquid phase transition in the phase diagram (Figure 2.5), above 1000 °C[32], which can lead to compositional segrega-

tion and abnormal grain growth.[27] The solidus line in Figure 2.5 is approximately at 1150 °C for the stoichiometric KNN composition.

There is some disagreement on what the optimal sintering temperature for KNN materials are. Malic *et al.* reports that the optimal sintering conditions are within the 1100-1125 °C temperature window.[33] However, Li *et al.* reported that optimization of the density was achieved at 1080 °C, but that sintering at 1060 °C resulted in the best piezoelectric properties.[34] Zang *et al.* reported that sintering in the range 1170-1200 °C lead to a high degree of secondary phases, melting and significant weight loss during sintering.[31] From the phase diagram of KNN (Figure 2.5) this temperature is clearly above the solidus line.

In addition to the sintering temperature, the heating and cooling rates also affect the sintering process. The mechanisms for coarsening generally have a lower activation energy than the mechanisms for densification.[35] An increase in the heating rate should therefore improve the densification. Du *et al.* and Liu *et al.* reported that a heating rate of 5 °C/min optimized the densification process as well as the piezoelectric properties in KNN[36] and Li-doped KNN[37]. Studies of the effect of the heating rate in $KNbO_3$ showed that 2 °C/min resulted in a higher densification compared to faster heating rates.[13] This is supported by the results of Haugen which also found a heating rate of 2 °C/min to be optimal, and that there is practically no difference in the sintering behaviour in nominally stoichiometric KNN sintered in air, nitrogen and pure oxygen.[2]

There are not a lot of studies on the cooling rate, but Zang *et al.* reported an inhomogeneous distribution of potassium and sodium rich phases and deteriorated piezoelectric response in quenched KNN samples.[31] A slow cooling rate will enable the system to establish compositional equilibrium. This will give a homogeneous potassium and sodium distribution, which is believed to be beneficial for enhanced piezoelectric properties.[31]

Highly volatile alkali species and evaporation of alkali during calcination and sintering makes stoichiometric control difficult in air.[23, 25, 38, 39] Flückiger *et al.* reported that potassium evaporation in $KNbO_3$ started at temperatures as low as 850 °C[40], but that the decomposition can be neglected up to 950 °C.[41] The amount of evaporation is affected by the atmosphere in which the sintering occurs, which again determines the stoichiometry deviation.[42] The evaporation of alkali species also effect the microstructure and the electrical properties. [38]

2.4.2 Stoichiometry changes

Alkali evaporation in nominally stoichiometric KNN will lead to a non-stoichiometric KNN compound, and the alteration of the stoichiometry may lead to drastic changes in densification behaviour. Haugen suggested that the sintering behaviour

of nominally A-site excess KNN also can explain the behaviour observed in nominally stoichiometric KNN.[2]

Acker *et al.* reported that $KNbO_3$ with nominal potassium excess starts to sinter at temperatures as low as 740 °C, but the densification rate is low and the shrinkage stops around 950 °C.[13] Excess niobium can occur in nominally stoichiometric KNN as a consequence of alkali evaporation. Haugen found that the sintering process in nominal B-site excess KNN was not significantly different from that of nominally stoichiometric KNN.[2] However, adding 3 mol% of excess alkali to nominally stoichiometric KNN resulted in a large densification at low temperatures (650-700 °C), and a reduction in the densification at higher temperatures.[2] Powders with less excess (1-2 mol%) did not show the same drastic densification at low temperatures.[2]

Acker *et al.* found that nominally stoichiometric KNN densifies faster and better than nominally A- or B-site excess KNN with respect to shrinkage and shirking rate.[12] Also, the non-stoichiometry will shift the temperature for the maximal shrinkage. A-site excess shifts the maximal shrinkage to lower temperatures and B-site excess shifts towards higher temperatures, compared to the stoichiometric composition.[12, 13]

Acker *et al.* also observed that sintering nominally A-site excess KNN in an atmosphere with a high alkali vapour pressure resulted in more spherical and smaller grains compared to conventional sintering.[42] The high alkaline vapour pressure was however not sufficient to enhance the sintering significantly.[42]

2.4.3 Coarsening and cubic grain formation

One of the main problems limiting the use of KNN is that the current reported grain sizes are to large for today's demand of piezoceramics, or depend on a processing technique that is not suitable for industrial scale production.[23] Limiting the coarsening still remains a challenge.

Haugen found that the average particle size increased with increasing calcination temperature.[2] Powders with 3 mol % nominal alkali excess showed dramatic coarsening and cubic grain formation when calcination was done at 800 °C. The same coarsening was not as severe in nominally stoichiometric KNN and KNN with 3 mol% nominal niobium excess.[2] The coarsening of excess alkali powders could be avoided by lowering the calcination temperature to 400 °C, which improved the green body densities.[2] These results are in agreement with the work of Bomlai *et al.*[11]

Cubic grains being formed during conventional sintering of KNN based materials at sufficiently high temperatures have been reported.[12] Cubic grains are highly undesirable, since they often have low-energy (low curvature) grain boundaries which will remove the driving force for densification and also the associated

the kinetics by reducing grain boundary diffusion.[12]

Also, abnormal grain growth seams to be difficult to avoid in KNN based materials.[43] The abnormal grain growth is ascribed to the difference in grain boundary mobility, caused by the presence of a liquid phase or impurities at the grain boundaries.[35, 44]. Fisher *et al.* explained this in terms of the 2D nucleation-control theory of grain growth.[45] Atomically ordered (faceted) grain boundaries are believed to be the cause of the abnormal grain growth, while normal grain growth occur on disordered (rough) grain boundaries.[45] Oxygen vacancies, induced by evaporation of alkali in inert and reducing atmospheres, will change the grain boundary from faceted to rough.[45]

2.4.4 Liquid phase formation

There have been several reports that a liquid forms in KNN with alkali excess. Acker *et al.* observed supercooled liquid wetting the grain boundaries in KNN with 2 mol% nominal A-site excess sintered at 970 °C.[12] Acker *et al.* also investigated the sintering behaviour of $KNbO_3$, and found that the excess potassium powders showed a double peak in the shrinking rate, and ascribed this to a formation of a liquid at 845 °C.[13] Bomlai *et al.* also found evidence of a liquid forming during calcination at 800 °C of KNN with excess alkali carbonates.[11] The coarsening of the powder and necking between cubic particles during calcination, suggested the presence of a liquid.[11] The liquid phase forming at low temperatures is believed to cause the cubic grain formation observed in KNN based materials, and also the severe coarsening.[2, 11, 14]

The work of Chowdhury *et al.* found that KNN powders react with the CO_2 in the air during storage, forming bicarbonates or weakly bound carbonate species from the adsorption of CO_2.[39] Haugen suggested the following possible reactions of KNN with alkali excess with the humidity and CO_2 in the air:

$$K_2O(s) + CO_2(g) = K_2CO_3(s, l) \tag{2.3}$$

$$K_2O(s) + H_2O(g) = KOH(s, l) \tag{2.4}$$

The reactions of Na_2O will be in the same fashion.[2] Due to this reactivity there should be alkali carbonates and hydroxides on the KNN particle surface when alkali excess powders are exposed to air. Haugen proposed these alkali carbonates and hydroxides to be the liquid phase that forms during heat treatment of KNN with alkali excess.[2] Haugen argued that liquid phases are known to induce faceted grain growth, which could explain the cubic grain formation in the calcined powders, well below the solidus line for KNN.[2] Due to this reactivity with air, Haugen suggested that there also should be a small amount of this liquid when heat treating nominally stoichiometric KNN.[2] This liquid could be responsible for

cubic grain formation and coarsening in nominally stoichiometric KNN as well.[2] The possible reactions for the formation of alkali hydroxides and carbonates in stoichiometric KNN in air (exemplified with $KNbO_3$ instead of KNN) are:

$$4KNbO_3(s) + CO_2(g) = K_2CO_3(s) + K_2Nb_4O_{11}(s) \quad (2.5)$$

$$4KNbO_3(s) + H_2O(g) = 2KOH(s) + K_2Nb_4O_{11}(s) \quad (2.6)$$

2.4.5 Reducing conditions during sintering

Kobayashi *et al.* studied the effects of a reducing sintering atmosphere in KNN-LiF ceramics, and found that the grains were larger and rounder-shaped than air sintered KNN ceramics.[25] A higher density was also achieved.[25] The piezoelectric properties were not affected by the reducing atmosphere, and the resistivity was improved.[25] Shimizu *et al.* studied the effect of a reducing atmosphere on $NaNbO_3$ ceramics. A significantly higher density was found for reduced sintered sodium niobate.[38] Fisher *et al.* found that sintering nominally stoichiometric KNN in hydrogen improved the densification.[46]

Several studies have reported small traces of a niobium-rich phase after sintering or calcination in nitrogen[2] or powders with Nb excess[2, 12, 13], corresponding to alkali evaporation. Haugen suggested that the following reaction occur at high temperature:

$$4KNbO_3(s) = 2K(g) + \tfrac{1}{2}O_2(g) + K_2Nb_4O_{11}(s) \quad (2.7)$$

The observed $K_2Nb_4O_{11}$ in stoichiometric KNN by Haugen[2] indicates that the reaction in equation 2.7 does occur.

The work of Haugen indicates that the evaporation of alkali oxide from the surface of the KNN particles only occurs at high temperature. That means that the reaction in equation 2.8 occurs during sintering, and not during heating.[2]

$$K_2O(s) = 2K(s) + \tfrac{1}{2}O_2(g) \quad (2.8)$$

Sintering in a reducing (or inert) atmosphere should increase the evaporation of alkali in equation 2.7 and 2.8.[2] It should also destabilize the alkali carbonates and hydroxides, even at low temperatures[2]:

$$K_2CO_3(s,l) \longrightarrow 2K(g) + \tfrac{1}{2}O_2(g) + CO_2(g) \quad (2.9)$$

$$KOH(s,l) \longrightarrow 2K(g) + \tfrac{1}{2}O_2(g) + H_2O(g) \quad (2.10)$$

Haugen therefore concluded that the increased density and improved microstructure resulting from sintering in a reducing atmosphere demonstrated by Kobayashi *et al.*[25] and Fisher *et al.*[46] was due to evaporation of the alkali hydroxides and carbonates.[2]

2.4.6 Piezoelectric performance

The piezoelectric performance of a material is not only affected by the density, but also by the composition or changes in stoichiometry and the grain sizes. Therefore optimization of the densification process is not enough to produce good piezoelectric components; stoichiometric control is also important.[14]

Fang *et al.* observed that the polarization hysteresis loops were rounder and had large leakage currents when the density was low.[10, 23] Shimizu *et al.* observed better loops and larger polarization in sodium niobates sintered in reducing conditions compared to air-sintered samples.[38]

Wu *et al.* investigated the influence of the K/Na ratio on physical properties of $K_xNa_{1-x}NbO_3$ materials.[47] This study found that the piezoelectric properties of KNN, like the piezoelectric coefficient (d_{33}), was practically independent of the K/Na ratio, in the composition range x=0.40-0.60.[47] However, the microstructure was found to be more homogeneous and consisted of large uniformly distributed faceted grains in the compositional range x=0.45-0.60.[47] Wu *et al.* suggested that the good piezoelectric properties in this compositional range were more dependent on the microstructure than on the effect of the morphotropic phase transition (near x=0.50) on the lattice parameters.[47]

Chapter 3

Experimental

3.1 Materials

The stoichiometric KNN powder ($K_{0.5}Na_{0.5}NbO_3$) studied in this master thesis was produced by spray pyrolysis, from CerPoTech AS.[48] Using the stoichiometric KNN powder, non-stoichiometric powders with respectively 3 mol% K excess and 3 mol% Na excess were made. The powders used in this master thesis were prepared and analysed by Bakken[1]. The excess alkali powders were prepared by mixing stoichiometric KNN with potassium and sodium nitrates. The powders were calcined at 400 °C and then ball milled for 18 h.[1]

3.2 Sintering

3.2.1 Conventional sintering

The green body pellets was prepared using 5 mmØ and 10 mmØ pressing tools and a pressure of 75 MPa, with stearic acid as lubricant. Pellets of all three KNN powders were sintered at 700 °C, 1100 °C, 1140 °C in a tube-furnace (ETF 15 Tube furnace, Entech, Ängelholm, Sweden). The heating and cooling rate was 200 °C/h, and the sintering temperature was held for 2 hours. At each temperature pellets were sintered in both synthetic air, nitrogen and a 5 % H_2 in nitrogen.

3.2.2 Dilatometry

The green body pellets were prepared by using a 5 mmØ pressing tool and a pressure of 75 MPa, with stearic acid as lubricant. Dilatometry (DIL 402E, Netzsch, Selb, Germany) was used to study the sintering process for the nominally stoichiometric KNN and KNN with nominal alkali excess powders in synthetic air,

nitrogen and 2 % H_2 in argon. A maximal temperature of 1100 °C and a heating rate of 2 °C/min was used. The dilatometry measurements in air and nitrogen were conducted by Bakken.[1]

3.3 Characterization of sintered pellets

Investigation of the microstructure, phase composition and electrical properties was done only for the conventionally sintered samples. Density was measured for both the conventionally sintered samples and the samples from the dilatometry measurements.

3.3.1 Density

The density of the sintered pellets were measured using Archimedes method in isopropyl alcohol, according to the ISO standard 5017. The density was averaged over three separate measurements on two samples sintered at equal conditions. The densities of the green bodies were calculated using a scale and a calliper.

3.3.2 Microstructure

Microstructure and grain sizes were studied using SEM (S-3400N, Hitachi, Japan). Microstructure analysis was done by investigating a fracture surface of each pellet, covered with a thin layer of gold by a sputter coater (S150B, Edwards, Crawley, England) to ensure conductivity. The reported grain sizes were determined from the obtained SEM pictures by manual inspection.

3.3.3 Phase composition

Phase composition was determined using XRD (D8 Focus, Bruker AXS, Karlsruhe, Germany). Diffractograms, of crushed pellets, were recorded with a step size of 0.0143, a scan time of 0.5 seconds and a slit size of 1.0 mm. This instrument used Cu-K_α radiation and linear detectors. Using the TOPAS-software, refinement of the lattice parameters was done using Pauli fitting.

Possible presence of secondary phases was investigated using infrared spectroscopy. Pulverized samples were diluted by dried KBr, mixed in a mortar and pressed into a thin 13 mmØ pellet by use of a uniaxial press. The applied pressure was varied in accordance with the concentration of the sample in relation to the KBr (see Table 3.1). The pellets were then studied in a FT-IR spectrometer (VERTEX 80, Bruker Optik, Ettlingen, Germany), in the transmission mode with a pure KBr-pellet as the background.

Table 3.1: Relationship between the sample concentration and the applied uniaxial pressure for preparing samples for infrared spectroscopy measurements.

Concentration [wt%]	**KBr [g]**	**Sample [g]**	**Pressure [MPa]**
0	0.200	0	590
2	0.200	0.004	590
5	0.200	0.010	520
10	0.200	0.020	520
15	0.200	0.030	480
20	0.200	0.040	440
23	0.200	0.046	295

3.3.4 Electrical properties

Samples for electrical measurements were prepared by removing at least 0.1 μm of the top and bottom surface by grinding. Parallel surfaces were achieved through grinding, with a final grit size of 10 μm. Electrodes were created by spraying Ag on top and bottom surfaces and then curing for 12 h at 200 °C, or by sputtering the sample with gold for 15 minuets on each side using a sputter coater (S150B, Edwards, Crawley, England).

The conductivity of the samples was measured by using a Novocontrol Alpha-A impedance analyzer (Hundsangen, Germany). The AC conductivity was measured as a function of frequency in the range 10^{-2}-10^{7} Hz by applying an AC voltage of 1 Vrms.

The samples sintered in nitrogen and a reducing atmosphere were reoxidized before the piezoelectric measurements. The reoxidation was achieved by heating the samples to 1000 °C and holding this temperature for 1 hour in air, with a heating and cooling rate of 200 °C/h.

A piezoelectric testing system (TF Analyzer 2000, aixACCT Systems GmbH, Aachen, Germany) was used to investigate strain and polarization behaviour of the samples in relation to an applied electric field. To avoid arching, the samples were immersed in silicone fluid, and a triangular waveform with frequency 0.25 Hz was applied. Bipolar pulses were applied with stepwise increasing amplitude to investigate the polarization and strain loops. Unipolar pulses with stepwise decreasing amplitude were applied to record the electric field-induced strain and the corresponding normalized strain S_{max}/E_{max}. At each amplitude the pulses were applied several times to stabilize the response (3 times for the bipolar pulses and 10-15 times for the unipolar). This treatment left the samples in a poled state afterwards.

The direct piezoelectric longitudinal response was measured by the use of a d_{33}-

meter (90-2030, APC Products Inc, Mackeyville, PA, USA). The reported values are averaged over 5 separate measurements.

Chapter 4

Results

4.1 Densification

The densities of the conventionally sintered samples are shown in Table 4.1, and in Figure 4.1. The densities do not improve significantly from the green body densities when heat treated at 700 °C, independent of the atmosphere and stoichiometry of the powder. The apparently higher densities of the samples sintered in a reducing atmosphere (5 % H_2 in nitrogen) can be ascribed to the uncertainty of the measurements, (Table 4.1).

Figure 4.1 show the densities of the samples sintered at high temperature. The highest observed densities were found in nominally stoichiometric KNN sintered in nitrogen at 1100 °C (90 %) and 1140 °C (92 %) and the sample sintered in a reducing atmosphere at 1140 °C (93 %).

The densities of KNN with nominal potassium and sodium excess behave similarly with increasing temperature (Figure 4.1). At 1100 °C the samples sintered in a reducing atmosphere shows the highest densities. At 1140 °C the densities are about the same, namely just below 90 %, independent of sintering atmosphere for both powder stoichiometries. Generally, sintering in air results in low density independently of powder stoichiometry, but the difference is largest for

Table 4.1: Green body density and the densities of the KNN samples heat treated at 700 °C in different atmospheres.

Powder sample	*Green body density [%]*	*Density after heat treatment [%]*		
		Air	Nitrogen	Red.atm.
KNN	45 ± 4.4	47 ± 0.2	46 ± 1.2	48 ± 2.5
KNN+K	46 ± 2.8	47 ± 1.1	50 ± 1.4	53 ± 3.2
KNN+Na	46 ± 2.3	47 ± 0.9	48 ± 1.0	53 ± 2.8

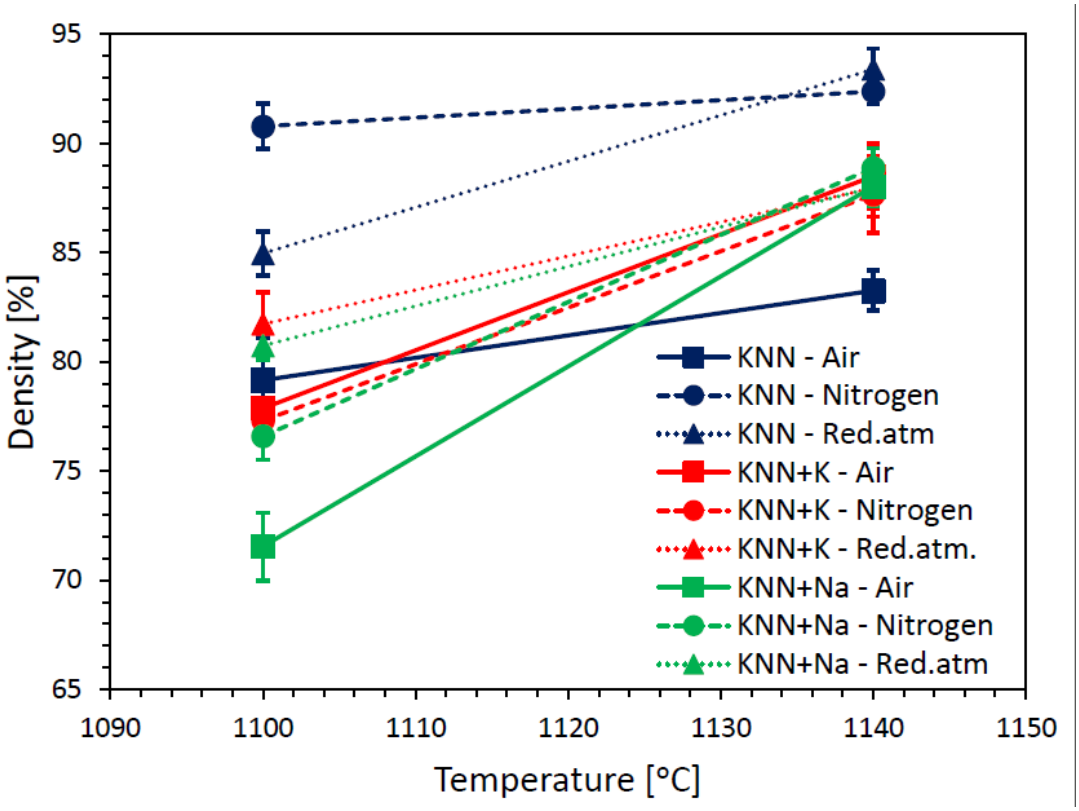

Figure 4.1: *The increase in density with temperature of nominally stoichiometric KNN, KNN with 3 mol% nominal potassium excess and KNN with 3 mol% nominal sodium excess sintered in air, nitrogen and a reducing atmosphere (5 % H_2 in nitrogen). Sintering in air generally results in low densities, while sintering in a reducing atmosphere gives high densities.*

nominally stoichiometric KNN.

The density of nominally stoichiometry KNN sintered in a reducing atmosphere (5 % H_2 in nitrogen) was also measured before and after the reoxidizing treatment. The density increases from 93 % to 95 % during the reoxidation.

The sintering process was studied by dilatometry measurements. Figure 4.2-4.4 shows the linear shrinkage and shrinking rate of nominally stoichiometric KNN, KNN with nominal potassium excess and nominal sodium excess, all sintered in air, nitrogen and a reducing atmosphere (2 % H_2 in argon).

The linear shrinkage in nominally stoichiometric KNN (Figure 4.2(a)) seems to be more or less the same for the different sintering atmospheres, but the curve

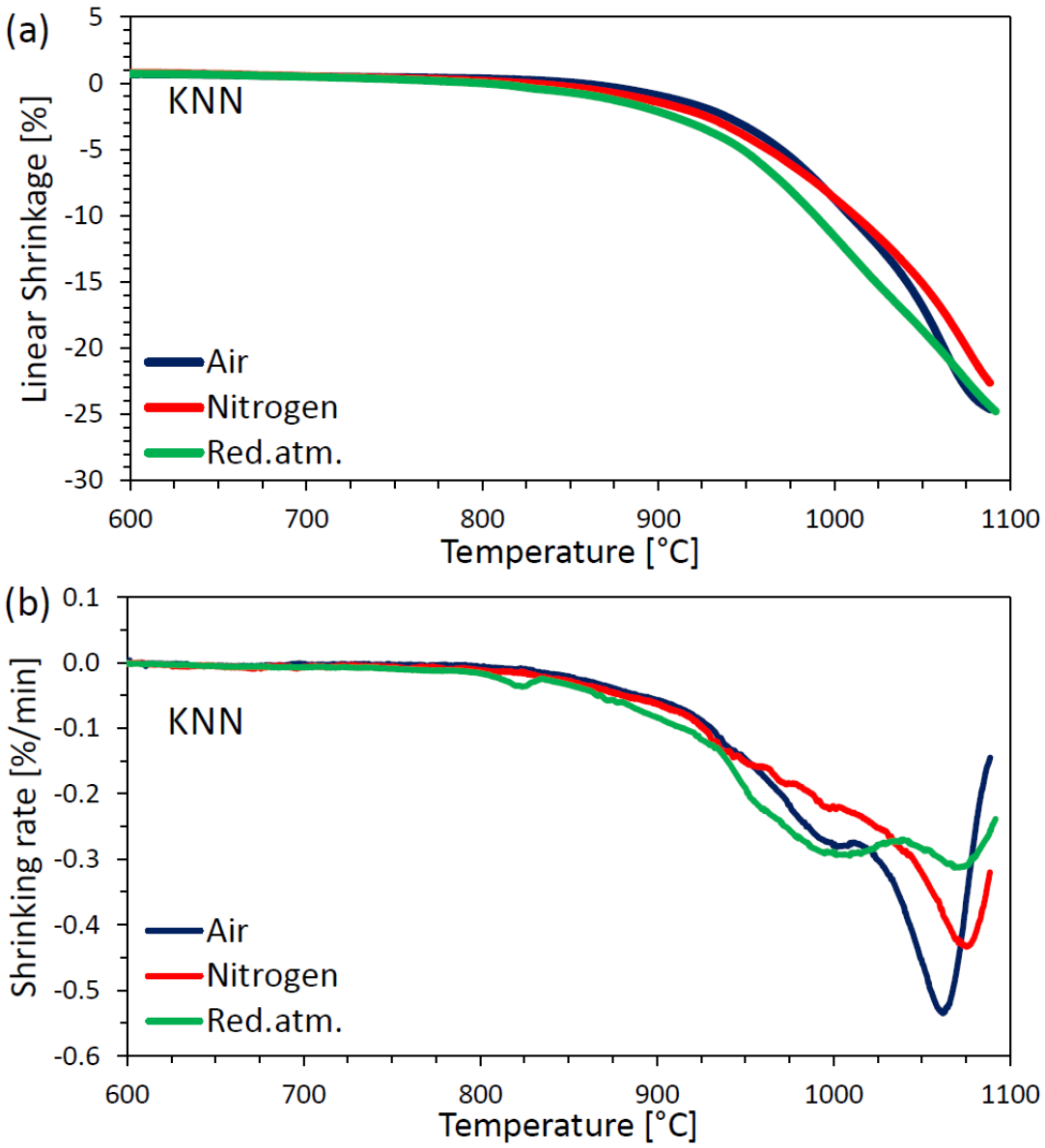

Figure 4.2: *Dilatometry curves for nominally stoichiometric KNN sintered in air, nitrogen and a reducing atmosphere (2 % H_2 in argon). (a) Linear shrinkage as a function of temperature. (b) Shrinking rate as a function of temperature. A wider temperature range for densification can be seen for the reducing atmosphere.*

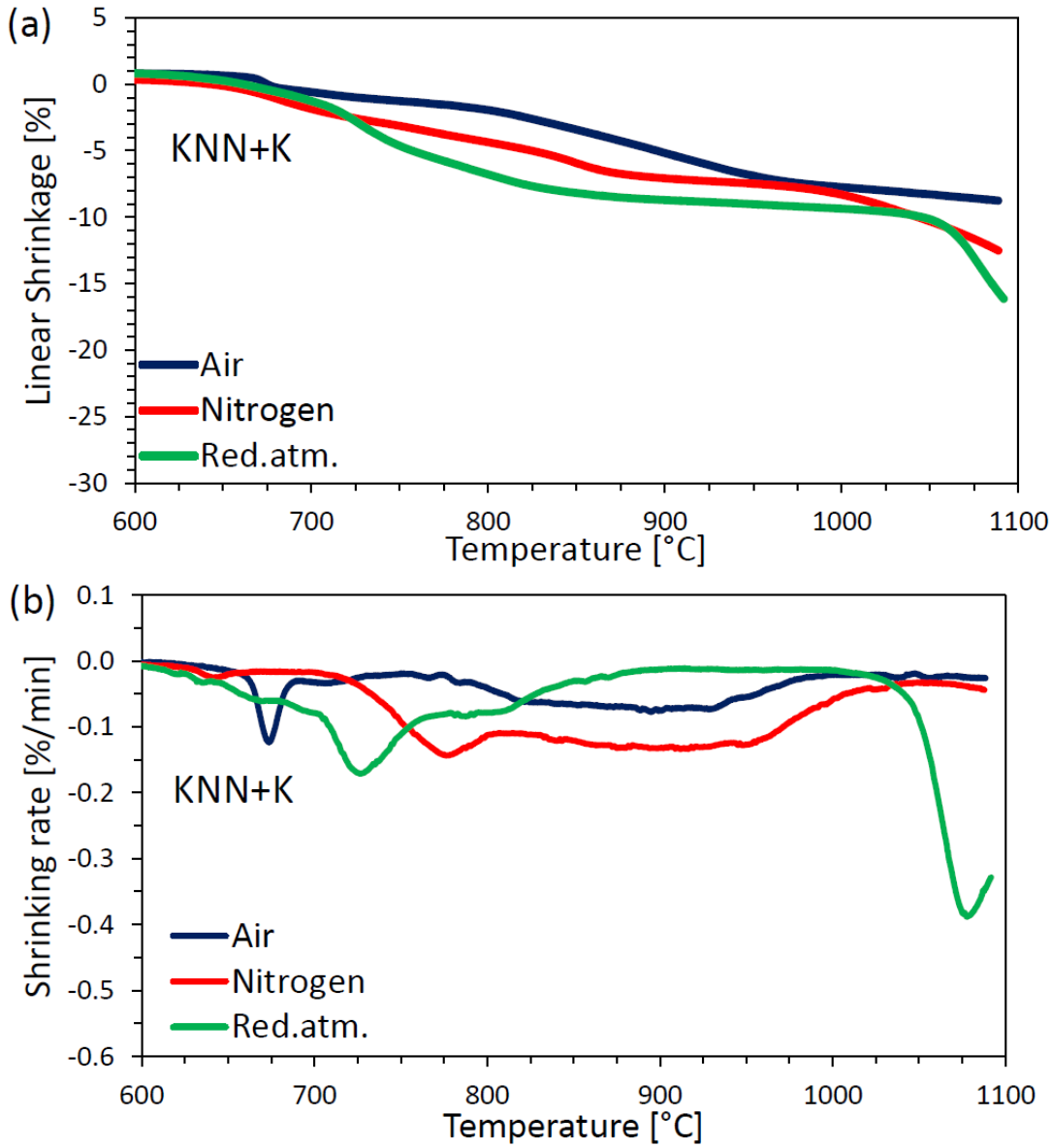

Figure 4.3: *Dilatometry curves for KNN with 3 mol% nominal potassium excess sintered in air, nitrogen and a reducing atmosphere (2 % H_2 in argon). (a) Linear shrinkage as a function of temperature. (b) Shrinking rate as a function of temperature. A liquid forming at low temperatures reduce the driving force for sintering at higher temperatures.*

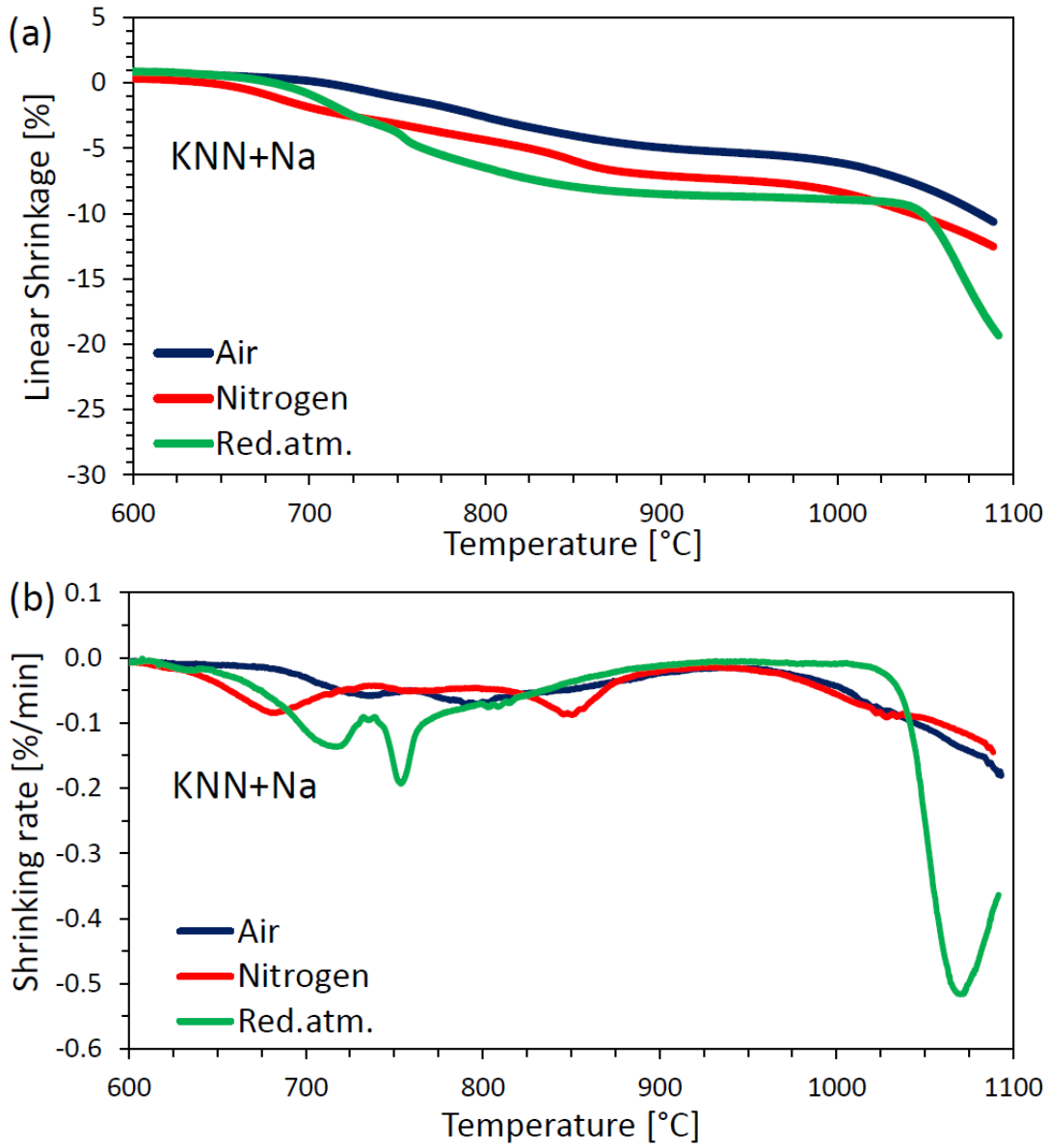

Figure 4.4: *Dilatometry curves for KNN with 3 mol% nominal sodium excess sintered in air, nitrogen and a reducing atmosphere (2 % H_2 in argon). (a) Linear shrinkage as a function of temperature. (b) Shrinking rate as a function of temperature. A liquid forming at low temperatures reduce the driving force for sintering at higher temperatures.*

of the sample sintered in a reducing atmosphere starts to sinter at a lower temperature than in air or nitrogen. However, the shrinking rates (Figure 4.2(b)) differ significantly. In a reducing atmosphere, there is a small increase in the shrinking rate at 825 °C, and after this the shrinking rate steadily increase. The maximal shrinking rate is lower for a reducing atmosphere in nominally stoichiometric KNN compared to air and nitrogen, but the temperature range for the shrinkage is wider. The density of the nominally stoichiometric KNN sample sintered in the reducing atmosphere was measured afterwards to 94 %.

Adding excess alkali to the nominally stoichiometric KNN powder drastically changes the sintering behaviour. KNN with nominal potassium excess (Figure 4.3) and KNN with nominal sodium excess (Figure 4.4) shows the same kind of densification behaviour in their dilatometry curves. In Figure 4.3(b) there is a small increase in the shrinking rate in KNN with nominal potassium excess at lower temperature in nitrogen (at 640 °C) and in the reducing atmosphere (at 635 °C). However, a large and sharp increase in the shrinking rate is observed at 675 °C in air, 780 °C in nitrogen and 725 °C in a reducing atmosphere. After the initial increase the shrinking rate, further shrinkage seams limited. This indicating that the initial shrinkage removes the driving force for further densification. Only for the reducing atmosphere does the shrinking rate increase significantly again when the temperature reaches 1040 °C. The density of the KNN with nominal potassium excess sample sintered in the reducing atmosphere was measured afterwards to be 76 %.

The same trends in the dilatometry curve of KNN with nominal potassium excess (Figure 4.3), can be found in KNN with nominal sodium excess (Figure 4.4), only not as pronounced. Also in KNN with nominal sodium excess is there a small increase in the shrinking rate (Figure 4.4(b)) at low temperatures in nitrogen (at 625 °C) and in the reducing atmosphere (at 630 °C), but the increase is not as pronounced as in the excess potassium curves (Figure 4.3(b)).

The sharp increase in the shrinking rate observed in KNN with nominal potassium excess (Figure 4.3(b)) is not observed in KNN with nominal sodium excess (Figure 4.4(b)). There is however a slight increase, but in the dilatometry curve in air and nitrogen this is wider and with a lower amplitude. A peak in shrinking rate is observed at 730 °C in air. In nitrogen and the reducing atmosphere, there is a double peak in the shrinking rate. These occur for nitrogen at 685 °C and again at 850 °C. The peaks in the reducing atmosphere curve are much sharper and closer together, and occur at 715 °C and again at 755 °C.

As for KNN with excess potassium, after the initial increase the shrinking rate for excess sodium, further shrinkage seams limited. This indicating that the initial shrinkage removes the driving force for further densification. Only for the reducing atmosphere does the shrinking rate increase significantly again when the

temperature reaches 1030 °C. The density of the KNN with nominal sodium excess sample sintered in the reducing atmosphere was measured afterwards to be 76 %.

4.2 Microstructure

Fracture surfaces of nominally stoichiometric KNN (Figure 4.5), KNN with nominal potassium excess (Figure 4.6) and KNN with nominal sodium excess (Figure 4.7) were investigated in a scanning electron microscope. At 700 °C (Figure 4.5(a)-(c), 4.6(a)-(c) and 4.5(a)-(c)) the grains are all small (< 1 μm) and spherical. No notable difference can be found between the different stoichiometries and atmospheres.

Formation of cubic grains and severe coarsening is evident in nominally stoichiometric KNN sintered in air and nitrogen as the temperature increase to 1100 °C and 1140 °C (Figure 4.5(d)-(e) and (g)-(h)). However, the microstructure of the samples sintered in a reducing atmosphere at high temperature (Figure 4.5(f) and (i)) are fundamentally different. Some small cubic grains can be observed. This fundamental difference in microstructure between the samples sintered in air

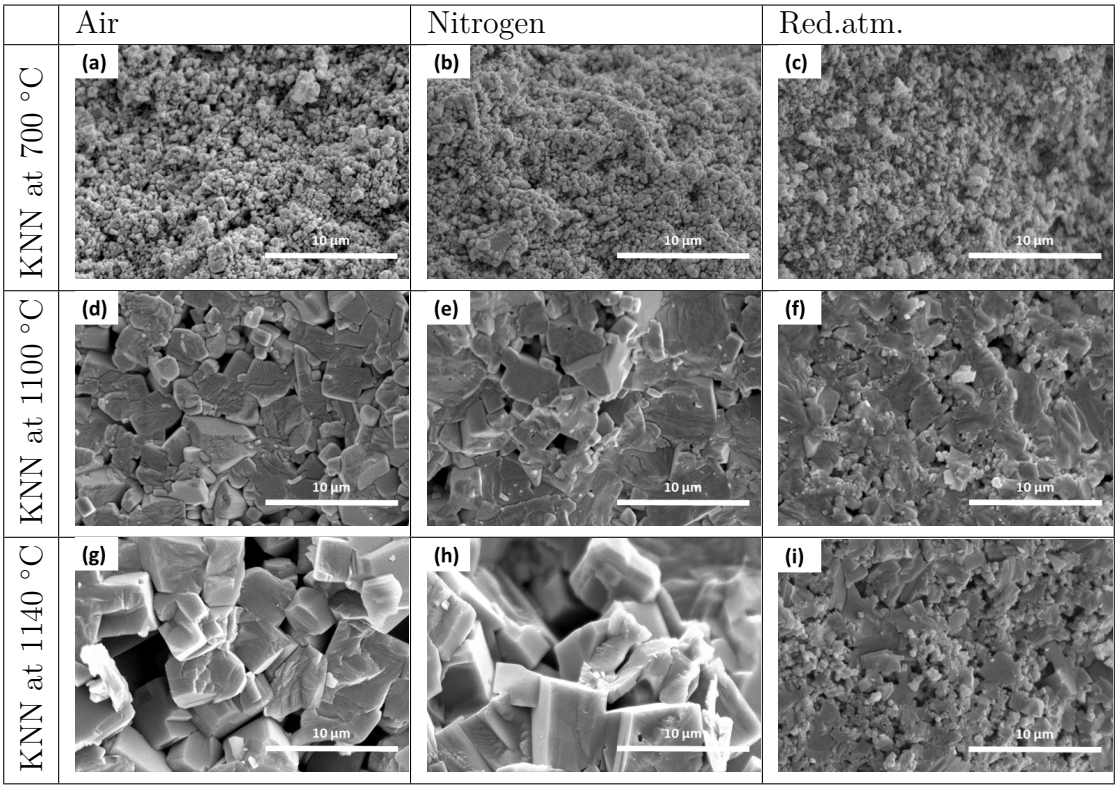

Figure 4.5: *Microstructure of nominally stoichiometric KNN with different sintering temperatures and atmospheres. The formation of cubic grains is evident in nominally stoichiometric KNN sintered in both air and nitrogen. The microstructure of samples sintered in a reducing atmosphere indicated a different sintering mechanism than in air and nitrogen.*

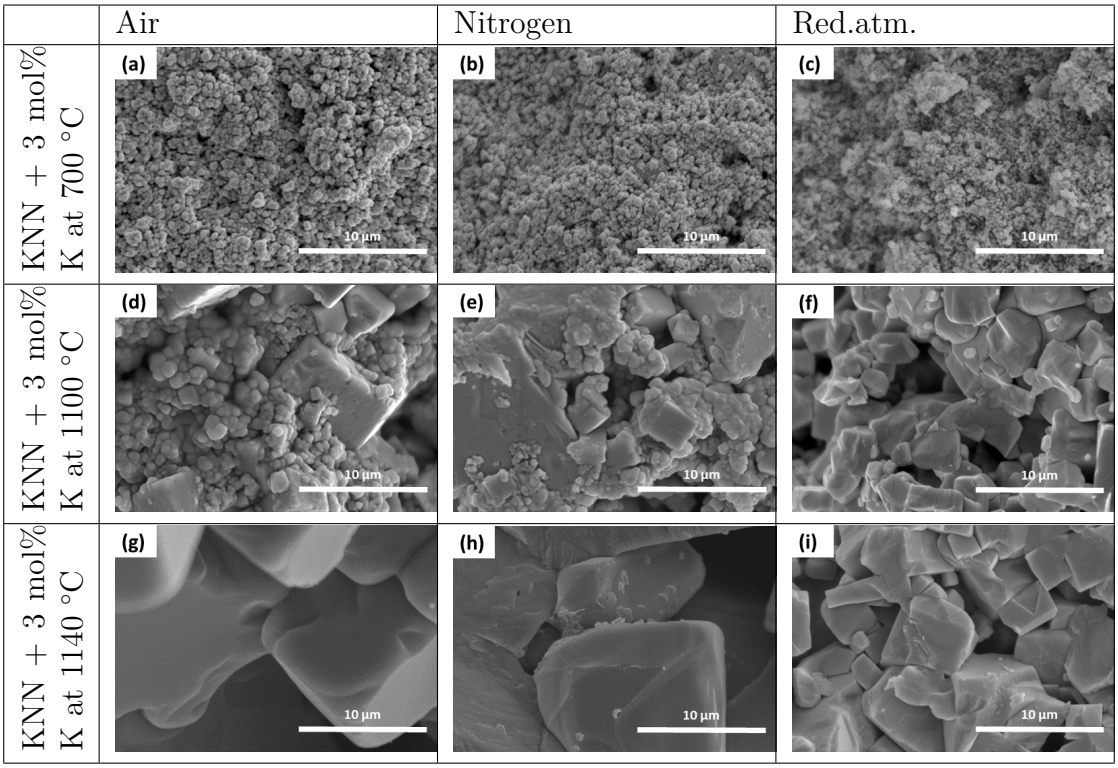

Figure 4.6: *Microstructure images of KNN with nominally 3 mol% excess potassium at different sintering temperatures and atmospheres. The formation of cubic grains is evident in KNN with excess potassium independent of atmosphere during sintering. Abnormal grain growth occur when sintering in air and nitrogen, while a reducing atmosphere appears to reduce the amount of coarsening, but the grains are still large.*

and nitrogen, and the samples sintered in a reducing atmosphere (Figure 4.5), indicates that a different densification mechanism is at work for the sintering process in reducing conditions for nominally stoichiometric KNN compared to in air and nitrogen.

The microstructure of samples with nominal alkali excess in different atmospheres and temperatures are similar (Figure 4.6 and 4.7). Cubic grains form at 1100 °C, and abnormal grain growth has occurred at 1100 °C and 1140 °C. The reducing atmosphere seems to limit the coarsening and abnormal grain growth to some degree, but large cubic grains are still found.

Figure 4.8 shows the microstructure of nominally stoichiometric KNN sintered at 1140 °C in a reducing atmosphere, before and after reoxidation. During the reoxidation there is some grain growth, but still the grains are much smaller than any of the nominally stoichiometric KNN samples sintered in air and nitrogen.

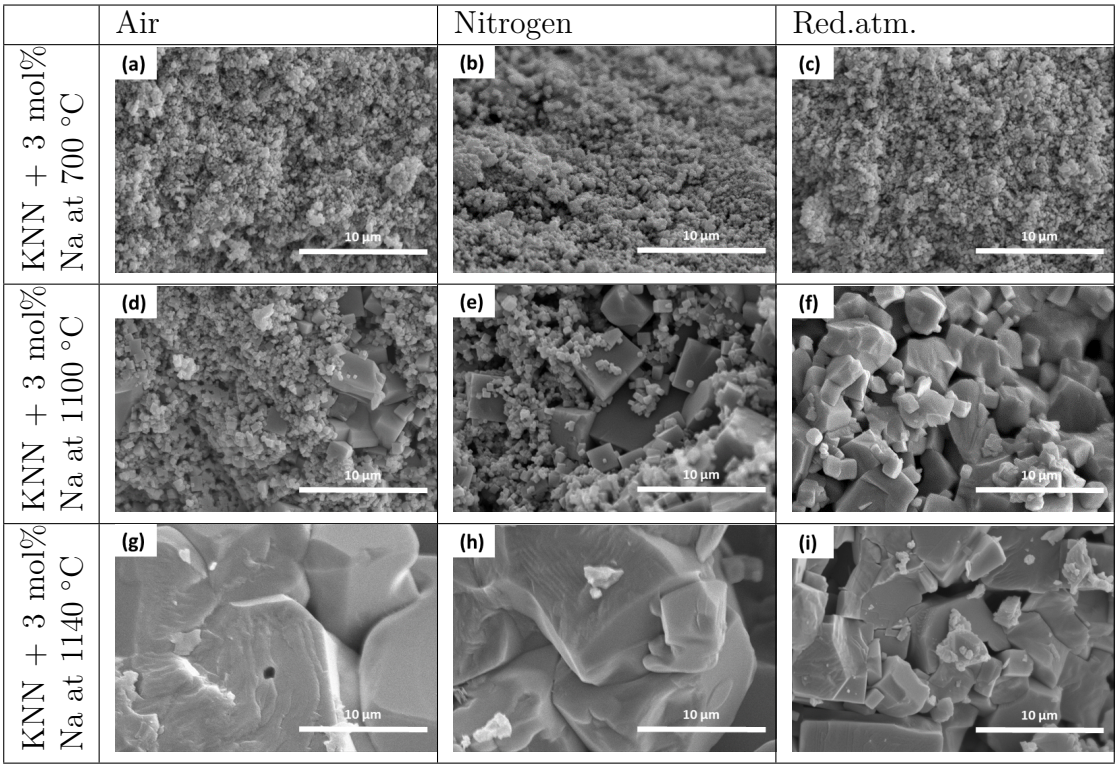

Figure 4.7: *Microstructure of KNN with nominally 3 mol% excess sodium at different sintering temperatures and atmospheres. The formation of cubic grains is evident in KNN with excess sodium independent of atmosphere during sintering. Abnormal grain growth occur when sintering in air and nitrogen, while a reducing atmosphere appears to reduce the amount of coarsening, but the grains are still large.*

Figure 4.9 shows the grain sizes with increasing temperature. These values are estimated from the SEM pictures (Figure 4.5-4.7). A wide size distribution and many small grains, with a few abnormally large grains, causes low average values at 1100 °for KNN with excess alkali (Figure 4.9). The average particle sizes are smallest in a reducing atmosphere, especially for nominally stoichiometric KNN. The coarsening and abnormal grain growth in A-site excess powders is clearly illustrated both in Figure 4.6-4.7 and 4.9.

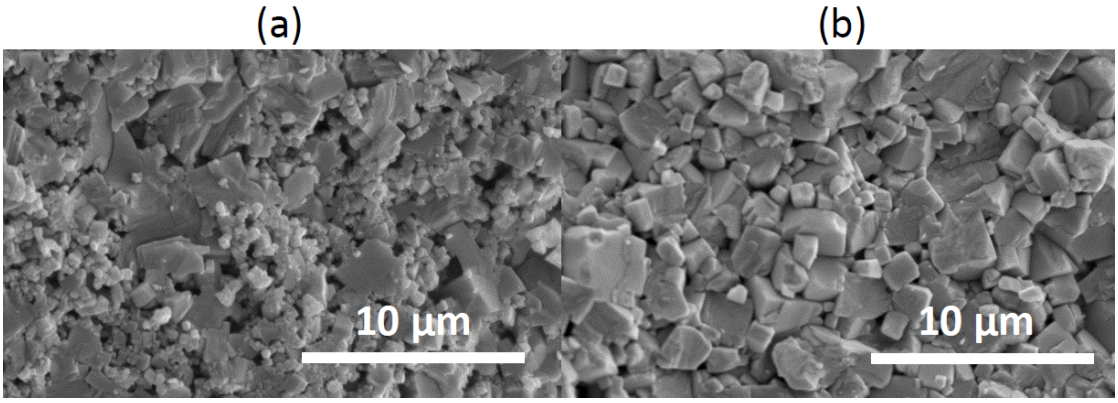

Figure 4.8: *Microstructure of nominally stoichiometric KNN sintered at 1140 °C in a reducing atmosphere (a) before and (b) after reoxidizing at 1000 °C. Some grain growth occur during the oxidizing, but the grains are still small afterwards.*

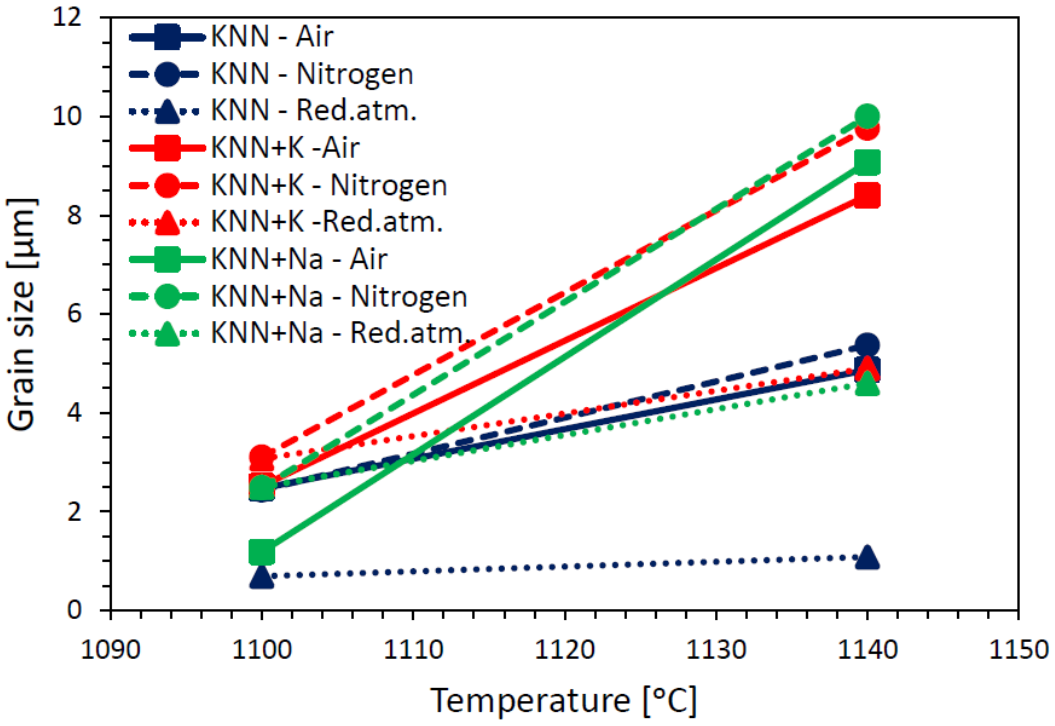

Figure 4.9: *Estimated grain sizes from SEM pictures for nominally stoichiometric KNN, KNN with nominal potassium excess and KNN with nominal sodium excess. Abnormal grain growth occur in KNN with nominal alkali excess, especially in air and nitrogen.*

Table 4.2: Schematics over which samples showed small amount of a Nb-rich secondary phase ($K_2Nb_4O_{11}$) after sintering, corresponding to alkali evaporation.

Nominally stoichiometric KNN			
Temperature [°C]	*Atmosphere*		
	Air	Nitrogen	Red.atm.
700	No	No	No
1100	Yes	Yes	Yes
1140	Yes	Yes	Yes
KNN with nominal potassium excess			
Temperature [°C]	*Atmosphere*		
	Air	Nitrogen	Red.atm.
700	No	No	No
1100	No	No	Yes
1140	No	No	Yes
KNN with nominal sodium excess			
Temperature [°C]	*Atmosphere*		
	Air	Nitrogen	Red.atm.
700	No	No	No
1100	No	No	Yes
1140	No	No	Yes

4.3 Phase composition

The phase composition of the sintered KNN samples was investigated using X-ray diffraction. Figure 4.10 showed the diffractograms of nominally stoichiometric KNN sintered in air at different temperatures. The main reflections were assigned to orthorhombic KNN (PDF card 04-016-9141). All the diffractograms show the same main reflections as Figure 4.10, and only small deviations occur, like shifts in peak intensities and peak sharpening. The rest of the diffractograms can be found in appendix A.

Small traces of a secondary phase were observed in some of the samples. The reflections of the secondary phase were assigned to $K_2Nb_4O_{11}$.[49] Table 4.2 shows which samples that had small amounts of this niobium rich phase. No other significant crystalline secondary phases were observed in any of the diffractograms.

In Figure 4.11 the difference in the diffractograms of nominally stoichiometric KNN and KNN with nominal alkali excess is illustrated. The peaks becomes sharper and overlap between adjacent peaks decrease from the nominally stoichiometric KNN powder to the powders with nominal alkali excess, indicating increased crystallite sizes in excess alkali powders. A small shift in the diffraction

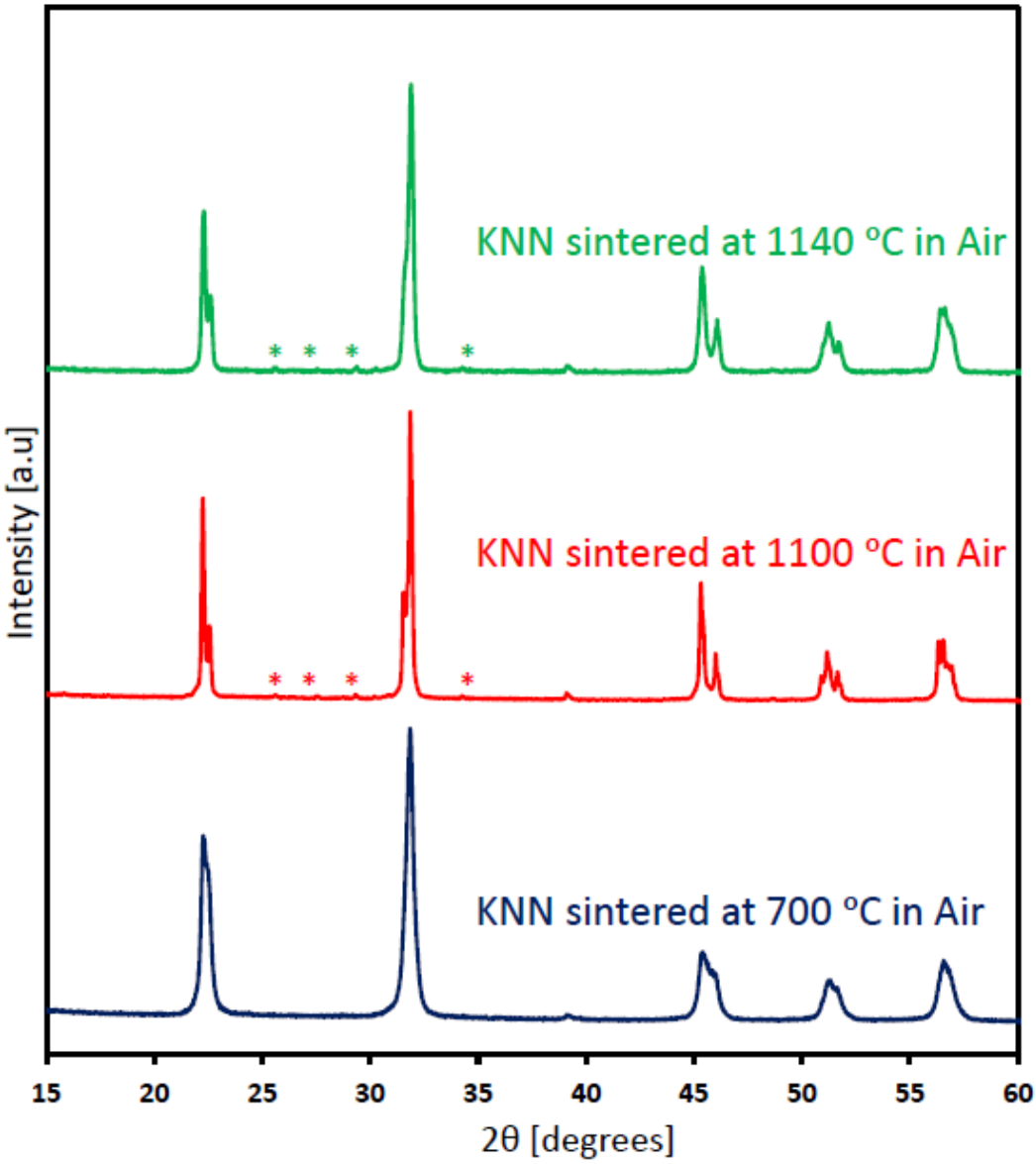

Figure 4.10: *X-ray diffractograms of nominally stoichiometric KNN sintered in air at various temperatures. Small peaks from a secondary Nb-rich phase ($K_2Nb_4O_{11}$, marked *) are visible between 25° and 35° in the diffractograms of pellets sintered at 1100 °C and 1140 °C.*

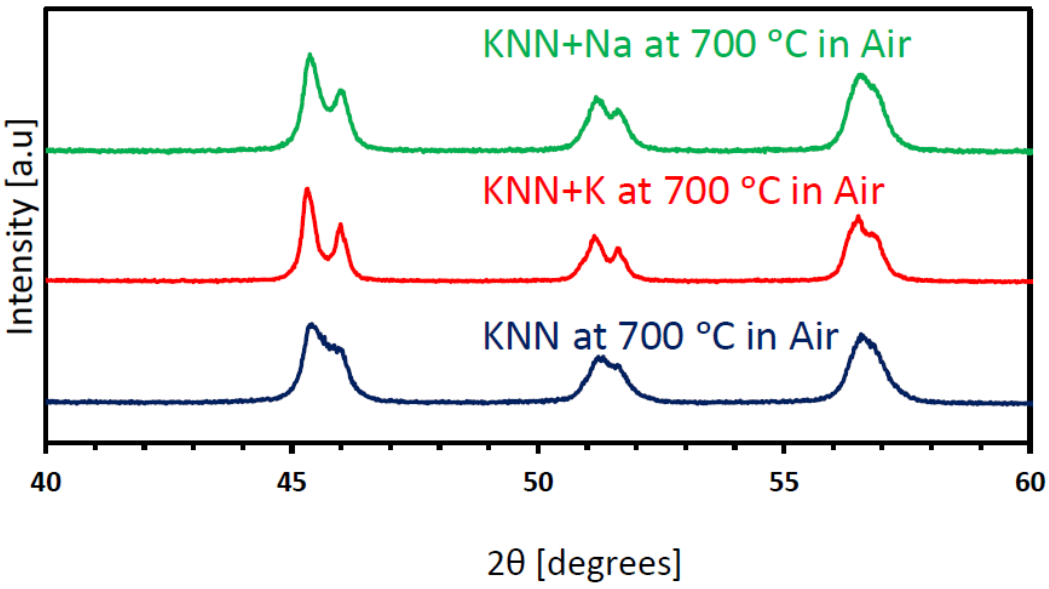

Figure 4.11: *X-ray diffractograms of nominally stoichiometric KNN, KNN with nominal potassium excess and KNN with nominal sodium excess, all heat treated at 700 °C in air. Peak sharpening and splitting are observed for the samples with alkali excess.*

Table 4.3: Pauli fitting of the lattice parameters of nominally stoichiometric KNN

	Orthorhombic KNN[50]	Sintered stoichiometric KNN		
		Atm.	1100 °C	1140 °C
a [Å]	3.9576(2)	Air	3.946(6)	3.946(0)
		N_2	3.945(4)	3.948(2)
		Red.	3.953(2)	3.952(8)
b [Å]	5.6388(4)	Air	5.644(0)	5.642(1)
		N_2	5.641(5)	5.644(0)
		Red.	5.641(2)	5.641(8)
c [Å]	5.6662(6)	Air	5.676(3)	5.675(8)
		N_2	5.673(6)	5.677(4)
		Red.	5.668(0)	5.671(6)

Table 4.4: Pauli fitting of the lattice parameters of KNN with nominal potassium excess

	Orthorhombic KNN[50]	Sintered KNN with excess potassium		
		Atm.	1100 °C	1140 °C
a [Å]	3.9576(2)	Air	3.947(9)	3.950(5)
		N_2	3.945(5)	3.949(2)
		Red.	3.948(6)	3.947(6)
b [Å]	5.6388(4)	Air	5.647(0)	5.648(9)
		N_2	5.644(7)	5.648(2)
		Red.	5.641(9)	5.640(4)
c [Å]	5.6662(6)	Air	5.677(2)	5.681(5)
		N_2	5.673(2)	5.681(7)
		Red.	5.670(4)	5.668()

Table 4.5: Pauli fitting of the lattice parameters of KNN with nominal sodium excess

	Orthorhombic KNN[50]	Sintered KNN with excess potassium		
		Atm.	1100 °C	1140 °C
a [Å]	3.9576(2)	Air	3.944(6)	3.945(2)
		N_2	3.944(6)	3.945(2)
		Red.	3.947(8)	3.947(0)
b [Å]	5.6388(4)	Air	5.642(6)	5.644(0)
		N_2	5.641(2)	5.644(4)
		Red.	5.639(2)	5.638(2)
c [Å]	5.6662(6)	Air	5.674(0)	5.675(2)
		N_2	5.672(5)	5.676(6)
		Red.	5.667(9)	5.665(8)

peaks can also be seen, indicating a change in the unit cell parameters.

The result of the Pauli fitting of the X-ray diffractogram is shown in Tables 4.3-4.3 and A.1-A.3. The high temperature values (Tables 4.3-4.3) are generally in agreement with the results obtained by Madaro.[50] There is more deviation in the values for the raw powders and the samples heat treated at 700 °C (Tables A.1-A.3). For all the samples the R_{wp}-values were in the range 6-10.

Infrared spectroscopy was done to see if there were alkali hydroxides and carbonates in the samples. Based on the results of Bakken[1] and the work of Garand *et al.*[51] and Rudolph *et al.*[52] the absorption bands in the spectra (Figure 4.12-4.14) around 1350, 1505 and 1640 cm^{-1} were assigned to alkali carbonates.

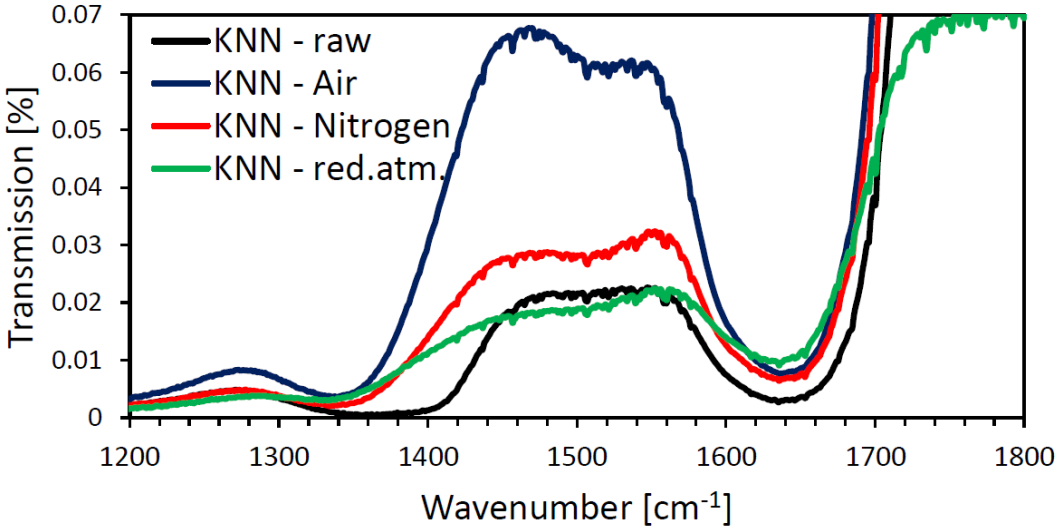

Figure 4.12: *Infrared spectra of 23 wt% nominally stoichiometric KNN heat treated at 700 °C in air, nitrogen and a reducing atmosphere. Also included are the spectra of the stoichiometric KNN raw powder. The absorption bands at 1350, 1505 and 1640 cm^{-1} indicates alkali carbonates.*

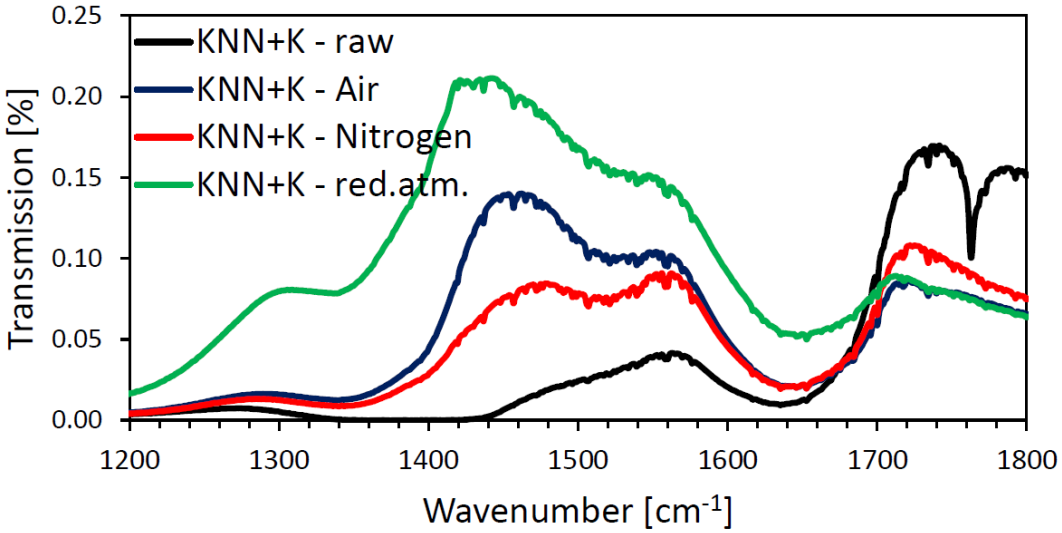

Figure 4.13: *Infrared spectra of 23 wt% KNN with nominal potassium excess heat treated at 700 °C in air, nitrogen and a reducing atmosphere. Also included are the spectra of the KNN with potassium excess raw powder. The absorption bands at 1350, 1505 and 1640 cm^{-1} indicates alkali carbonates. The absorption from these alkali carbonates seams to be less for the sample sintered in a reducing atmosphere.*

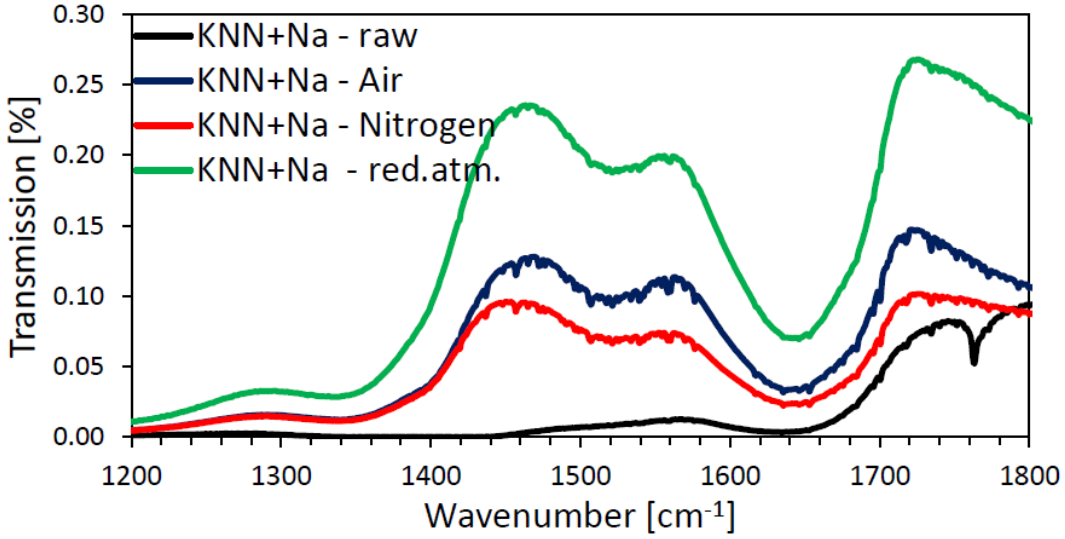

Figure 4.14: *Infrared spectra of 23 wt% KNN with nominal sodium excess heat treated at 700 °C in air, nitrogen and a reducing atmosphere. Also included are the spectra of KNN with sodium excess raw powder. The absorption bands at 1350, 1505 and 1640 cm^{-1} indicates alkali carbonates. The absorption from these alkali carbonates seams to be less for the sample sintered in a reducing atmosphere.*

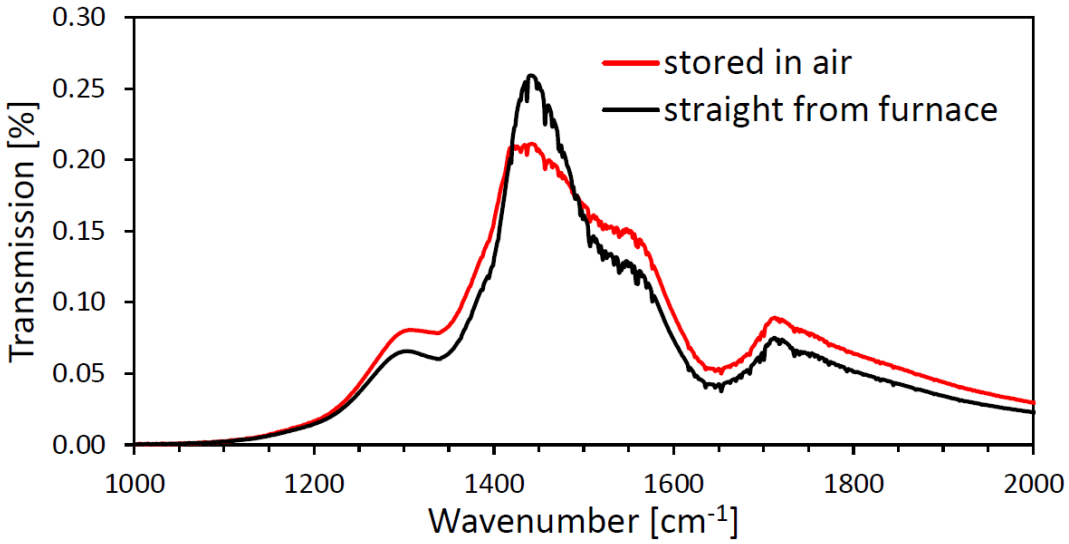

Figure 4.15: *Infrared spectra of 23 wt% KNN with 3 mol% nominal potassium excess heat treated in a reducing atmosphere at 700 °C. The spectra show that there is no significant difference in absorption from alkali carbonates after storage in air.*

The amount of alkali carbonate absorption seems to be equal in the nominally stoichiometric KNN samples. In the spectra of KNN with nominal alkali excess (Figure 4.13 and 4.14) there is a sharp absorption band at 1760 cm^{-1}, which is likely due to gas absorption in the raw powders during storage.[39] In the excess alkali spectra the absorption in the sample sintered in a reducing atmosphere seams to be less compared to the other samples, which may imply that there are less carbonates in those samples.

It was not possible to normalize the infrared spectra presented in section 4.3. This was due to saturation of the absorption band of Nb-O stretching (Figure B.2), observed by Bakken to be around 630 cm^{-1}[1, 53, 54]. This absorption band should be of the same amplitude in all the spectra, independent on the carbonate content and also the stoichiometry. Since this band saturates, quantitative considerations on the carbonate content in the different samples could not be done in the present work.

A KNN with potassium excess sample heat treated in a reducing atmosphere at 700 °C was prepared and infrared spectroscopy was conducted of the sample straight form the furnace. In Figure 4.15 this sample is compared to one that had been stored in air several weeks before the measurement. It is evident from Figure 4.15, there is practically no difference in absorption between the air stored and the sample measured straight form the furnace. Both show absorption bands at approximately 1350, 1505 and 1640 cm^{-1}, indicating alkali carbonate in both samples.

Infrared spectra of samples sintered at 1100 °C were also recorded for nominally stoichiometric KNN (Figure 4.16) and KNN with nominal potassium excess (Figure 4.17). Small traces of residue alkali carbonates were observed in both nominally stoichiometric KNN and KNN with nominal potassium excess after sintering in air, but not for the samples sintered in a reducing atmosphere. However, the spectra are saturated, due to scattering effects from the large grains in these samples.

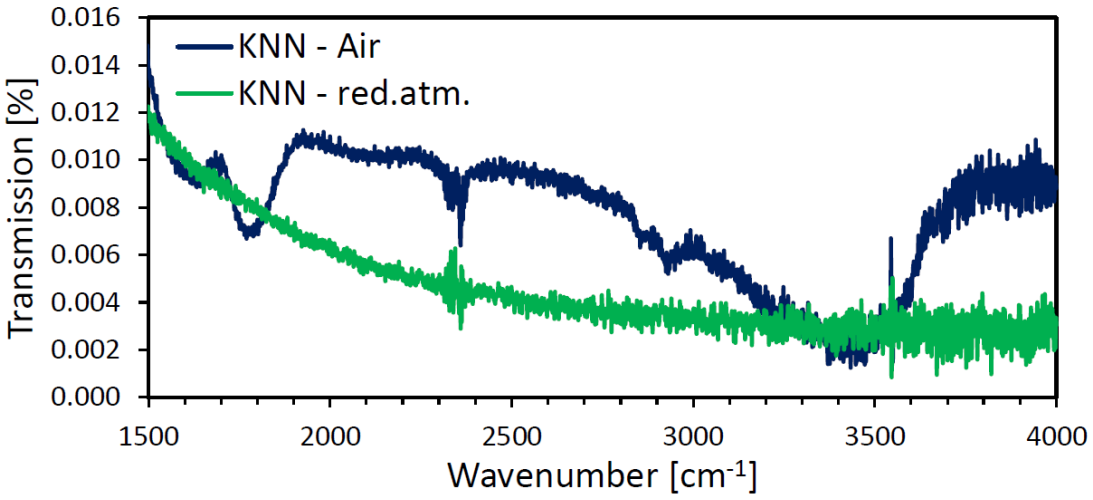

Figure 4.16: *Infra red spectra of 23 wt % nominally stoichiometric KNN sintered at 1100 °C in both air and a reducing atmosphere. Some residue alkali carbonates can be seen in the spectrum of air sintered KNN, but not for the sample sintered in a reducing atmosphere.*

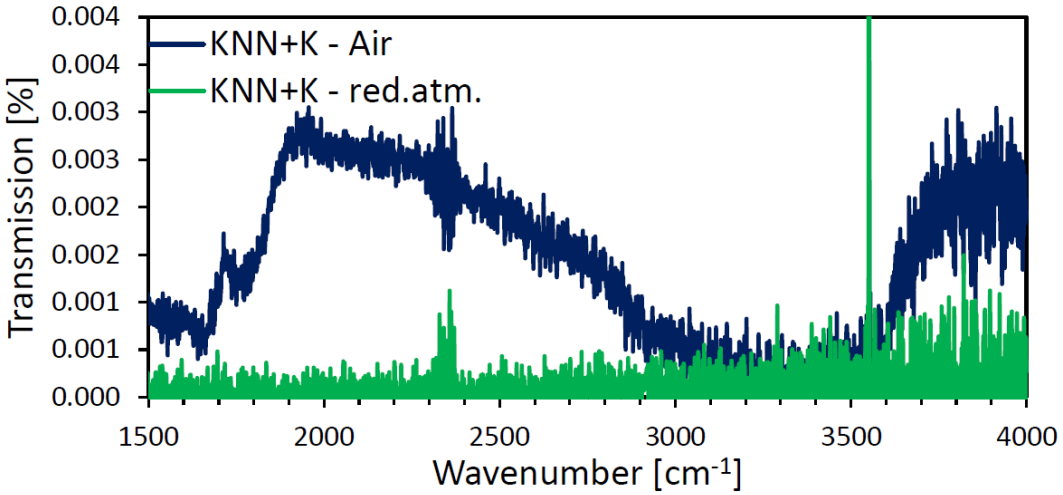

Figure 4.17: *Infra red spectra of 23 wt % KNN with nominal potassium excess sintered at 1100 °C in both air and a reducing atmosphere. Some residue alkali carbonates can be seen in the spectrum of the air sintered sample, but not for the sample sintered in a reducing atmosphere.*

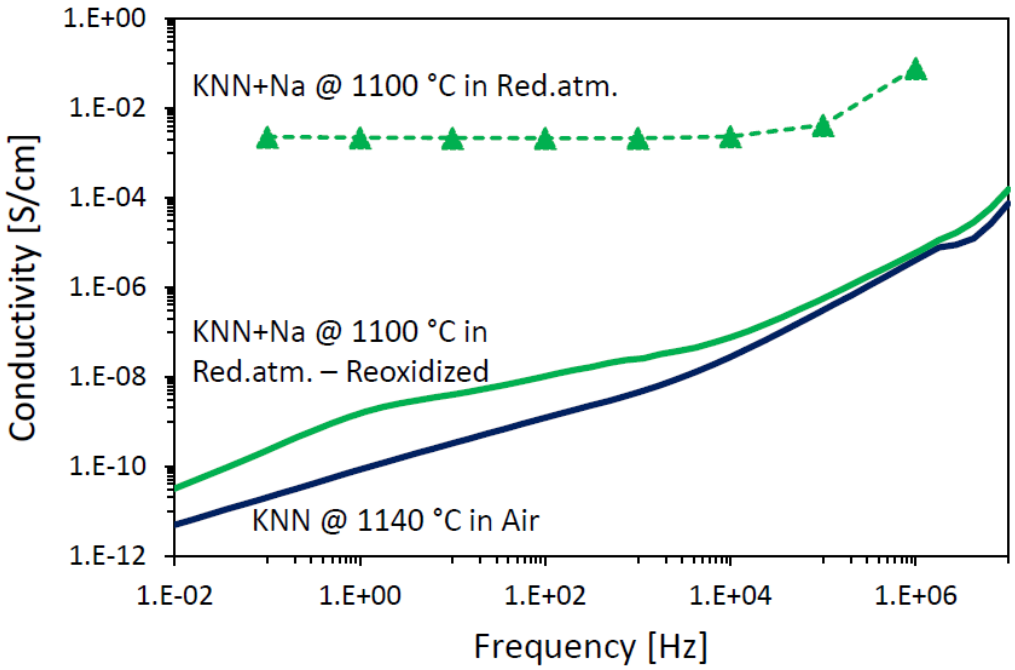

Figure 4.18: *The AC conductivity of KNN samples. The sample sintered in a reducing atmosphere has a significant conductivity, but after reoxidation this is reduced to the values of air sintered KNN.*

4.4 Piezoelectric properties

The samples sintered in a reducing atmosphere had to be reoxidized before any piezoelectric measurement could be done on them. This was due to a significant conductivity in these samples (Figure 4.18). After reoxidizing the samples sintered in a reducing atmosphere, the conductivity decreased to almost as low values as the samples sintered in air. The samples sintered in nitrogen were also reoxidized, due to poor initial piezoelectric results.

Figure 4.19-4.21 shows the polarization and strain loops of the samples sintered at 1140 °C. These samples are the ones with the highest density, and therefore should have the best piezoelectric response. The result of the samples sintered at 1100 °C can be found in appendix C. It is clear that all of the samples are ferroelectric, as they all show hysteresis behaviour.

From the polarization loops of nominally stoichiometric KNN sintered at 1140 °C (Figure 4.19(a)), it is clear that all the samples have leakage currents, but the loop of the sample sintered in a reducing atmosphere more so than the others, due to the round shape of the polarization loops. Also the discontinuity in the polarization loops is evidence of the leakage current. The largest polarization is

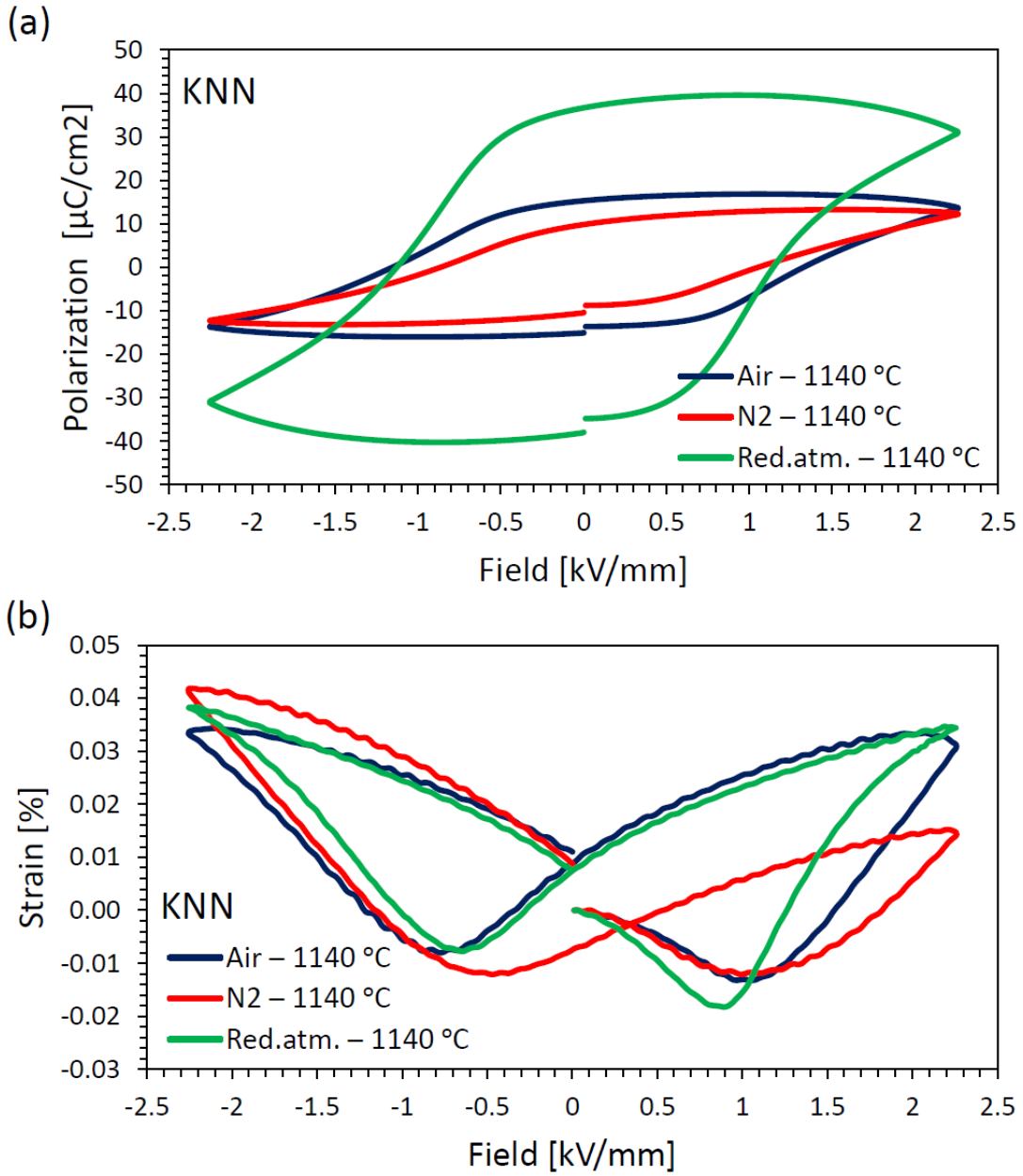

Figure 4.19: *(a) Polarization loop and (b) strain loop of nominally stoichiometric KNN sintered at 1140 °C in air, nitrogen and a reducing atmosphere.*

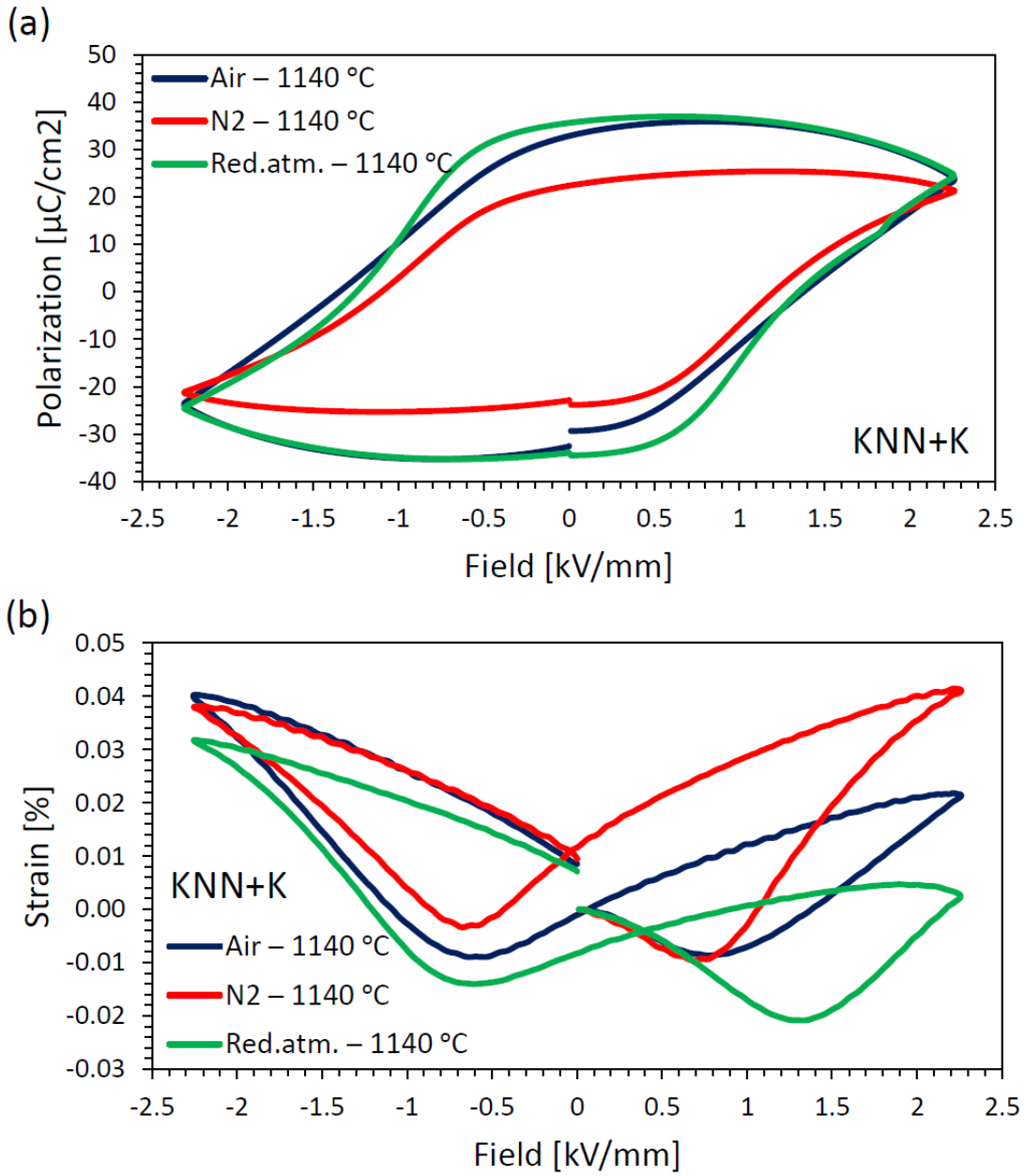

Figure 4.20: *(a) Polarization loop and (b) strain loop of KNN with nominal potassium excess sintered at 1140 °C in air, nitrogen and a reducing atmosphere.*

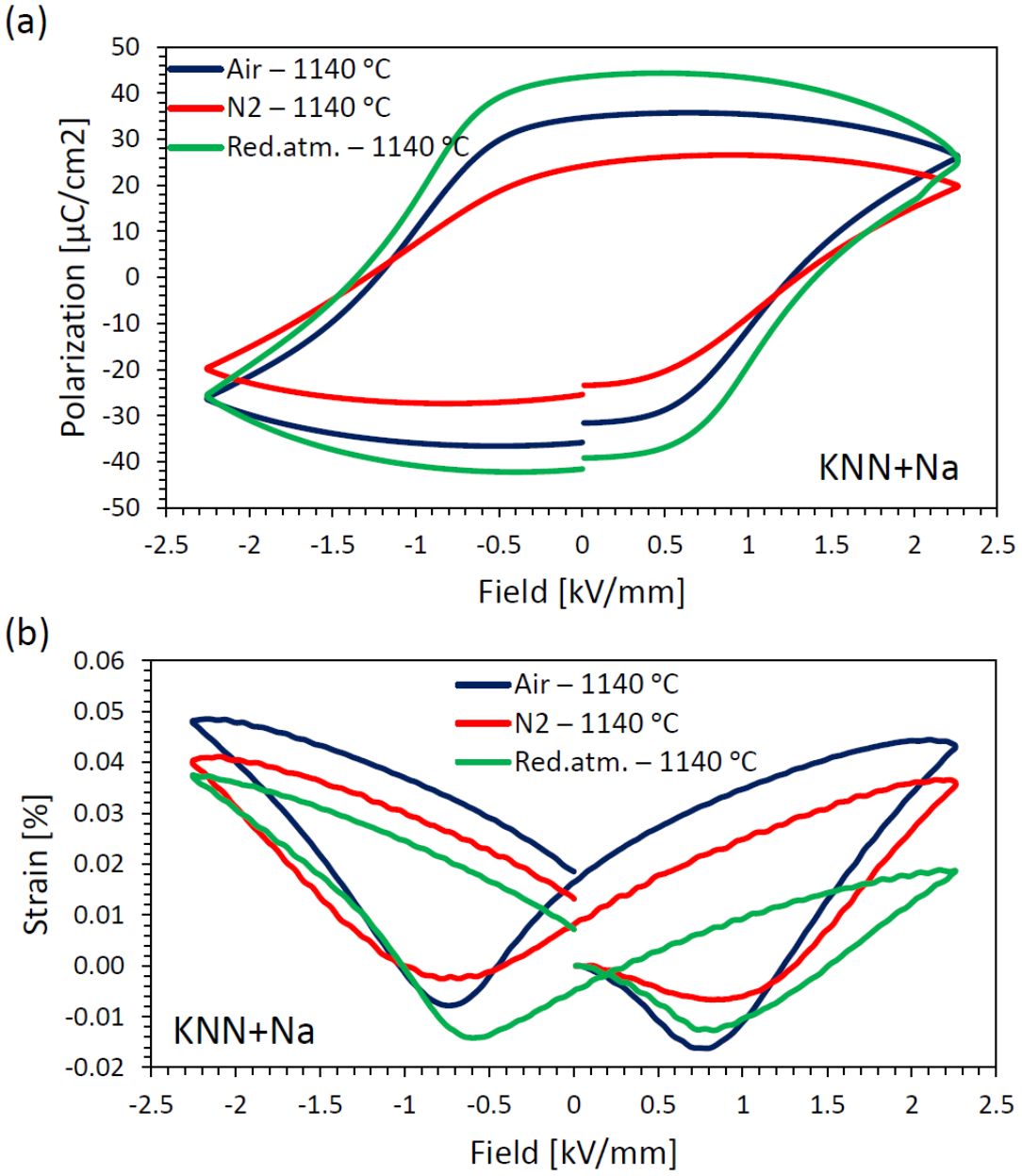

Figure 4.21: *(a) Polarization loop and (b) strain loop of KNN with nominal sodium excess sintered at 1140 °C in air, nitrogen and a reducing atmosphere.*

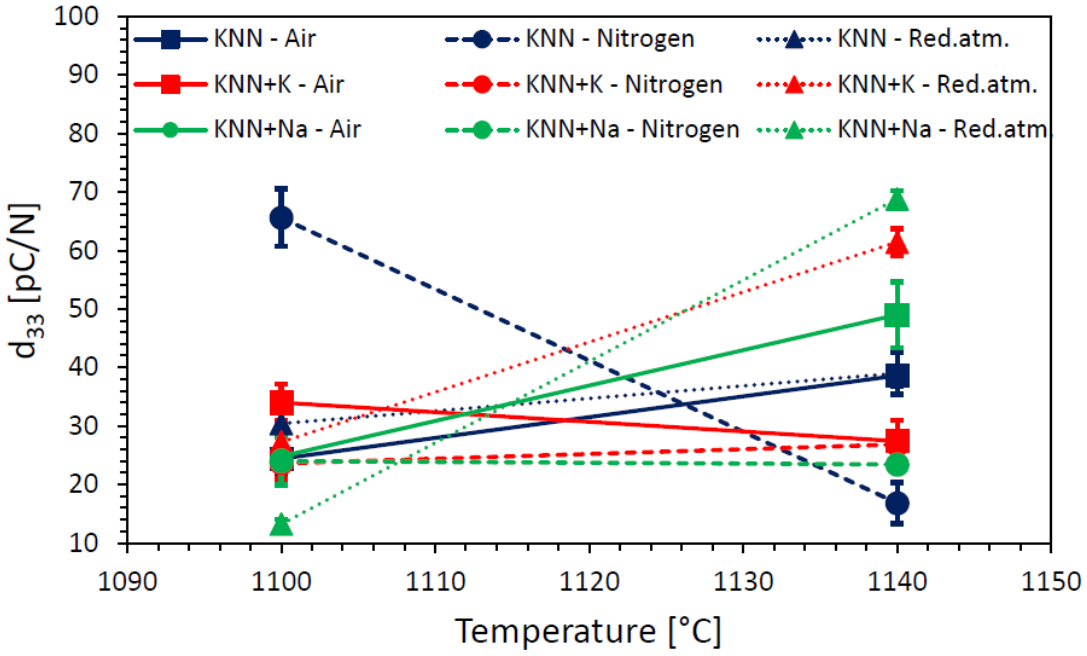

Figure 4.22: *The direct longitudinal piezoelectric coefficient* (d_{33}) *as a function of temperature, for nominally stoichiometric KNN, KNN with nominal potassium excess and KNN with nominal sodium excess. The achieved values are generally low.*

found in the sample sintered in a reducing atmosphere, while the loop of the sample sintered in air and nitrogen are very similar. The corresponding strain loops in Figure 4.19(b) show that there is asymmetry, especially in the nitrogen curve.

Also the polarization curves of KNN with nominal potassium excess show large leakage currents due to the round loops (Figure 4.20(a)). The polarization loops in the different sintering atmospheres are more similar than in nominally stoichiometric KNN (Figure 4.19(a)), but the total polarization is less than that of the nominally stoichiometric KNN sample sintered in a reducing atmosphere. Asymmetry is also present here in the strain loops (Figure 4.20(b)), especially in the air and reducing atmosphere loops. The same observations can be done for KNN with nominal sodium excess (Figure 4.21), although here the total polarization is about the same as for nominally stoichiometric KNN in a reducing atmosphere (Figure 4.19(a)).

Figure 4.22 shows the direct longitudinal piezoelectric coefficient (d_{33}) as a function of temperature. The decrease observed in the piezoelectric coefficient for the nominally stoichiometric KNN sample sintered in nitrogen deviate from the general trend in all the d_{33}-values, which is an increase with increasing temperature. For KNN with nominal potassium excess the piezoelectric coefficient of

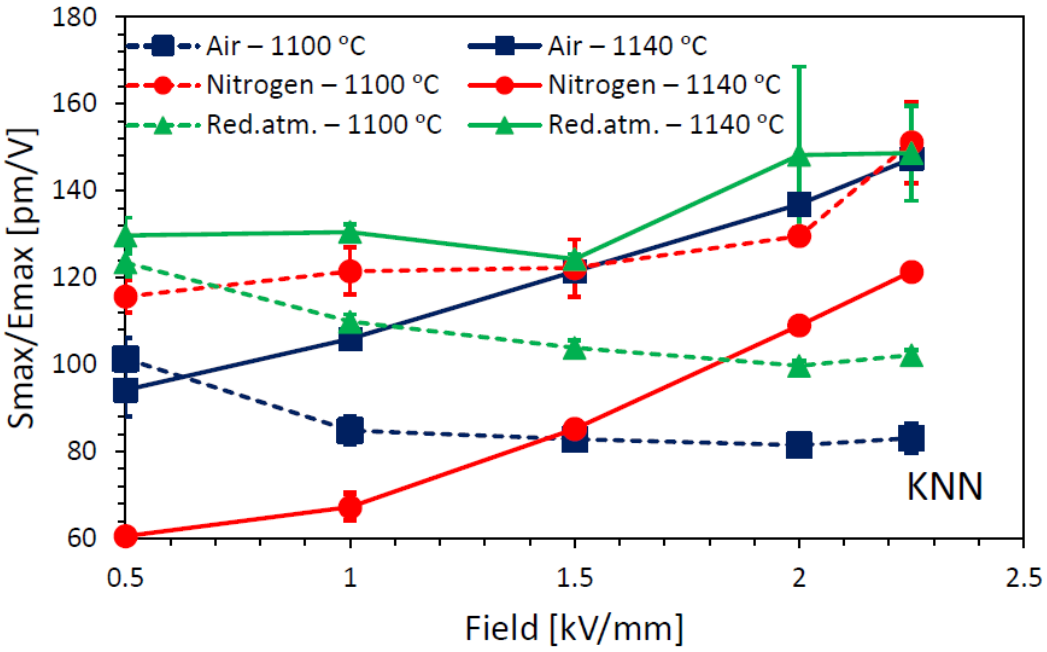

Figure 4.23: *The normalized strain for nominally stoichiometric KNN sintered at 1100 °C and 1140 °C in air, nitrogen and a reducing atmosphere.*

the sample sintered in a reducing atmosphere at 1140 °C is the highest, while the samples in air and nitrogen decrease slightly with increasing temperature. The piezoelectric coefficients of KNN with nominal sodium excess increase with increasing temperature in air and a reducing atmosphere, which is also the highest, while in nitrogen the value decrease slightly. Generally the achieved d_{33}-values are low compared to the values found in literature (see Table 2.2).

Figure 4.23-4.25 shows the normalized strain for nominally stoichiometric KNN, KNN with nominal potassium excess and KNN with nominal sodium excess. In nominally stoichiometric KNN (Figure 4.23) there is a large deviation in the normalized strain values at high fields for the sample sintered in a reducing atmosphere, but the general trend is that the normalized strain increase for an increasing electric field. In both nominally stoichiometric KNN (Figure 4.23) and KNN with nominal potassium excess (Figure 4.24), the highest normalized strain is found in the samples sintered in a reducing atmosphere, and also here is there an increase for increasing electric field. The normalized strain curves of KNN with nominal sodium excess (Figure 4.25) are equally increasing, and there is almost no deviation on the measured values. The values for the measurement done on the air sample seems to be slightly better than that of the nitrogen and reducing atmosphere sample.

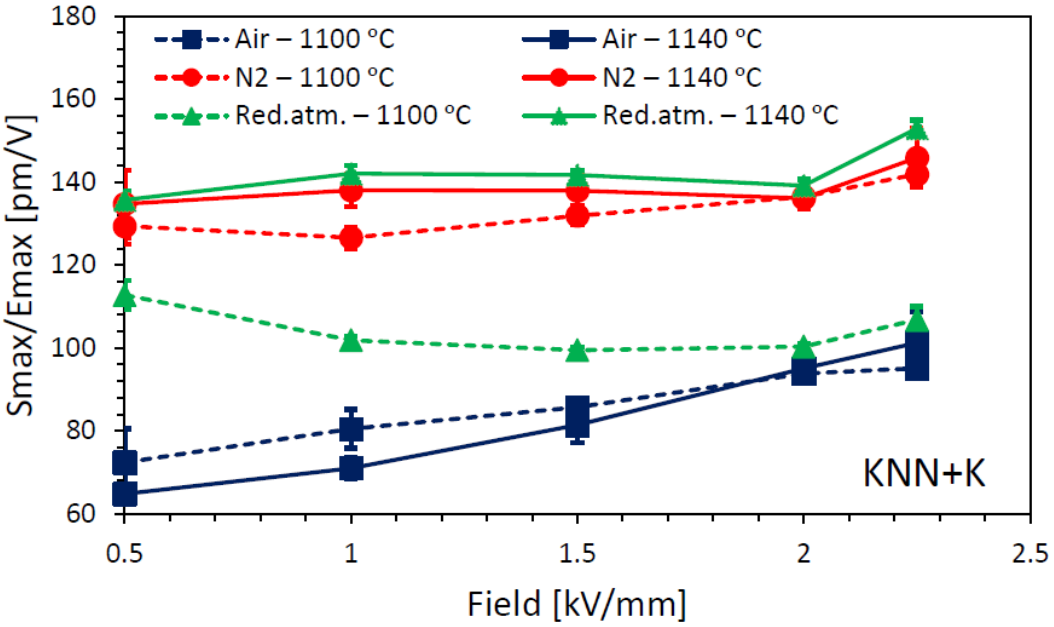

Figure 4.24: *The normalized strain for KNN with nominal potassium excess sintered at 1100 °C and 1140 °C in air, nitrogen and a reducing atmosphere.*

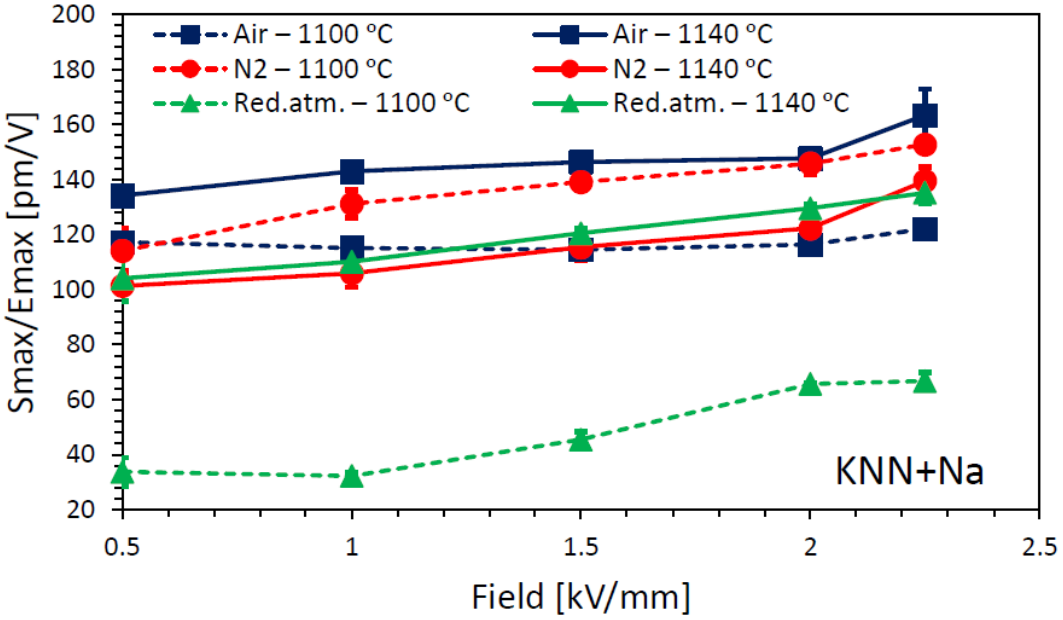

Figure 4.25: *The normalized strain for KNN with nominal sodium excess sintered at 1100 °C and 1140 °C in air, nitrogen and a reducing atmosphere.*

Chapter 5

Discussion

5.1 Alkali carbonates and hydroxides liquid phase formation

A mentioned in the introduction (section 2.4.4) several literature reports indicate that a liquid forms at low temperature (650-700 °C). From the reactions in equations 2.3-2.6, it is assumed that this liquid consists of alkali hydroxides and carbonates. The infrared spectra presented in section 4.3 clearly show that the nominally stoichiometric KNN and KNN with nominal alkali excess samples heat treated at 700 °C contains alkali carbonates, independent of the atmospheres. This confirms that the liquid forming at low temperature consists of melted alkali carbonates.

According to equation 2.3-2.6, the liquid forming is most likely a mixture of alkali hydroxides and carbonates. Bakken[1] observed the infrared spectra of a KNN powder wafer (Figure B.3), before and after drying it in a furnace. In the spectrum recorded after drying, the absorption bands had moved closer together, centred around the absorption band at approximately 1465 cm^{-1}. This band was assigned to pure a carbonate specie.[55] The splitting of the carbonate absorption band in the powder wafer, is evidence that the liquid phase is not a pure carbonate phase, but a mixture of alkali carbonates, bicarbonates and hydroxides. The movement of the split bands closer to the pure carbonate band after drying, can be ascribed to evaporation of hydroxides. Therefore, the liquid forming in KNN must also contain alkali hydroxides.

The spectra of the raw powders (Figure 4.12-4.14) also show that there are alkali hydroxides and carbonates in the raw powders. Meaning that the reactions in equations 2.3-2.6 occur during storage of the raw powders, before any heat treatment. Formation of alkali hydroxides and carbonates therefore seems to be unavoidable if the KNN powder is exposed to air.

The infrared spectra in Figure 4.15 and B.2 show that there is practically no difference between the the sample measured right after sintering in a reducing atmosphere, and after the same sample have been stored in air for several weeks. This implies that the alkali hydroxides and carbonates are present in the samples during sintering. They are not just a result of reactions with the humidity and CO_2 in the air during storage of the heat treated samples.

The infrared spectra of the 1100 °C samples (Figure 4.16 and 4.17) shows that there no longer are alkali hydroxides and carbonates present in the samples after sintering at high temperatures. Since these samples have been stored in air between the sintering and the measurement, they also show that there is no longer any reaction between the sample and the humidity and CO_2 in the air.

5.2 The effect of additional alkali oxides in KNN

Addition of excess alkali to the nominally stoichiometric KNN powder is done to compensate for the alkali evaporation during sintering. A nominal excess of 3 mol% alkali oxides is enough to change the sintering process drastically. The dilatometry curves for the nominal alkali excess samples (Figure 4.2-4.4) show peaks in the shrinking rate at low temperatures corresponding to a liquid formation. These curves confirm the results obtained by Acker *et al.*[12, 13] and Haugen[2]. The alkali hydroxide and carbonate liquid phase gives a rearrangement of the particles, but then at higher temperatures there is no longer any driving force for sintering. This reduction in the driving force is not observed in the dilatometry curve for the nominally stoichiometric KNN compound, and is responsible for the lower density in excess alkali samples (Figure 4.1).

The addition of the alkali excess is done by addition of alkali oxides, which will react with the humidity and CO_2 in the air to form the alkali hydroxide and carbonate liquid phase, in accordance with equation 2.3 and 2.4. When the alkali excess is added to the stoichiometric compound, the reducing atmosphere does not seam to be sufficient to destabilize all the alkali carbonates and hydroxides, before they melt. Additional alkali oxides will therefore lead to more of the liquid phase. This liquid induce abnormal grain growth and severe coarsening. This can clearly be seen in the SEM pictures (Figure 4.5-4.7). The coarsening is much more severe in the nominal alkali excess samples compared to the nominally stoichiometric KNN. In the alkali excess samples abnormal grain growth occur, but the extent is much more pronounced in air and nitrogen, resulting in grains that are up to 10 µm. The peak sharpening and splitting observed in the X-ray diffractograms also testify about the changes in lattice parameters and increase in crystallite sizes, due to the coarsening.

The effect of the additional alkali oxide on the surface of the KNN particles

limits the densification, gives more liquid formation and severe coarsening. However, the alkali excess also compensate for the alkali evaporation during sintering. The secondary phase, $K_2Nb_4O_{11}$, do not form in the powders with nominal alkali excess, which is why it is interesting to investigate the sintering behaviour of KNN with nominal alkali excess.

5.3 The effect of the sintering atmosphere

The effect of the sintering atmosphere is more important for the sintering process in KNN, than the stoichiometry. A reducing atmosphere during sintering gives a higher density compared to sintering in air and nitrogen, as can be seen form the density graphs (Figure 4.1). The densities presented in section 4.1 shows that the highest densities is achieved for nominally stoichiometric KNN sintered in a reducing atmosphere at 1140 °C. Highest densities for samples sintered in a reducing atmosphere are expected from the reactions in equations 2.9 and 2.10, presented in the introduction (section 2.4.5). The reoxidizing treatment also contribute to the densification, as the density increase, but also to the coarsening. The observed grains in nominally stoichiometric KNN sintered at 1140 °C are larger after reoxidation, but not nearly as large as the ones found in the air or nitrogen sintered samples.

The densities found for nominally stoichiometric KNN sintered in nitrogen are generally high compared to in the reducing atmosphere, especially at 1100 °C. These high densities in nitrogen are unexpected. According to the theory presented in the introduction, the density of the samples sintered in a reducing atmosphere should be the highest. Also the microstructure of the samples (Figure 4.5) indicate that the density should be highest in the reduced samples. There are some uncertainty to the density data, but the samples of nominally stoichiometric KNN sintered in nitrogen and a reducing atmosphere were measured several times, and additional samples were made to be sure of the data. The same trend was observed each time.

Also the dilatometry curves (Figure 4.2-4.4) show that a reducing atmosphere is beneficial for the sintering of KNN. The shrinkage curves of nominally stoichiometric KNN looks more or less the same for all sintering atmospheres. However, there is a wider temperature range for which a high shrinking rate can be found in the reducing atmosphere. The increase in shrinking rate starts at 840 °C, but in the temperature range 980 to 1090 °C the shrinking rate is at its highest, and densification occur. The reducing atmosphere also enhance the densification of KNN with nominal alkali excess. At higher temperatures, above 1030-1040 °C there is a new increase in the shrinking rate in the reducing atmosphere. This corresponds to destabilization of the liquid phase. This induce solid state sintering,

since the liquid has not yet caused coarsening to the point that the driving force for sintering disappears.

The reducing atmosphere also limits the grain growth, especially in nominally stoichiometric KNN. The fine homogeneous microstructure testify about a different sintering mechanism at work in nominally stoichiometric KNN sintered in a reducing atmosphere. Destabilization of the alkali carbonates and hydroxides at low temperature, before they can form a liquid phase, induce solid state sintering with out the severe coarsening. In samples with nominal alkali excess, the abnormal grain growth seems to be inhibited, but severe coarsening still occur in a reducing atmosphere. It is also clear from the microstructure that faceted grain growth do occur in KNN materials. Cubic grain formation is hard to avoid in any atmosphere and for all stoichiometries.

The reducing atmosphere destabilize the alkali carbonates and hydroxides, but also increase the alkali evaporation. This results in formation of the secondary phase, $K_2Nb_4O_{11}$, after sintering. There are several reports of secondary niobium rich phases forming in KNN corresponding to evaporation of alkali oxides.[2, 12, 13, 42] The observed secondary phase in the X-ray diffractograms (Table 4.2) further confirms that the reaction in equation 2.7 stated in section 2.4.5 occur.

5.4 The effect of stoichiometry and sintering atmosphere on the piezoelectric performance

The high conductivity caused by the reducing atmosphere by reduction of a small amount of the niobium ions, disappears during the reoxidation. This is promising since it was not possible to measure the piezoelectric properties of the reduced samples before the reoxidation.

The normalized strain and the piezoelectric coefficient recorded is generally very low compared to the data reported in the literature (Table 2.2). The measured samples were all 5 mmØ pellets with silver electrodes. A few 10 mmØ pellets with gold electrodes of nominally stoichiometric KNN sintered in a reducing atmosphere at 1140 °C were also prepared. They could unfortunately not be measured, due to problems with the piezoelectric measurement set-up. The plan was to see if better properties could be achieved by the latter sample preparation procedure. The 10 mmØ samples were easier to make than the 5 mmØ, and also easier to handle during sample preparation.

Generally the 1140 °C samples showed the best properties. From the density data, this is expected, since porosity will lead to higher leakage current, and deteriorated performance. The highest normalized strains and piezoelectric coefficients observed were for all stoichiometries the sample sintered in a reducing atmosphere.

The highest polarization was also found for samples sintered in a reducing atmosphere. A high polarization is desired, but the polarization loops should also be flat, like the one presented in section 2.2.1 (Figure 2.3). Flat polarization loops are advantageous because it means the leakage currents are low or non existent.

These results do indicate that high density is important for the piezoelectric properties. A reducing atmosphere have been demonstrated to result in higher density and improve the sintering process. A reducing atmosphere also results in a better microstructure compared to sintering in air or nitrogen, especially for nominally stoichiometric KNN. The work of Wu *et al.* suggested that optimizing the microstructure should result in the best piezoelectric properties.[47] By that reasoning, it is expected that the nominally stoichiometric KNN sintered in a reducing atmosphere samples should have the best piezoelectric properties. A reducing atmosphere might therefore be beneficial for enhancing the piezoelectric performance.

5.5 Finding the balance between competing mechanisms in KNN materials

In KNN materials there is a competition between two different mechanisms. Evaporation of alkali (equation 2.7 and 2.8) will lead to the formation of secondary phases, such as $K_2Nb_4O_{11}$. These niobium phases are undesirable since they deteriorate the ferroelectric properties of KNN.[56] Addition of excess alkali in the form of alkali oxides on the surface of the KNN particles will compensate for the alkali evaporation. However, the alkali oxides will also lead to more liquid phase formation. The liquid phase, consisting of alkali hydroxides and carbonates, induce abnormal grain growth and severe coarsening in KNN.

Liquid phase sintering can be beneficial for densification, but only if the liquid is present at the sintering temperature.[3] Liquid formation at low temperatures, which is found in KNN materials, is not beneficial and will enhance coarsening. According to the dilatometry curves (Figure 4.2-4.4), the alkali liquid phase seams to evaporate, before the sintering can start. This makes it hard to achieve densification in the degree that is necessary to achieve good piezoelectric properties.

Sintering in a reducing atmosphere on the other hand, seems to limit the coarsening and grain growth, but it will also lead to increased alkali evaporation. The ultimate goal is to find the balance between these two competing mechanisms, so that the piezoelectric properties are optimizes. Ideally it would be possible to remove the liquid without the formation of these secondary phases, although this do not seem to be possible. Sintering nominally stoichiometric KNN in a reducing atmosphere is therefore promising with respect to the obtained microstructure,

but also the sintering process. The only concern is to what degree this leads to formation of the secondary phase ($K_2Nb_4O_3$) and how this affect the piezoelectric performance.

Chapter 6

Conclusion

The recorded infrared spectra show that the liquid forming at low temperatures (650-700 °C) in KNN materials consists of alkali carbonates and hydroxides. These alkali carbonates and hydroxides form when the raw powder is exposed to air. The alkali oxides and alkali niobates in the raw powder will react with the humidity and CO_2 in the air at room temperature.

The sintering process of KNN materials in different atmospheres have been investigated. The effect of the partial pressure of oxygen on the microstructure has also been demonstrated. A reducing atmosphere results in a better microstructure, especially in nominally stoichiometric KNN. In nominally stoichiometric KNN the grain growth was limited during sintering in a reducing atmosphere, resulting in small but cubic grains. Sintering in the reducing atmosphere also resulted in higher densities and a larger temperature range for sintering in nominally stoichiometric KNN.

The enhanced sintering process in a reducing atmosphere can be attributed to a destabilization of the alkali hydroxides and carbonates. Increased evaporation of alkali will limit the amount of liquid formation. Less liquid will result in less coarsening and inducing solid state sintering.

The coarsening in KNN with nominal alkali excess was limited by the reducing atmosphere, but not sufficient to retain the sub-micron particles of the raw powders. However, the reduction in the driving force for sintering, due to severe coarsening is observed in KNN with nominal alkali excess in air and nitrogen, but not in a reducing atmosphere. Therefore solid state sintering is possible at temperatures above 1000 °C.

The samples sintered in a reducing atmosphere had to be reoxidized due to high conductivity. The reoxidation contribute to the coarsening, but also the densification. After the reoxidation the conductivity was reduced to the values of KNN sintered in air.

The observed piezoelectric performance is generally poor, probably due to the

sample preparation. Low values for the normalized strain and piezoelectric coefficient were found. The polarization loops were generally round with large leakage currents. However, the obtained piezoelectric data suggest that achieving high densities are important. Sintering in a reducing atmosphere may therefore be beneficial for a enhanced piezoelectric performance.

Chapter 7

Further work

This work has demonstrated the benefits of the reducing atmosphere on the sintering process of KNN materials. A reducing atmosphere resulted in high density. Increasing the dwell time at the sintering temperature may lead to a further increase, as should lowering the heating rate to 2 °/min.

Further work should include infrared spectroscopy. Lowering the sample concentration when recording the infrared spectra may give less saturation. Concentration in the range 0-10 wt% should give less saturation so the Nb-O stretching absorption band might be visible. This will make quantitatively determination of the amount of liquid in the samples possible. Also it would be interesting to do measurements on samples sintered at temperatures in-between 700 °C and 1100 °C to see when the evaporation of the liquid phase occur.

The microstructures obtained indicate that the sintering process in nominally stoichiometric KNN is better than for KNN with nominal alkali excess. A more thorough investigation of the piezoelectric properties of nominally stoichiometric KNN sintered in a reducing atmosphere at temperatures ranging from 980-1140 °C would be interesting to determine the optimal sintering temperature and atmosphere for nominally stoichiometric KNN.

Appendix A

X-Ray diffractograms of sintered pellets

The Pauli fitting for the lattice parameters of nominally stoichiometric KNN and KNN with nominal alkali excess raw powders and the samples heat treated at 700 °C are presented in Table A.1-A.3. The diffractograms of the conventional sintered samples of nominally stoichiometric KNN and KNN with nominal alkali excess sintered in different atmospheres and temperatures are included in this chapter. The diffractograms of nominally stoichiometric KNN sintered in air can be found in chapter 4.3.

Table A.1: Pauli fitting of the lattice parameters of nominally stoichiometric KNN

	Orthorhombic KNN[50]	Raw powder	Heat treated KNN	
			Atm.	700 °C
a [Å]	3.9576(2)	3.997(5)	Air	3.954(1)
			N_2	3.998(1)
			Red.	3.999(5)
b [Å]	5.6388(4)	5.528(8)	Air	5.637(0)
			N_2	5.534(6)
			Red.	5.552(9)
c [Å]	5.6662(6)	5.660(7)	Air	5.666(1)
			N_2	5.659(8)
			Red.	5.654(1)

Table A.2: Pauli fitting of the lattice parameters of KNN with nominal potassium excess

	Orthorhombic KNN[50]	Raw powder	Heat treated KNN+K	
			Atm.	700 °C
a [Å]	3.9576(2)	3.997(5)	Air	3.949(0)
			N_2	3.951(9)
			Red.	3.948(7)
b [Å]	5.6388(4)	5.530(9)	Air	5.644(5)
			N_2	5.644(8)
			Red.	5.644(9)
c [Å]	5.6662(6)	5.661(0)	Air	5.673(9)
			N_2	5.675(0)
			Red.	5.674(8)

Table A.3: Pauli fitting of the lattice parameters of KNN with nominal sodium excess

	Orthorhombic KNN[50]	Raw powder	Heat treated KNN+Na	
			Atm.	700 °C
a [Å]	3.9576(2)	3.997(1)	Air	4.002(8)
			N_2	3.998(9)
			Red.	3.948(5)
b [Å]	5.6388(4)	5.530(3)	Air	5.582(3)
			N_2	5.516(2)
			Red.	5.639(6)
c [Å]	5.6662(6)	5.660(5)	Air	5.610(7)
			N_2	5.659(2)
			Red.	5.668(4)

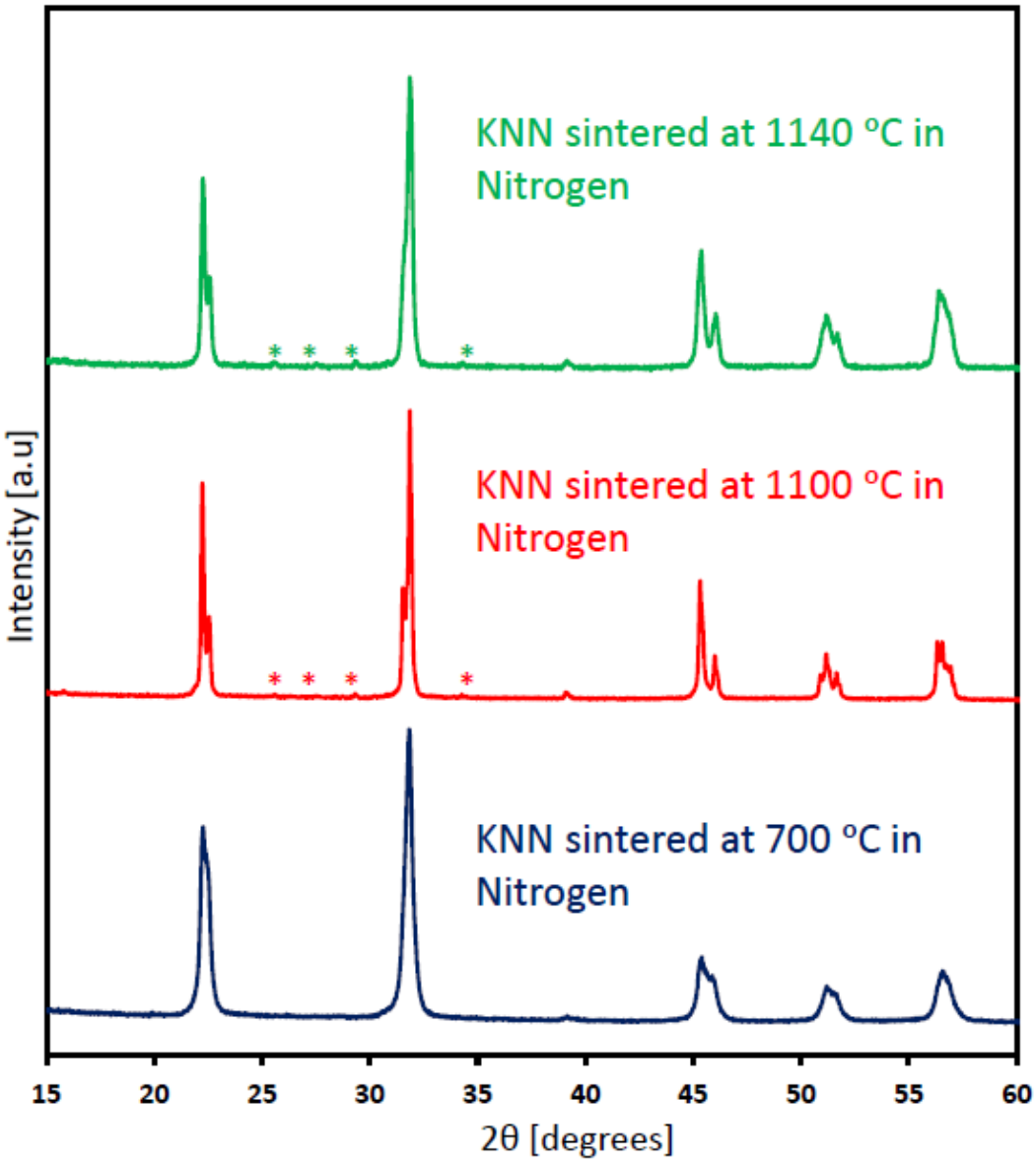

Figure A.1: *X-ray diffractograms of nominally stoichiometric KNN sintered in nitrogen at various temperatures. Small peaks from a secondary Nb-rich phase ($K_2Nb_4O_{11}$, marked *) are visible between 25° and 35° in the diffractograms of pellets sintered at 1100 °C and 1140 °C.*

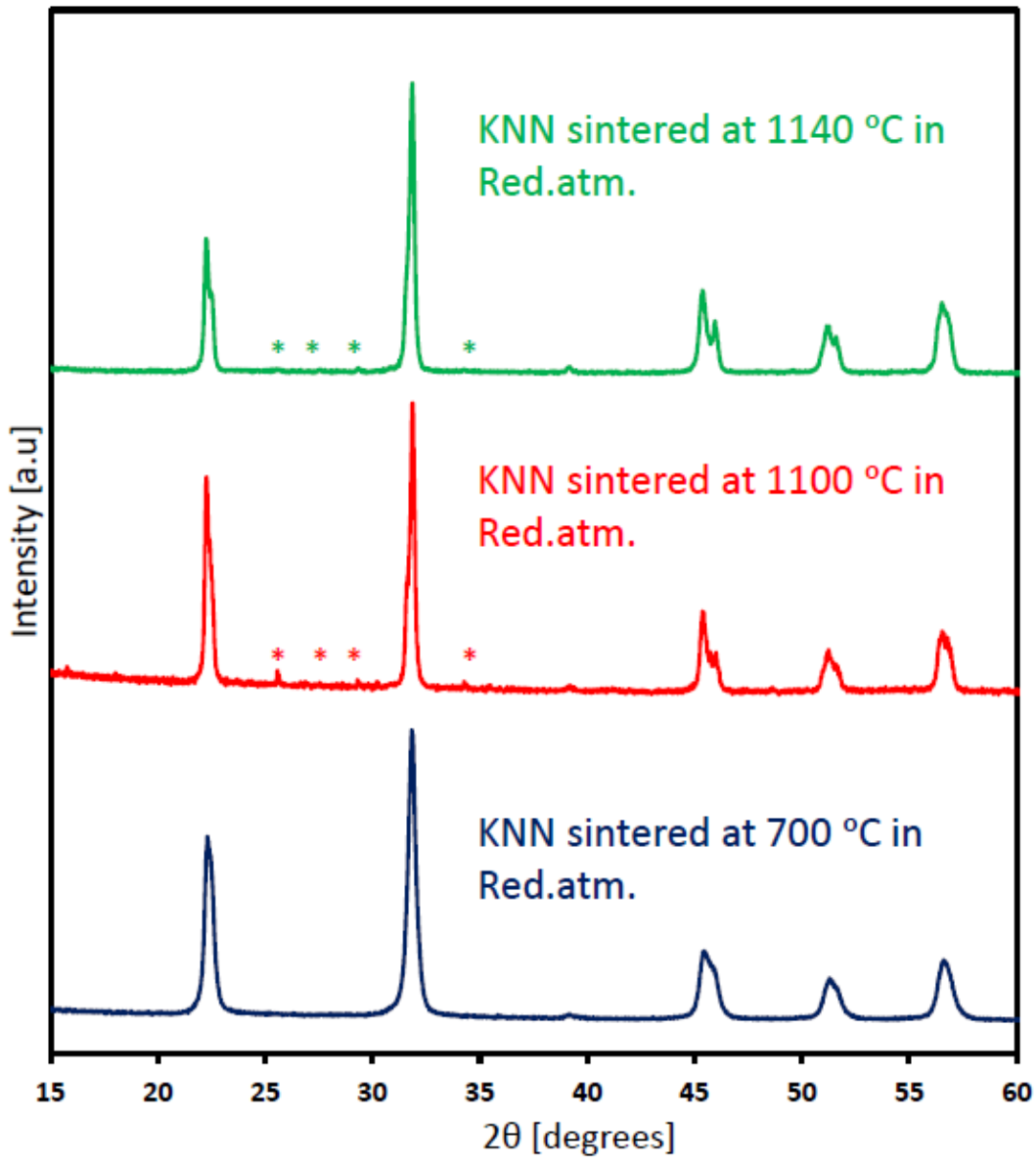

Figure A.2: *X-ray diffractograms of nominally stoichiometric KNN sintered in a reducing atmosphere at various temperatures. Small peaks from a secondary Nb-rich phase ($K_2Nb_4O_{11}$, marked *) are visible between 25° and 35° in the diffractograms of pellets sintered at 1100 °C and 1140 °C.*

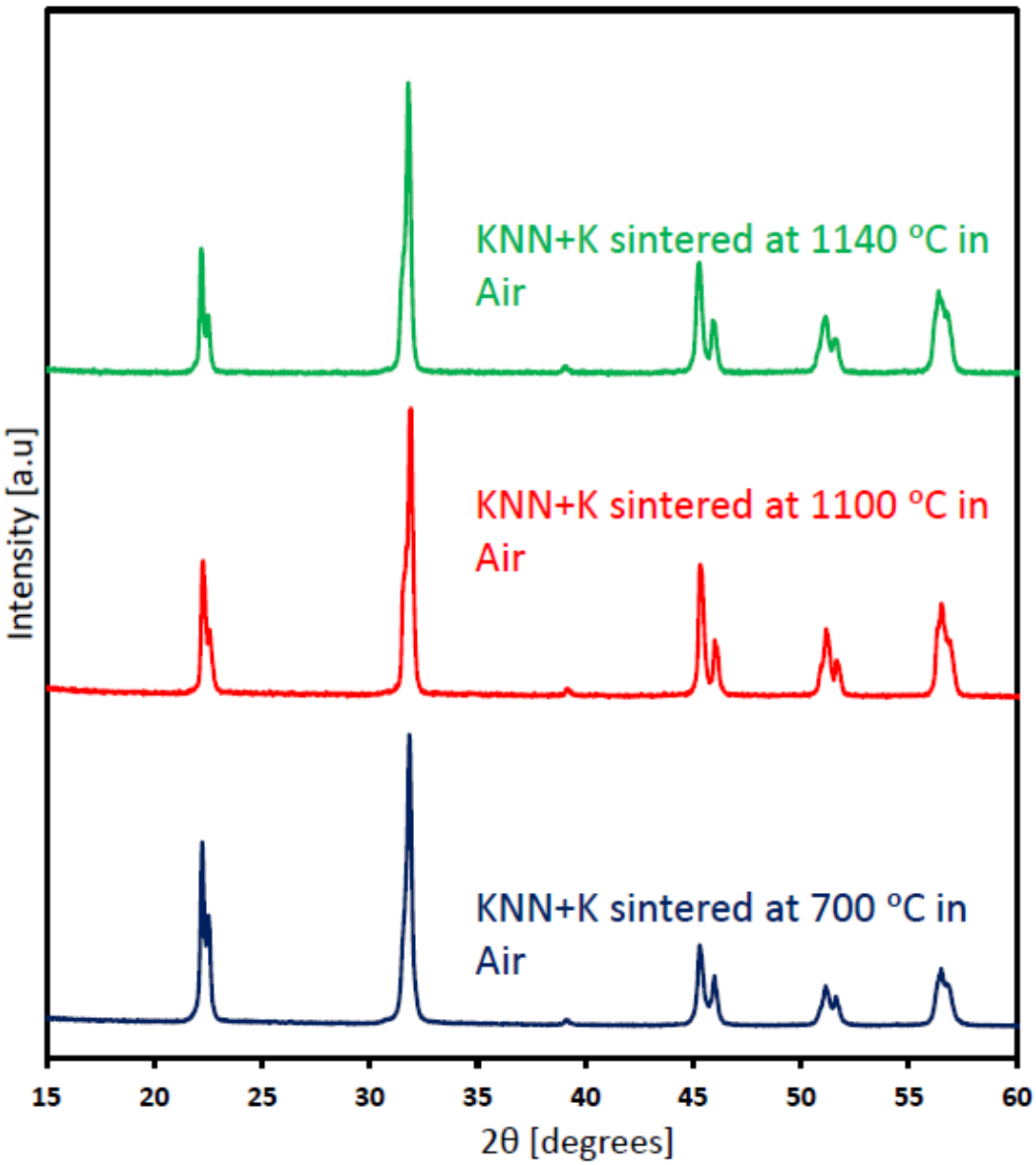

Figure A.3: *X-ray diffractograms of KNN with nominal potassium excess sintered in air at various temperatures.*

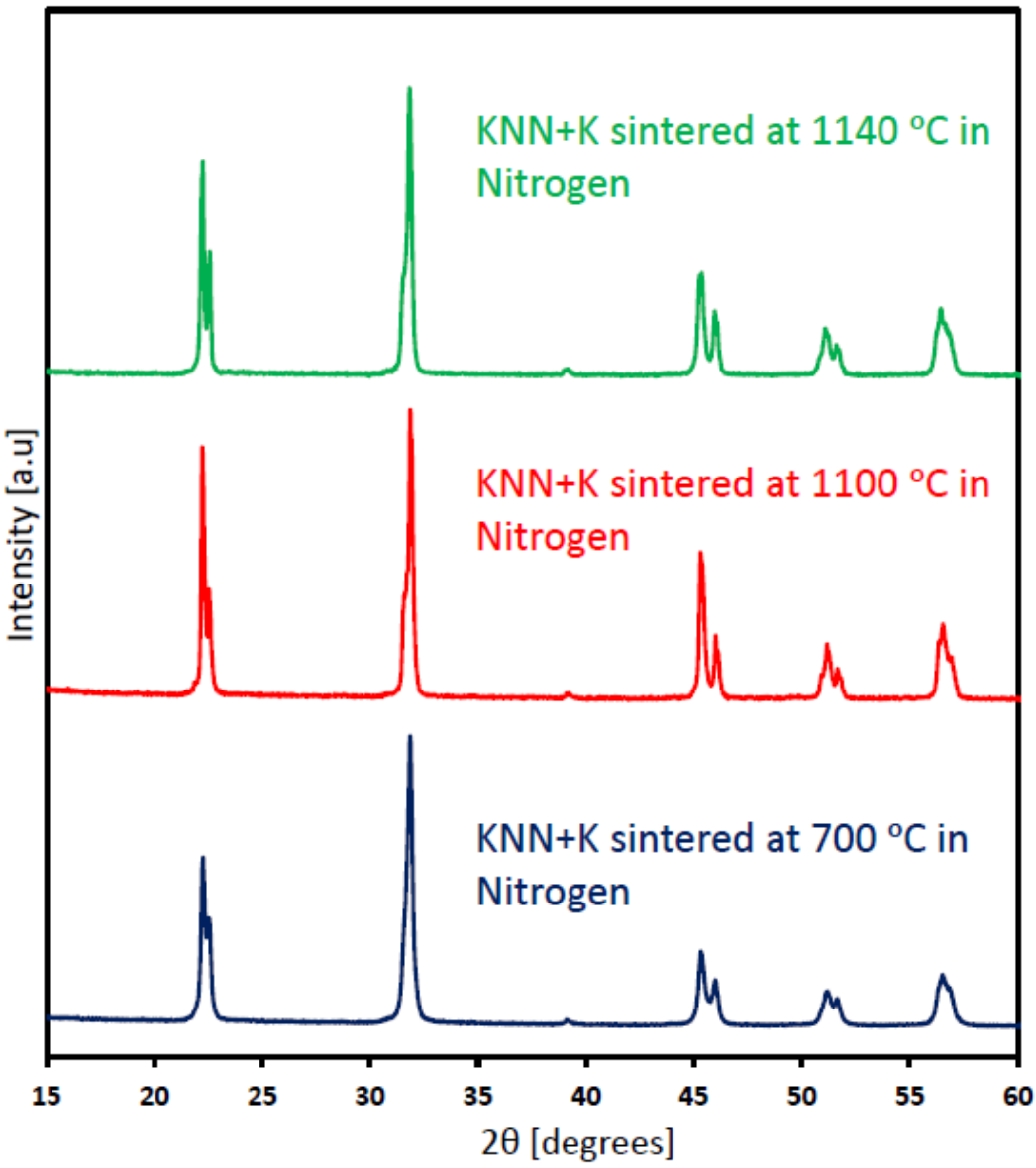

Figure A.4: *X-ray diffractograms of KNN with nominal potassium excess sintered in nitrogen at various temperatures.*

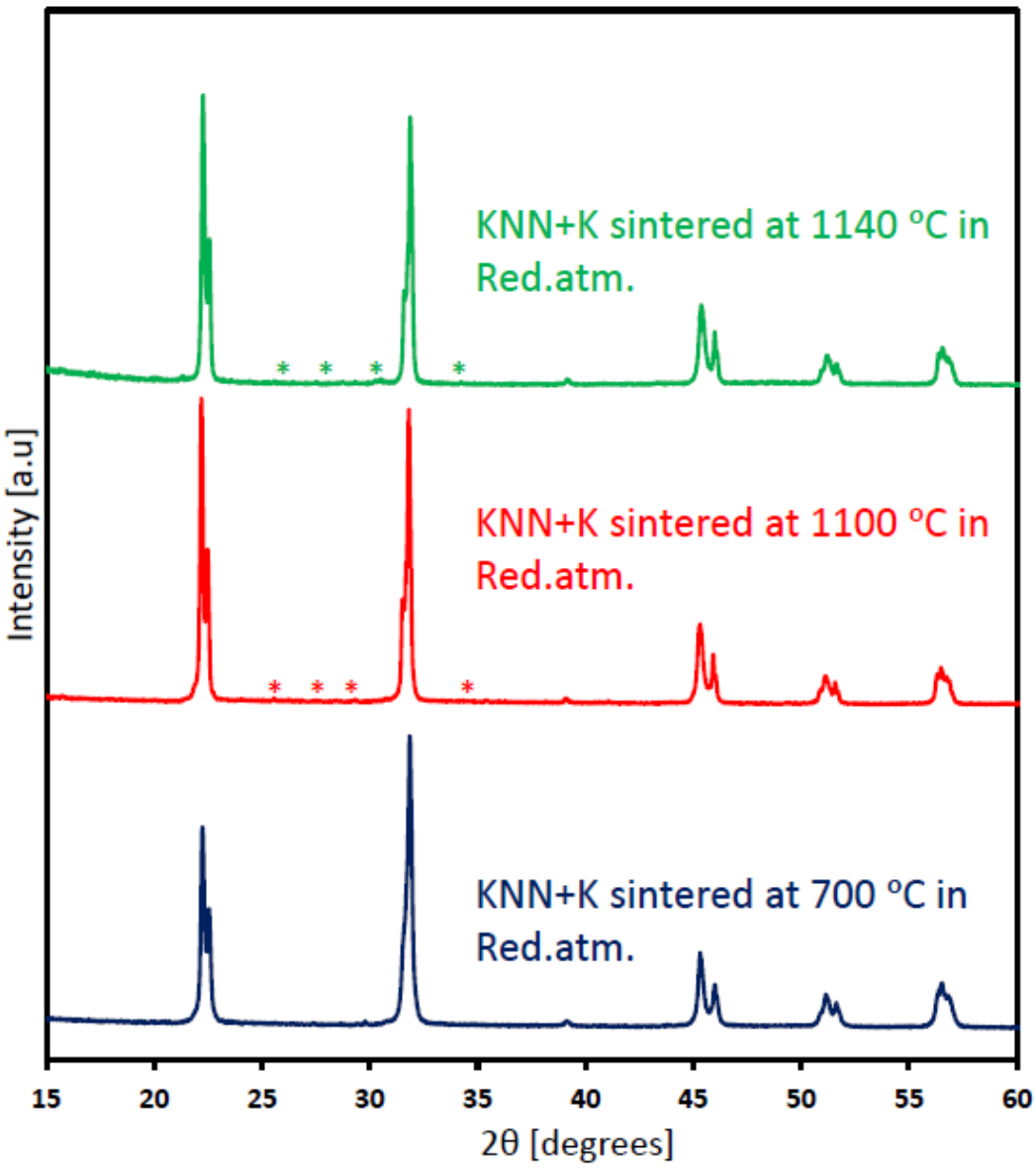

Figure A.5: *X-ray diffractograms of KNN with nominal potassium excess sintered in a reducing atmosphere at various temperatures. Small peaks from a secondary Nb-rich phase ($K_2Nb_4O_{11}$, marked *) are visible between 25° and 35° in the diffractograms of pellets sintered at 1100 °C and 1140 °C.*

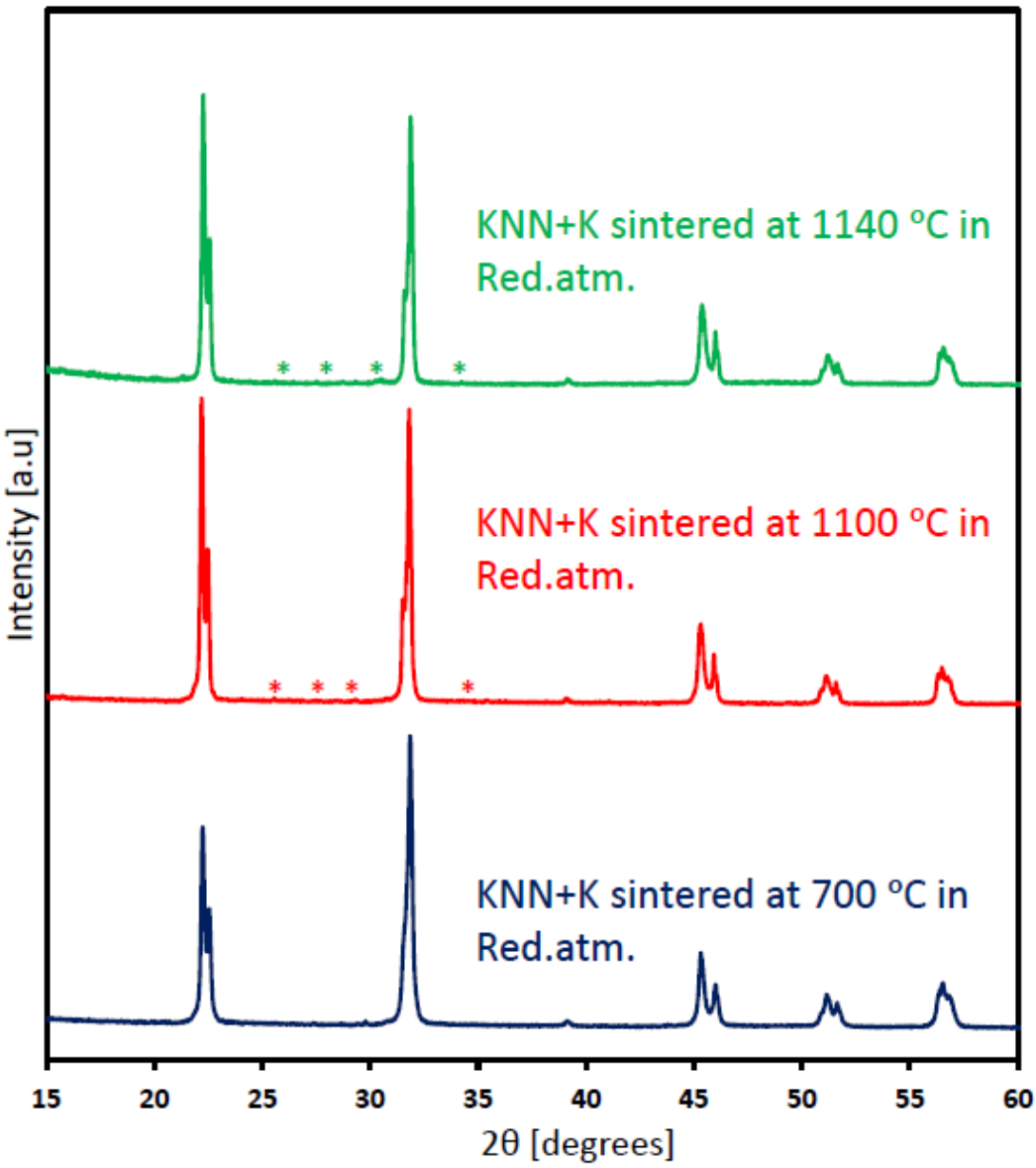

Figure A.6: *X-ray diffractograms of KNN with nominal sodium excess sintered in air at various temperatures.*

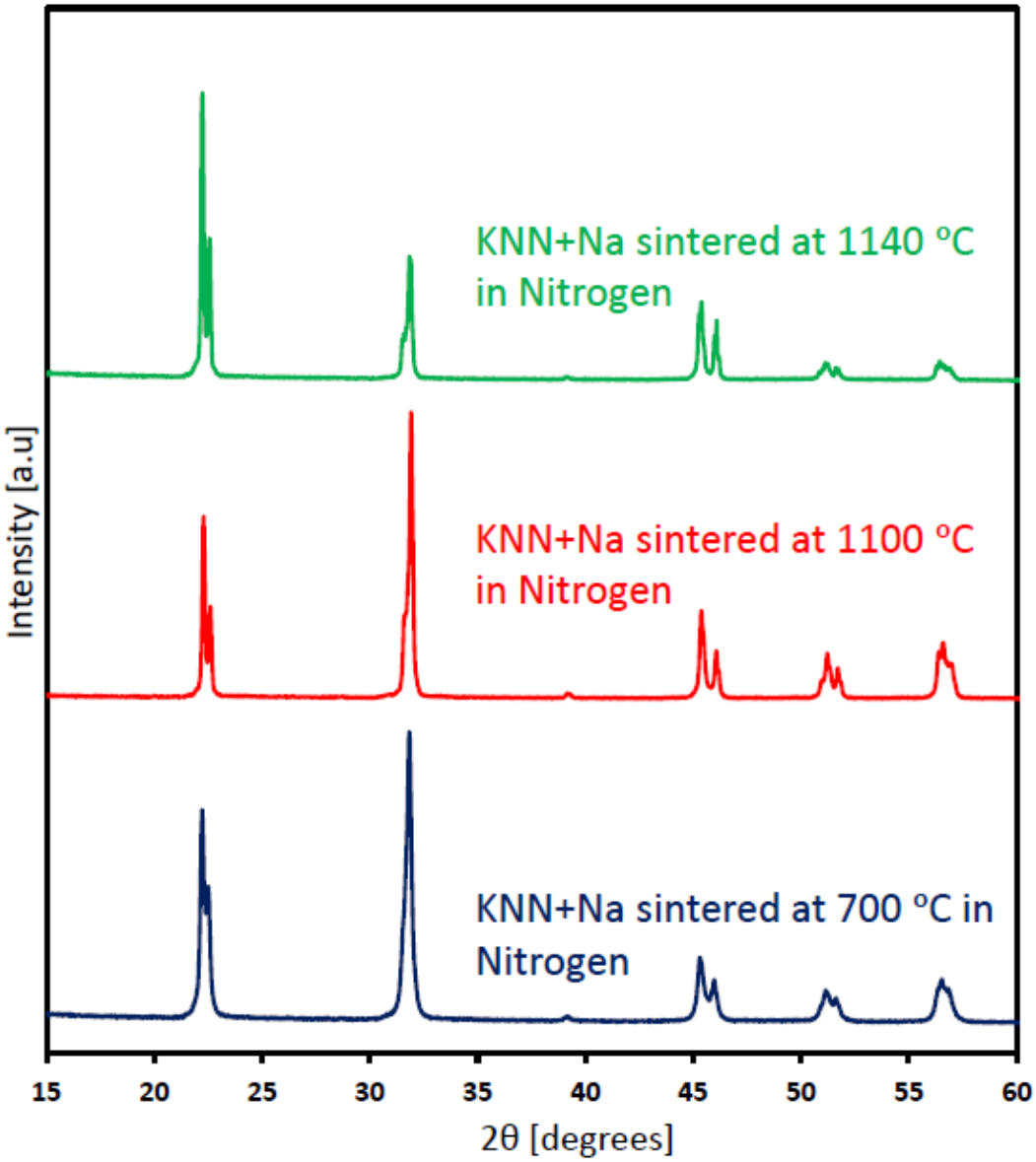

Figure A.7: *X-ray diffractograms of KNN with nominal sodium excess sintered in nitrogen at various temperatures.*

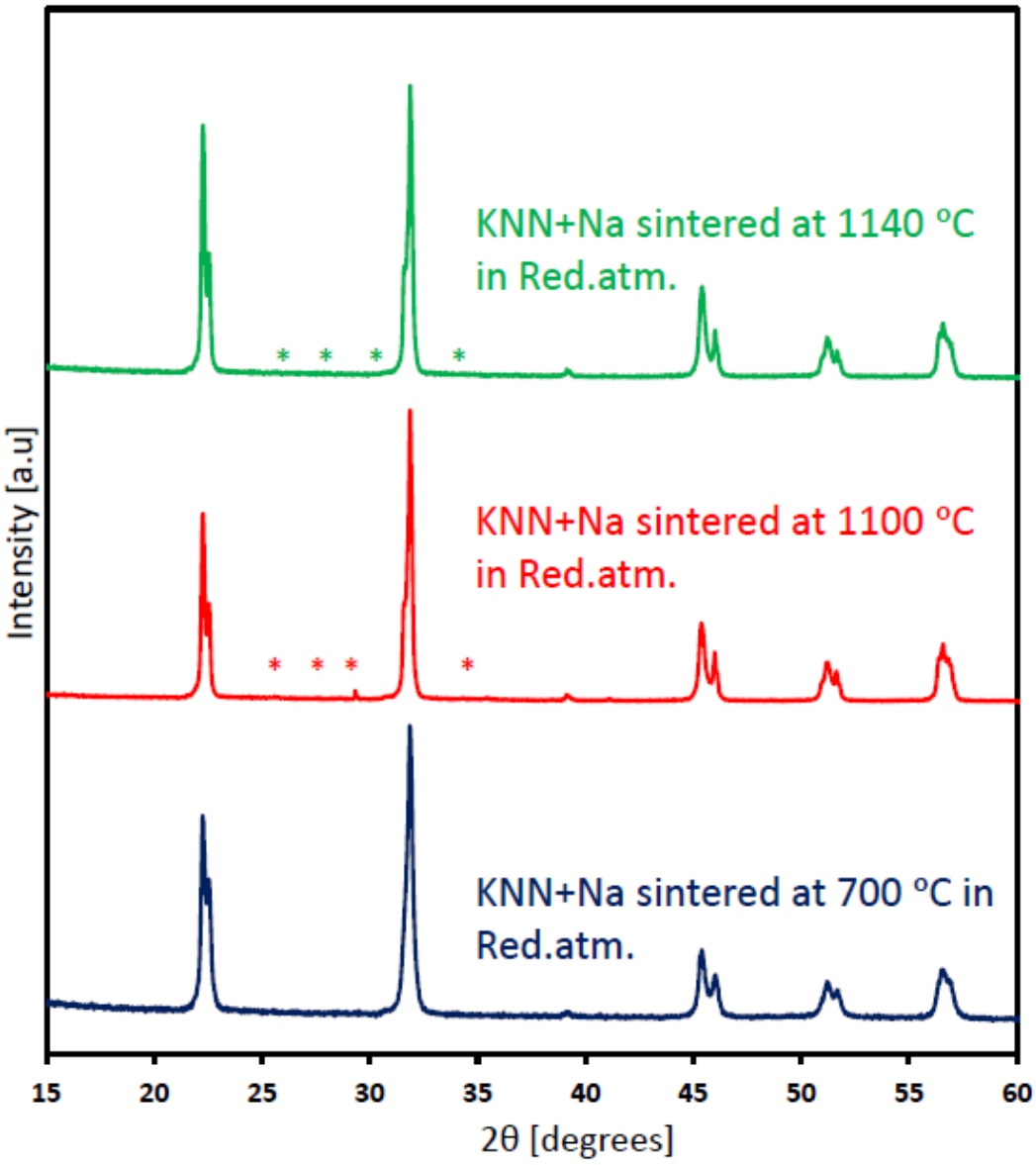

Figure A.8: *X-ray diffractograms of KNN with nominal sodium excess sintered in a reducing atmosphere at various temperatures. Small peaks from a secondary Nb-rich phase ($K_2Nb_4O_{11}$, marked *) are visible between 25° and 35° in the diffractograms of pellets sintered at 1100 °C and 1140 °C.*

Appendix B

Additional Infrared Spectra

Additional infrared spectra are included. The spectra of the 2 wt % KNN with nominal potassium excess heat treated at 700 °C in a reducing atmosphere and then stored in air presented in Figure B.1 and B.2 were recorded as part of the specialization project.[1] The infrared spectra in Figure B.3 were also recorded as part of the specialization project.[1] From these spectra evaporation of alkali hydroxides during drying in a furnace (at 100 °C for 24 h) is evident.

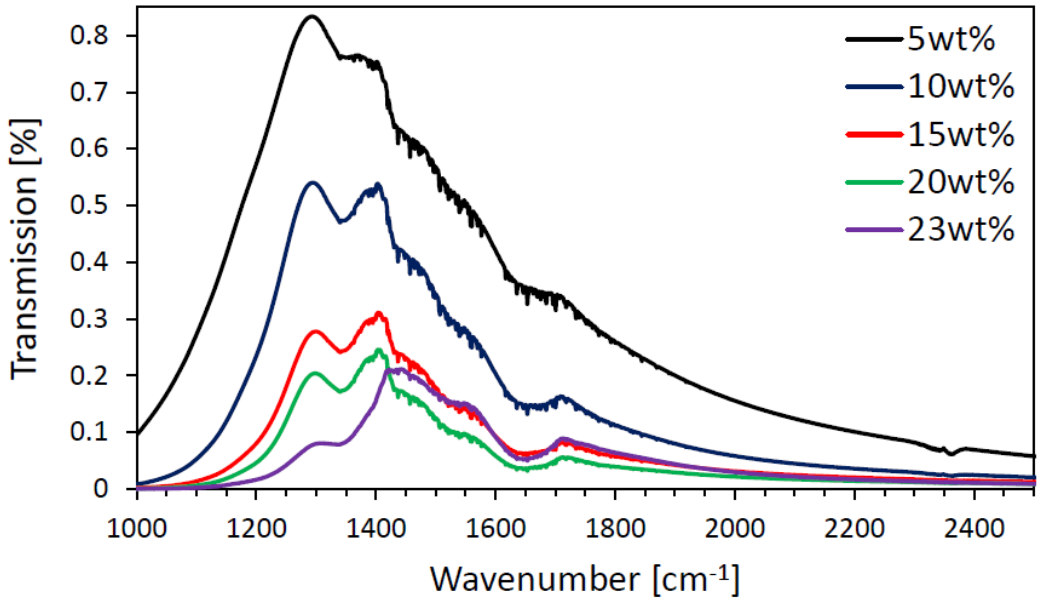

Figure B.1: *Infrared spectra of KNN with nominal potassium excess heat treated at 700 °C in reducing atmosphere. The spectra show that there is little difference in the absorption due to a change in concentration of the sample in relation to the KBr. No additional peaks appear at lower concentrations.*

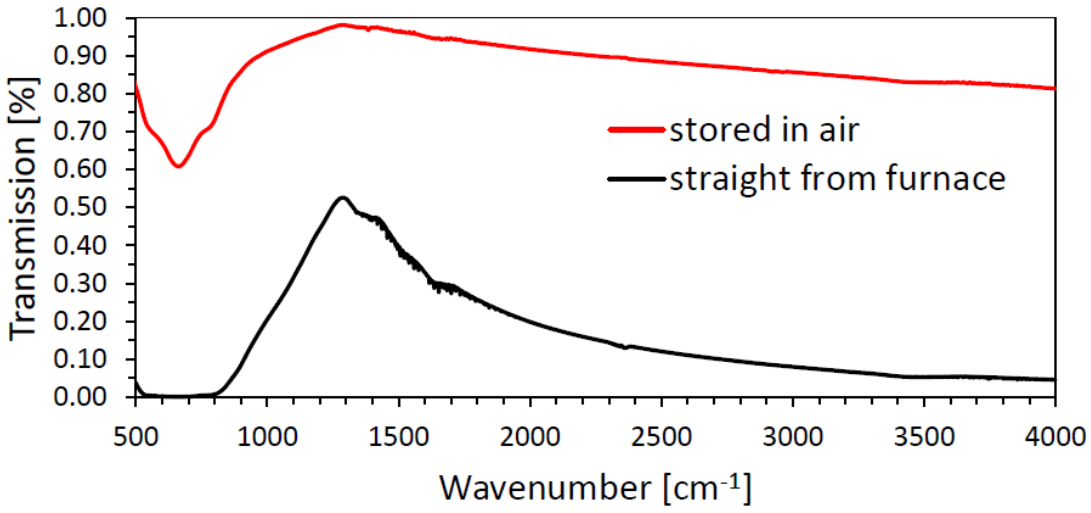

Figure B.2: *Infrared spectra of 2 wt % KNN with nominal potassium excess heat treated at 700 °C in reducing atmosphere. The spectra show the that there is little difference in absorption in a sample stored in air and a sample measured right after the heat treatment.*

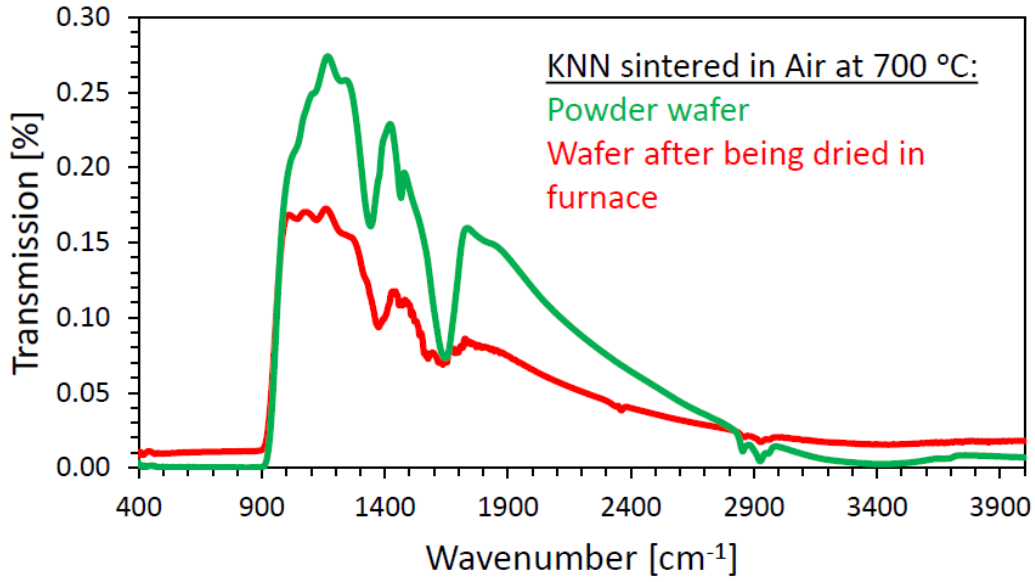

Figure B.3: *Infrared spectra of a pure powder nominally stoichiometric KNN wafer heat treated at 700 °C in air. The absorption band at 1465 cm^{-1} is ascribed to pure carbonate. After drying the absorption bands, originally at 1340 and 1640 cm^{-1}, move closer to the pure carbonate absorption band, indicating evaporation of hydroxides.*

Appendix C

Piezoelectric properties - 1100 °C samples

The polarization and strain loops of nominally stoichiometric KNN and KNN with nominal alkali excess sintered at 1100 °C in different atmospheres are included.

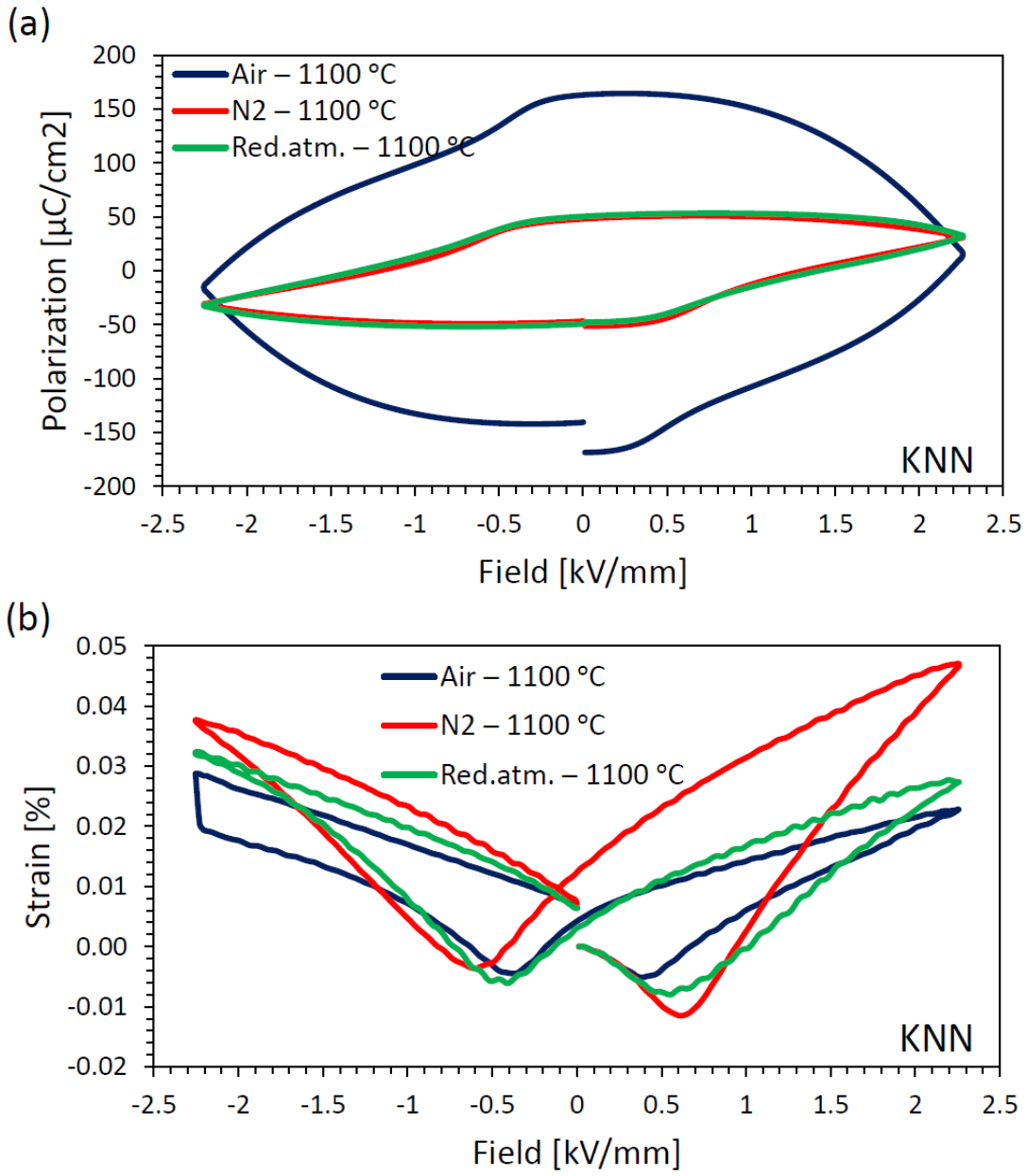

Figure C.1: *The (a) polarization and (b) strain loops of nominally stoichiometric KNN sintered at 1100 °C in air, nitrogen and a reducing atmosphere.*

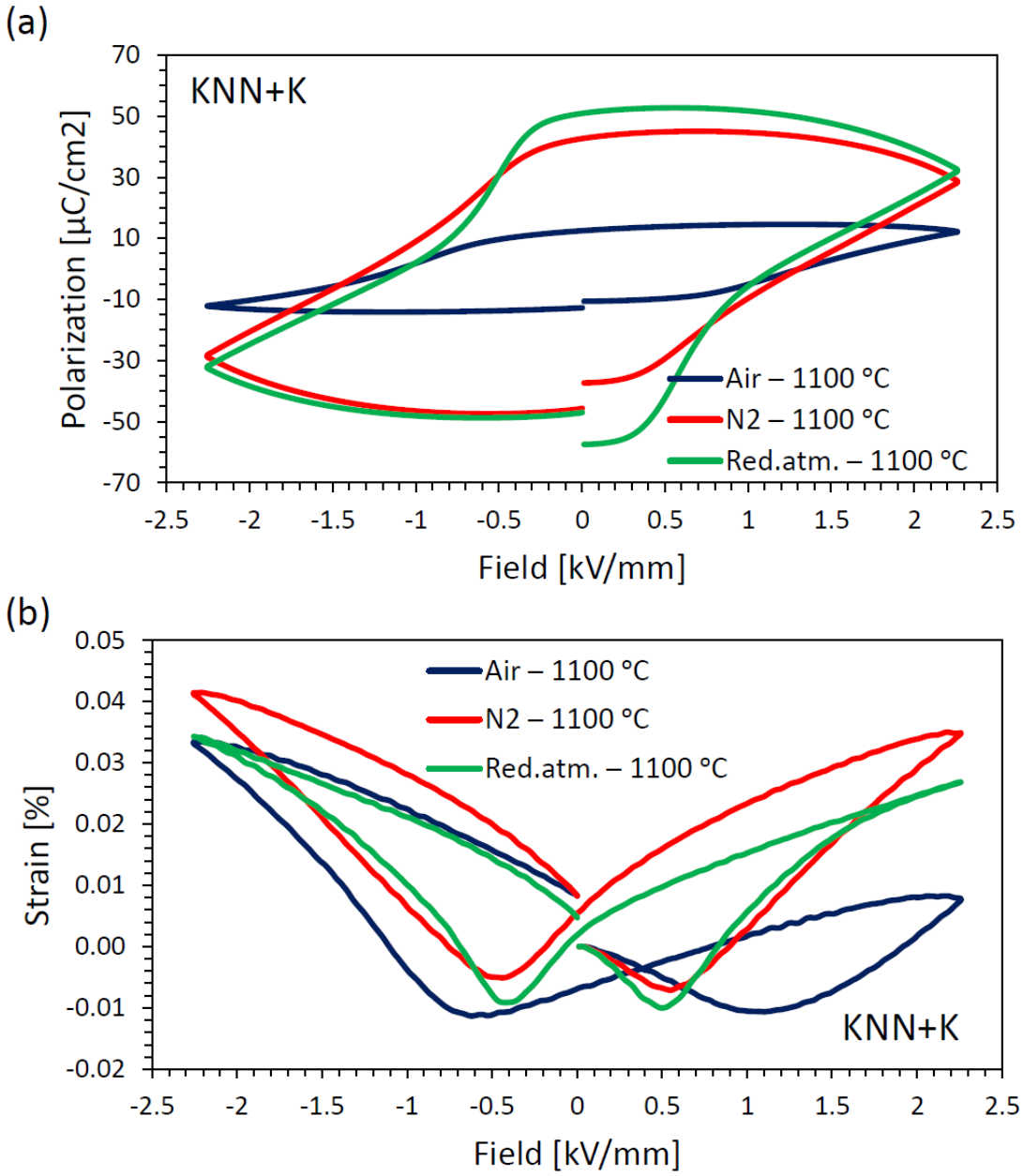

Figure C.2: *The (a) polarization and (b) strain loops of KNN with nominal potassium excess sintered at 1100 °C in air, nitrogen and a reducing atmosphere.*

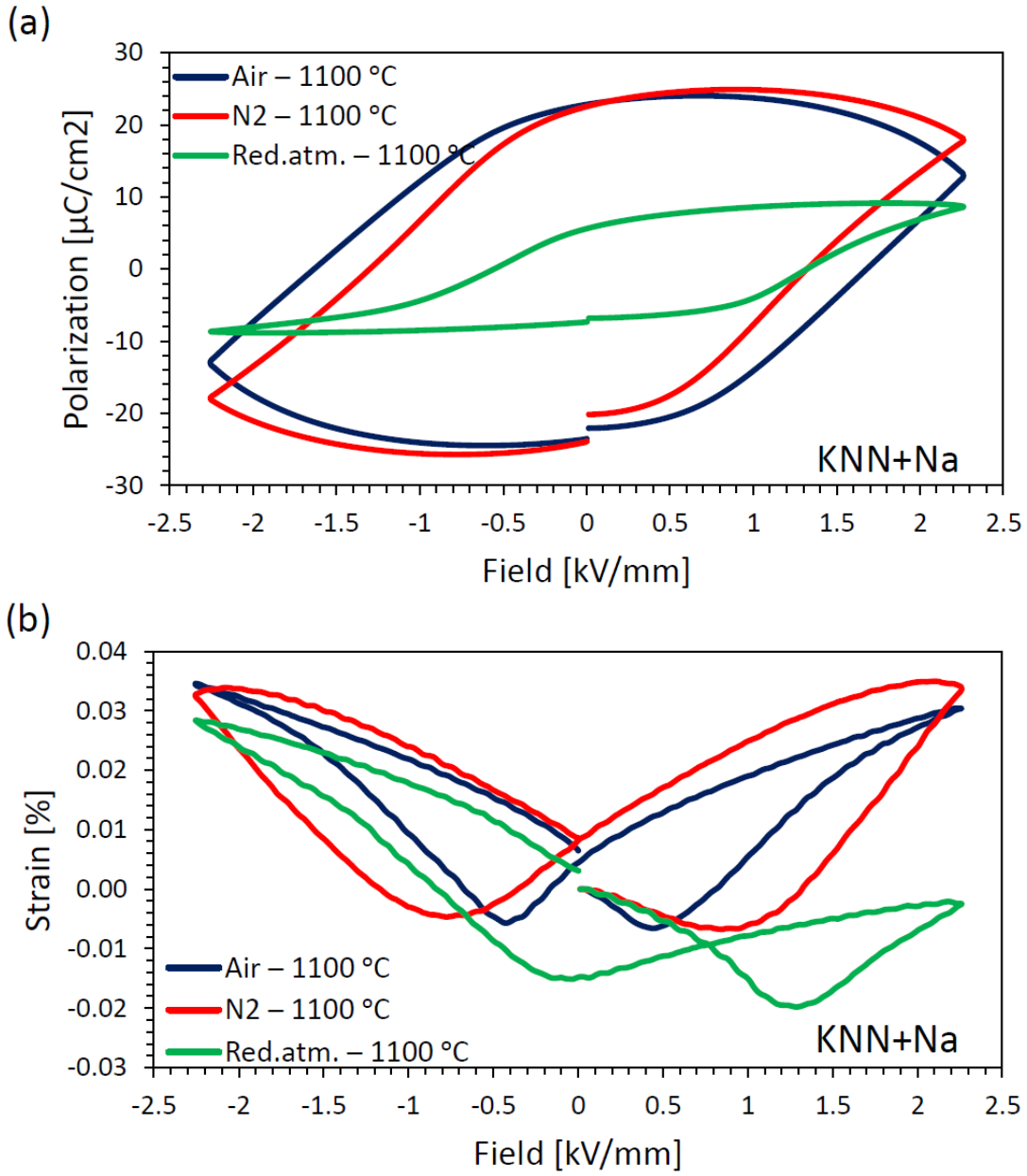

Figure C.3: *The (a) polarization and (b) strain loops of KNN with nominal sodium excess sintered at 1100 °C in air, nitrogen and a reducing atmosphere.*

Bibliography

[1] K. Bakken, *Sintering of lead-free piezoelectric materials*. Norwegian University of Science and Technology, 2014. Specialization project.

[2] A. B. Haugen, *Synthesis and characterisation of textured lead-free piezoelectric ceramics*, vol. 2014:139. Trondheim: Norges teknisk-naturvitenskapelige universitet, 2014. Delvis opptrykk av artikler.

[3] D. W. Richerson, *Modern ceramic engineering: properties, processing, and use in design*. Boca Raton, Fla.: CRC Press, 2006. 3rd ed.

[4] M. D. Maeder, D. Damjanovic, and N. Setter, "Lead free piezoelectric materials," *Journal of Electroceramics*, vol. 13, no. 1-3, pp. 385–392, 2004.

[5] "Directive 2002/95/EC of the European Parliament and of the Council of 27 January 2003 on the restriction of the use of certain hazardous substances in electrical and electronic equipment," *Official Journal of the European Union*, vol. 13, p. L37, 2003.

[6] J. Rödel, W. Jo, K. T. P. Seifert, E. M. Anton, T. Granzow, and D. Damjanovic, "Perspective on the development of lead-free piezoceramics," *Journal of the American Ceramic Society*, vol. 92, no. 6, pp. 1153–1177, 2009.

[7] Y. Saito, H. Takao, T. Tani, T. Nonoyama, K. Takatori, T. Homma, T. Nagaya, and M. Nakamura, "Lead-free piezoceramics," *Nature*, vol. 432, no. 7013, pp. 84–87, 2004.

[8] R. P. Wang, R. J. Xie, T. Sekiya, and Y. Shimojo, "Fabrication and characterization of potassium-sodium niobate piezoelectric ceramics by spark-plasma-sintering method," *Materials Research Bulletin*, vol. 39, no. 11, pp. 1709–1715, 2004.

[9] R. E. Jaeger and L. Egerton, "Hot pressing of potassium-sodium niobates," *Journal of the American Ceramic Society*, vol. 45, no. 5, pp. 209–213, 1962.

[10] J. Fang, X. Wang, Z. Tian, C. Zhong, L. Li, and R. Zuo, "Two-step sintering: An approach to broaden the sintering temperature range of alkaline niobate-based lead-free piezoceramics," *Journal of the American Ceramic Society*, vol. 93, no. 11, pp. 3552–3555, 2010.

[11] P. Bomlai, P. Wichianrat, S. Muensit, and S. J. Milne, "Effect of calcination conditions and excess alkali carbonate on the phase formation and particle morphology of $Na_{0.5}K_{0.5}NbO_3$ powders," *Journal of the American Ceramic Society*, vol. 90, no. 5, pp. 1650–1655, 2007.

[12] J. Acker, H. Kungl, and M. J. Hoffmann, "Influence of alkaline and niobium excess on sintering and microstructure of sodium-potassium niobate $K_{0.5}Na_{0.5}NbO_3$," *Journal of the American Ceramic Society*, vol. 93, no. 5, pp. 1270–1281, 2010.

[13] J. Acker, H. Kungl, and M. J. Hoffmann, "Sintering and microstructure of potassium niobate ceramics with stoichiometric composition and with potassium- or niobium excess," *European Ceramic Society. Journal*, vol. 33, no. 11, pp. 2127–2139, 2013. Date revised - 2013-07-01.

[14] Y. Zhen and J.-F. Li, "Normal sintering of (K,Na)NbO_3-based ceramics: Influence of sintering temperature on densification, microstructure, and electrical properties," *Journal of the American Ceramic Society*, vol. 89, no. 12, pp. 3669–3675, 2006.

[15] Z. Z. Fang, *Sintering of advanced materials: fundamentals and processes*. Oxford: Woodhead Pub., 2010.

[16] S. R. Elliott, *The physics and chemistry of solids*. Chichester: Wiley, 1998.

[17] L. Jin, F. Li, and S. Zhang, "Decoding the fingerprint of ferroelectric loops: Comprehension of the material properties and structures," *Journal of the American Ceramic Society*, vol. 97, no. 1, pp. 1–27, 2014.

[18] K. Momma and F. Izumi, "Vesta 3 for three-dimensional visualization of crystal, volumetric and morphology data," *Journal of Applied Crystallography*, vol. 44, pp. 1272–1276, 2011.

[19] A. Safari and M. Abazari, "Lead-free piezoelectric ceramics and thin films," *Ieee Transactions on Ultrasonics Ferroelectrics and Frequency Control*, vol. 57, no. 10, pp. 2165–2176, 2010.

[20] J. L. Jones, B. J. Iverson, and K. J. Bowman, "Texture and anisotropy of polycrystalline piezoelectrics," *Journal of the American Ceramic Society*, vol. 90, no. 8, pp. 2297–2314, 2007.

[21] G. Flora, D. Gupta, and A. Tiwari, "Toxicity of lead: A review with recent updates," *Interdisciplinary toxicology*, vol. 5, no. 2, pp. 47–58, 2012.

[22] L. Egerton and D. M. Dillon, "Piezoelectric and dielectric properties of ceramics in the system potassium sodium niobate," *Journal of the American Ceramic Society*, vol. 42, no. 9, pp. 438–442, 1959.

[23] J. Fang, X. Wang, and L. Li, "Properties of ultrafine-grained $Na_{0.5}K_{0.5}NbO_3$ ceramics prepared from nanopowder," *Journal of the American Ceramic Society*, vol. 94, no. 6, pp. 1654–1656, 2011.

[24] P. Zhao, B.-P. Zhang, R. Tu, and T. Goto, "High piezoelectric d_{33} coefficient in Li/Ta/Sb-codoped lead-free (Na,K)NbO_3 ceramics sintered at optimal temperature," *Journal of the American Ceramic Society*, vol. 91, no. 9, pp. 3078–3081, 2008.

[25] K. Kobayashi, Y. Doshida, Y. Mizuno, and C. A. Randall, "A route forwards to narrow the performance gap between PZT and lead-free piezoelectric ceramic with low oxygen partial pressure processed $Na_{0.5}K_{0.5}NbO_3$," *Journal of the American Ceramic Society*, vol. 95, no. 9, pp. 2928–2933, 2012.

[26] X. Pang, J. Qiu, K. Zhu, and J. Luo, "Study on the sintering mechanism of KNN-based lead-free piezoelectric ceramics," *Journal of Materials Science*, vol. 46, no. 7, pp. 2345–2349, 2011.

[27] M. Kosec, B. Malic, A. Bencan, T. Rojac, and J. Tellier, "Alkaline niobate-based piezoceramics: Crystal structure, synthesis, sintering and microstructure," *Functional Materials Letters*, vol. 3, no. 1, pp. 15–18, 2010.

[28] T. R. Shrout and S. J. Zhang, "Lead-free piezoelectric ceramics: Alternatives for PZT?," *Journal of Electroceramics*, vol. 19, no. 1, pp. 113–126, 2007.

[29] Z.-Y. Shen, Y. Zhen, K. Wang, and J.-F. Li, "Influence of sintering temperature on grain growth and phase structure of compositionally optimized high-performance Li/Ta-modified (Na,K)NbO_3 ceramics," *Journal of the American Ceramic Society*, vol. 92, no. 8, pp. 1748–1752, 2009.

[30] Y. Wang, D. Damjanovic, N. Klein, E. Hollenstein, and N. Setter, "Compositional inhomogeneity in Li- and Ta-modified (K,Na)NbO_3 ceramics," *Journal of the American Ceramic Society*, vol. 90, no. 11, pp. 3485–3489, 2007.

[31] S. Zhang, H. J. Lee, C. Ma, and X. Tan, "Sintering effect on microstructure and properties of (K,Na)NbO_3 ceramics," *Journal of the American Ceramic Society*, vol. 94, no. 11, pp. 3659–3665, 2011.

[32] J.-J. Zhou, L.-Q. Cheng, K. Wang, X.-W. Zhang, J.-F. Li, H. Liu, and J.-Z. Fang, "Low-temperature sintering of (K,Na)NbO_3-based lead-free piezoceramics with addition of lif," *Journal of the European Ceramic Society*, vol. 34, no. 5, pp. 1161–1167, 2014.

[33] B. Malic, A. Bencan, T. Rojac, and M. Kosec, "Lead-free piezoelectrics based on alkaline niobates: Synthesis, sintering and microstructure," *Acta Chimica Slovenica*, vol. 55, no. 4, pp. 719–726, 2008.

[34] J.-F. Li, Y. Zhen, B.-P. Zhang, L.-M. Zhang, and K. Wang, "Normal sintering of (K,Na)NbO_3-based lead-free piezoelectric ceramics," *Ceramics International*, vol. 34, no. 4, pp. 783–786, 2008.

[35] R. M. German, *Sintering theory and practice*. New York: Wiley. "A Wiley-Interscience publication.".

[36] H. Du, Z. Li, F. Tang, S. Qu, Z. Pei, and W. Zhou, "Preparation and piezoelectric properties of $(K_{0.5}Na_{0.5})NbO_3$ lead-free piezoelectric ceramics with pressure-less sintering," *Materials Science and Engineering B-Solid State Materials for Advanced Technology*, vol. 131, no. 1-3, pp. 83–87, 2006.

[37] D. Liu, H. Du, F. Tang, F. Luo, D. Zhu, and W. Zhou, "Effect of heating rate on the structure evolution of (K,Na)NbO_3-$LiNbO_3$ lead-free piezoelectric ceramics," *Journal of Electroceramics*, vol. 20, no. 2, pp. 107–111, 2008.

[38] H. Shimizu, K. Kobayashi, Y. Mizuno, and C. A. Randall, "Advantages of low partial pressure of oxygen processing of alkali niobate: $NaNbO_3$," *Journal of the American Ceramic Society*, vol. 97, no. 6, pp. 1791–1796, 2014.

[39] A. Chowdhury, J. Bould, M. G. S. Londesborough, and S. J. Milne, "Fundamental issues in the synthesis of ferroelectric $Na_{0.5}K_{0.5}NbO_3$ thin films by sol-gel processing," *Chemistry of Materials*, vol. 22, no. 13, pp. 3862–3874, 2010.

[40] U. Fluckiger, H. Arend, and H. R. Oswald, "Synthesis of $KNbO_3$ powder," *American Ceramic Society Bulletin*, vol. 56, no. 6, pp. 575–7, 1977.

[41] U. Fluckiger and H. Arend, "Preparation of pure, doped and reduced $KNbO_3$ single-crystals," *Journal of Crystal Growth*, vol. 43, no. 4, pp. 406–416, 1978.

[42] J. Acker, H. Kungl, R. Schierholz, S. Wagner, R.-A. Eichel, and M. J. Hoffmann, "Microstructure of sodium-potassium niobate ceramics sintered under high alkaline vapor pressure atmosphere," *Journal of the European Ceramic Society*, vol. 34, no. 16, pp. 4213–4221, 2014.

[43] J.-F. Li, K. Wang, F.-Y. Zhu, L.-Q. Cheng, and F.-Z. Yao, "(K,Na)NbO_3-based lead-free piezoceramics: Fundamental aspects, processing technologies, and remaining challenges," *Journal of the American Ceramic Society*, vol. 96, no. 12, pp. 3677–3696, 2013.

[44] Y.-M. Chiang, D. P. Birnie, and W. D. Kingery, *Physical ceramics: principles for ceramic science and engineering*. New York: Wiley, 1996.

[45] J. G. Fisher and S.-J. L. Kang, "Microstructural changes in $(K_{0.5}Na_{0.5})NbO_3$ ceramics sintered in various atmospheres," *Journal of the European Ceramic Society*, vol. 29, no. 12, pp. 2581–2588, 2009.

[46] J. G. Fisher, D. Rout, K.-S. Moon, and S.-J. L. Kang, "High-temperature x-ray diffraction and raman spectroscopy study of $(K_{0.5}Na_{0.5})NbO_3$ ceramics sintered in oxidizing and reducing atmospheres," *Materials Chemistry and Physics*, vol. 120, no. 2-3, pp. 263–271, 2010.

[47] L. Wu, J. L. Zhang, C. L. Wang, and J. C. Li, "Influence of compositional ratio K/Na on physical properties in $(K_xNa_{1-x})NbO_3$ ceramics," *Journal of Applied Physics*, vol. 103, no. 8, 2008.

[48] CerPoTech. http://cerpotech.com/. Accessed: 2015-6-5.

[49] F. Madaro, R. Saeterli, J. R. Tolchard, M. A. Einarsrud, R. Holmestad, and T. Grande, "Molten salt synthesis of $K_4Nb_6O_{17}$, $K_2Nb_4O_{11}$ and KNb_3O_8 crystals with needle- or plate-like morphology," *Crystengcomm*, vol. 13, no. 5, pp. 1304–1313, 2011.

[50] F. Madaro, *Synthesis of textured $K_xNa_{1-x}NbO_3$ materials*, vol. 2010:36. Trondheim: Norges teknisk-naturvitenskapelige universitet, 2010. Avhandling (ph.d.) - Norges teknisk-naturvitenskapelige universitet, Trondheim, 2010.

[51] E. Garand, T. Wende, D. J. Goebbert, R. Bergmann, G. Meijer, D. M. Neumark, and K. R. Asmis, "Infrared spectroscopy of hydrated bicarbonate anion clusters: $(HCO_3^-)(H_2O_{(1\text{-}10)})$," *Journal of the American Chemical Society*, vol. 132, no. 2, pp. 849–856, 2010.

[52] W. W. Rudolph, G. Irmer, and E. Koenigsberger, "Speciation studies in aqueous HCO_3^--CO_3^{2-} solutions: A combined Raman spectroscopic and thermodynamic study," *Dalton Transactions*, no. 7, pp. 900–908, 2008.

[53] F. Rubio-Marcos, J. Romero, M. Martín-Gonzalez, and J. Fernández, "Effect of stoichiometry and milling processes in the synthesis and the piezoelectric properties of modified KNN nanoparticles by solid state reaction," *Journal of the European Ceramic Society*, vol. 30, no. 13, pp. 2763 – 2771, 2010.

[54] J. S. de Andrade, A. G. Pinheiro, I. F. Vasconcelos, J. M. Sasaki, J. A. C. de Paiva, M. A. Valente, and A. S. B. Sombra, "Raman and infrared spectra of knbo3 in niobate glass-ceramics," *Journal of Physics-Condensed Matter*, vol. 11, no. 22, pp. 4451–4460, 1999.

[55] K. Nakamoto, *Infrared and Raman spectra of inorganic and coordination compounds, Part A, Theory and applications in inorganic chemistry.* Hoboken, N.J.: Wiley, 2009. 6th ed.

[56] F. Madaro, J. R. Tolchard, Y. D. Yu, M. A. Einarsrud, and T. Grande, "Synthesis of anisometric $KNbO_3$ and $K_{0.5}Na_{0.5}NbO_3$ single crystals by chemical conversion of non-perovskite templates," *Crystengcomm*, vol. 13, no. 5, pp. 1350–1359, 2011.